Aeromagnetic evidence of the jurassic rifting in the northwestern Chubut Province, Argentina,

Carlos J. Chernicoff [1,2,3],, Nora Cabaleri [1] and Flavia M. Salani [1,2], Consejo Nacional de Investigaciones Científicas y Técnicas, Universidad de Buenos Aires, Servicio Geológico-Minero Argentino , E-mail: jchern@secind.mecon.gov.ar

Abstract

The Jurassic sedimentary and volcanic sequence (Cañadón Asfalto Formation) of the northwestern Chubut province was started by an extensional regime. The precise location and geometry of a segment of the Jurassic rift, located in the Cerro Condor area, is distinguished as a narrow, north-south trending magnetic high rendered by the magnetite-rich basalts that lie at the base of the sedimentary sequence, which, in turn, are displaced by east-west wrench faults evidenced by cross magnetic lineaments.

Introduction

The aeromagnetic survey of the study area (Fig. 1) forms part of a larger, regional airborne geophysical survey carried out by a joint group of Argentine state agencies in the late 70´s in the Chubut province. The line spacing of the survey is 1000 m and the nominal altitude is 100 m.

No integrated geophysical-geological studies have been carried out in the Chubut province, with the exception of the preliminary interpretation of the Cerro Condor area that has recently been made available (Chernicoff and Cabaleri, 2000).

Synopsis and conclusions

In the Chubut Province, northern Patagonia, a sedimentary and volcanic sequence known as the Cañadón Asfalto Formation developed during Jurassic times.

The Cañadón Asfalto basin is thought to have been started by an extensional regime. In addition to the extensive work done in the field, the inspection of the aeromagnetic maps (Figs. 2 and 3) of the region (total magnetic intensity reduced to the pole and first vertical derivative of the total magnetic intensity reduced to the pole) has allowed the authors to identify the precise location and geometry of a segment of the Jurassic rift, as it is depicted by a

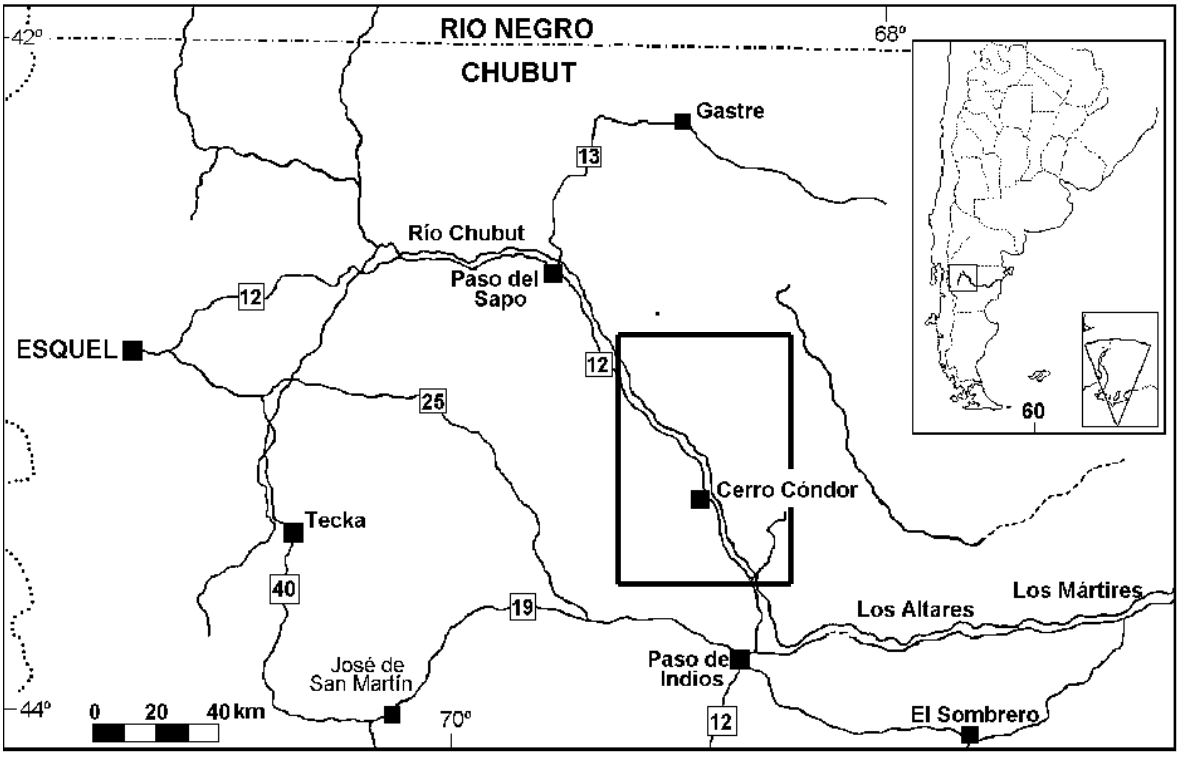

Figure 1. Locality map of the northwestern Chubut province. Argentina. See location of Figs. 2 and 3.

narrow, north-south trending magnetic high resulting from the magnetite-rich basalts lying at the base of the sedimentary sequence; this magnetic high is clearly displaced by east-west trending magnetic lineaments which are likely to represent wrench faults.

The identification of the rift segment is part of the overall structural picture established during the interpretation of the regional aeromagnetic survey of the study area. .

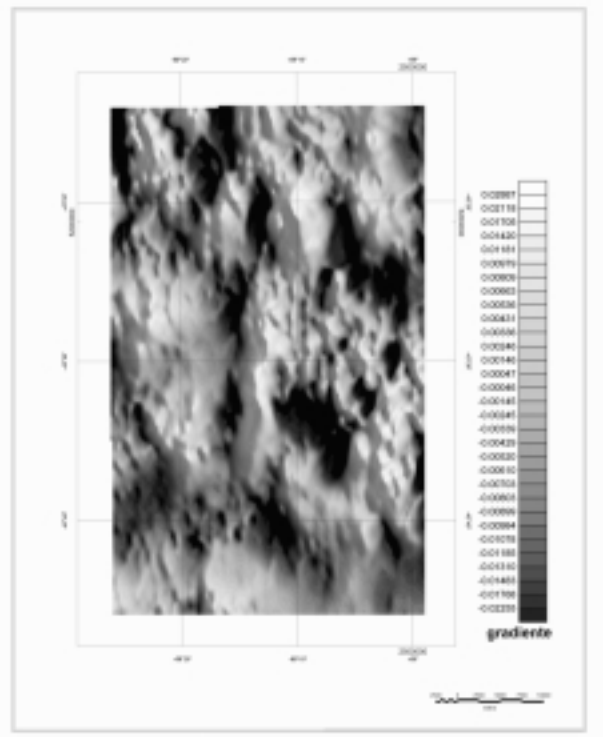

Figure 2. First vertical derivative of the total magnetic intensity reduced to the pole. Cerro Condor area, northwestern Chubut province, Argentina

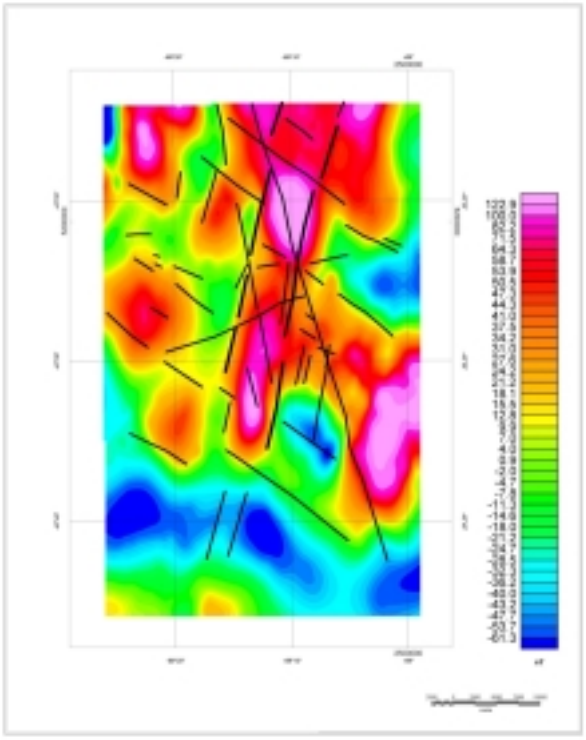

Figure 3. Total magnetic intensity reduced to the pole, and main magnetic lineaments. Cerro Condor area, northwestern Chubut province, Argentina

References

Chernicoff, C.J. and N. Cabaleri, 2000, Jurassic rifting in the northwestern Chubut Province, Argentina, as evidenced by an aeromagnetic survey. 31st International Geological Congress, Abstracts.

AEROMAGNETOMETRIC DATA PROCESSING REVEALING EMPLACEMENT HISTORY OF GRANITE COMPLEXES: Lavras do Sul Intrusive Complex and Jaguari Granite Intrusion study case (RS, Brazil)

Adelir J. Strieder [(1)]; Debora G. Roldão [(1)]; Francisco J.F. Ferreira [(2)] and Telmo F.P. Quadros [(3)];
(1) MODELAGE/UFRGS, (2) LPGA /UFPR, (3) DEMIN/UFRGS

Abstract

The Lavras do Sul Intrusive Complex (LSIC) is a shoshonite- to alkaline type intrusion, while Jaguari Granite Intrusion (JGI) shows just alkaline terms. These both intrusions are close together in western part of Sul-riograndense Shield. The aeromagnetic data processing revealed two types of lineaments around both intrusions (LSIC and JGI): i) regional lineaments and ii) intrusion related lineaments; both lineament types represent different shallow magnetic source. Regional magnetic lineaments are related to regional lithologies and deformational structures. Intrusion related lineaments show a circular distribution around both LSIC and JGI; they represent shallow source, positive magnetic anomalies that are caused by different types of mafic dikes: basaltic, lamprophyric and/or kersantitic ones. There are also felsic dikes around both LSIC and JGI, but they are controlled by radial fracture system. As both LSIC and JGI are circumscribed by circular dikes, at some time during the magmatic event, they must have evolved as a single magma chamber. Circular and radial dikes also point to a large caldera structure that must have evolved by multiple collapse episodes. The development of a caldera structure is compatible to a ballooning type emplacement mechanism for LSIC and JGI.

Introduction

Lavras do Sul Intrusive Complex (**LSIC**) and Jaguari Granite Intrusion (**JGI**) are located in the western part of Sul-riograndense Shield (Fig. 01).

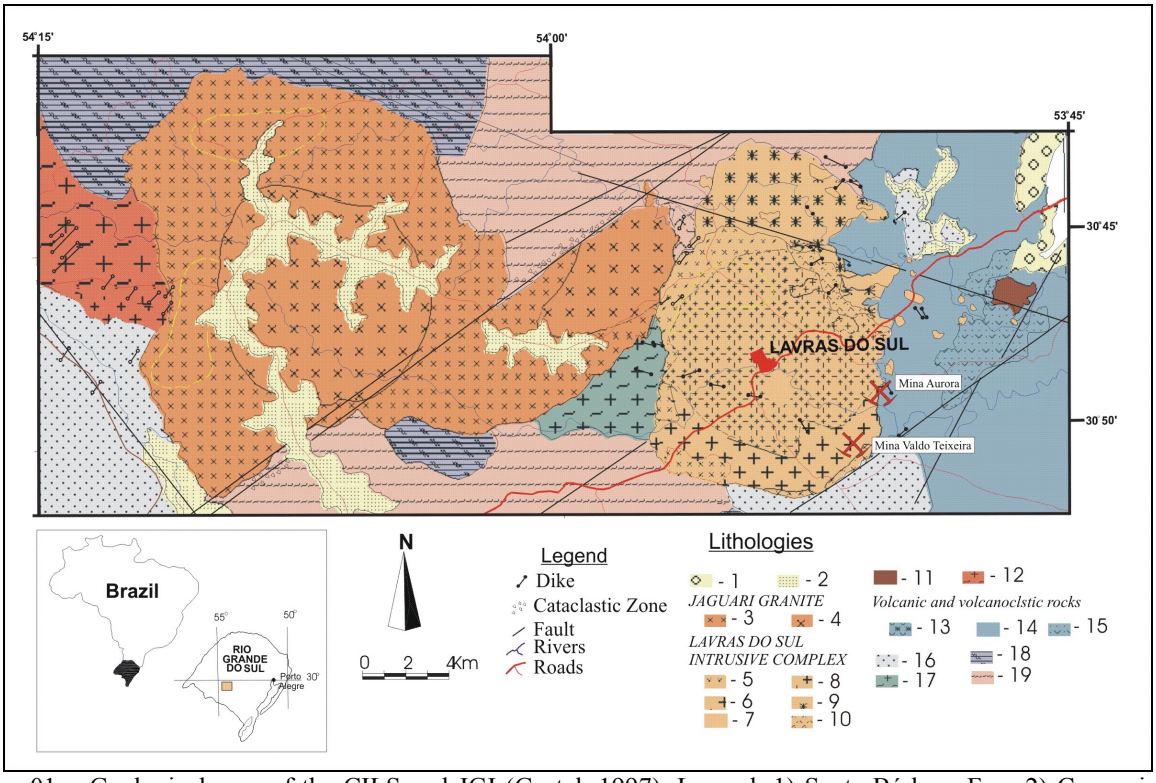

Figure 01 – Geological map of the CILS and JGI (Gastal, 1997). Legend: 1) Santa Bárbara Fm.; 2) Cenozoic and Gondwanic sedimentary cover; 3) Sienogranite; 4) Monzogranite; 5) Pertita granite; 6) Sieno-granite; 7) Porphyric quartz monzonite; 8) Granodiorite to monzogranite; 9) Quartz monzonite and monzonite; 10) Arroio do Jaques ortopirox. bearing monzodiorite; 11) Estrela granite; 12) Santa Rita monzogranite; 13) Latitic flows and breccias; 14) Andesitic flows and pyroclastic rocks; 15) epiclastic rocks; 16) Neoproterozoic cover (Maricá Fm. and Ibaré phylites); 17) Fazenda do Posto granodiorite; 18) Metamorphosed and deformed volcano-sedimentary sequences and mafic-ultramafic complexes; 19) Granite-gneissic complexes (Ortometamorphic Imbicui Suite).

They were characterized, in their actual configuration, by Gastal (1997) and they represent the last magmatic events during the Neoproterozoic orogenic cycle in Mantiqueira Province (RS). The LSIC has shoshonite-to-alkaline magmatic affiliation, while JGI shows just alkaline terms (Gastal, 1997). The LSIC is a multiphase intrusion composed by a range of rock types: from monzodiorite and quartz-monzodiorites, through granodiorite and monzogranites, to sieno and k-feldspar granites; these rock types are arranged in a zoned structure, but mafic rocks are placed in the NNE and northern part of the LSIC (Fig. 01). The JGI, on the other hand, includes just monzogranites and sienogranites (Fig. 01) and has a very poorly developed inner structure. Both intrusions were emplaced into volcano-sedimentary sequences (Palma Volcano-sedimentary Seq., Hilário Fm.) and into granite-gneisses (Cambaí Complex).

The multiphasic nature of LSIC can be pointed out as the reason for lode Au-quartz veins occurrences concentration around it (Andrade *et al*, 1998); it can be seen that JGI has not a multiphase character (Figure 01). General characteristics of the LSIC (shoshonite-to-alkaline granitic intrusion) and the mineralization (ore composition, hydrothermal alteration, etc…) permitted to assign these ore occurrences as related to Climax type intrusions (Andrade *et al*. 1998). But, it is to be realized that LSIC has not any more its root, eroded by subsequent processes.

The aim of this paper is to present some concerns about the emplacement of both, so close, intrusions. These concerns are base mainly on aeromagnetic data processing, but also in new fieldwork data.

Processing of aeromagnetic data

Aeromagnetic data is from Camaquã Airborne Geophysics Project (Jackson *et al.*, 1973) and was gently made available by CPRM (Companhia de Pesquisa de Recursos Minerais). Flight lines are spaced 1000 m apart, and the sampling interval in flight line is 127 m. In the pre-processing of airborne magnetic data, systematical errors were eliminated, such as: heading effects, removing diurnals, navigational effects, time variation in the magnetic field, aircraft effects and ground clearance variation.

Processing of aeromagnetic data included the subsequent steps: (i) statistical analysis of data; (ii) data filtering to eliminate artifacts, (iii) generation of total magnetic intensity map by minimum curvature girding method, and (iv) analytic signal, first vertical derivative over analytic signal filter and AGC filtering with oblique NW-SE illumination (Figure 2). The 1st vertical derivative filter is used to point out short wavelength components (shallow source) and to eliminate deep source effect. AGC filter and oblique illumination were applied to emphasize the amplitude of shallow source signals.

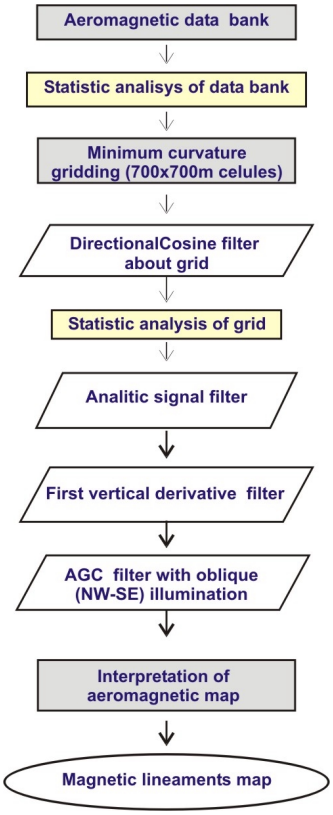

Figure 2 – Procedures applied for processing airborne magnetic data in Lavras do Sul region (RS, Brazil).

Magnetic lineament analysis

The aeromagnetic data processing (1st.vertical derivative and oblique illumination) revealed a series of lineaments around both intrusions (LSIC and JGI). The magnetic lineaments were interpreted in the inflection point from high to low magnetic intensity (Figure 02). The magnetic lineaments around LSIC and JGI can be distinguished into two types: i) regional lineaments (Figure 03) and ii) lineaments related to intrusions (Figure 04). Regional lineaments are related to shallow magnetic source that represent lithologies making up integral part of volcano-sedimentary sequences and/or granite-gneissic complexes were both intrusions were emplaced. Lineaments related to intrusions, on the other hand, circulate both intrusions at same time (Figure 04); these lineaments are also shallow

magnetic sources that are interpreted as circular dikes intruded in the country rocks during magmatic events. In this way, lineaments related to intrusions define an elliptical structure that circumscribes both LSIC and JGI.

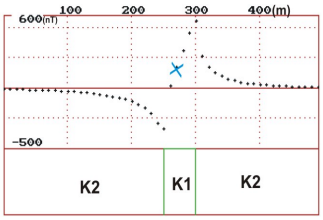

Magnetic inclination: -29.25
Magnetic declination: -8.04
Magnetic filed: 20782
Magnetic susceptibility: 0.010

Figure 02 – Definition of inflection point (x) for magnetic lineament interpretation.

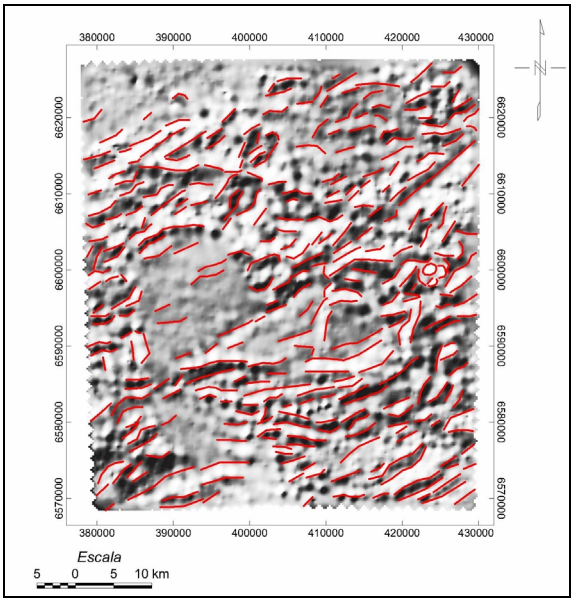

Figure 03 – Regional, shallow source magnetic lineaments interpreted over 1st vertical derivative anomaly map in the Lavras do Sul region (RS, Brazil).

Discussions of magnetic and field data implication for LSIC and JGI emplacement

Fieldwork data sampled after magnetic data processing show that circular lineaments are due to 1-4 m thick mafic dikes. These mafic dikes have basaltic composition (Strieder & d'Ávila, 1985), lamprophyric composition (amphibole bearing mafic dikes; Lima, 1985,1995), or kersantitic composition (phlogopite bearing mafic dikes; Gastal, 1997). These mafic dikes are, then, responsible for high frequency and large amplitude magnetic anomalies revealed by data processing (Figure 04). Fieldwork also showed another group of dikes: dacitic dikes that have porphyries of k-feldspar and amphibole; these dacitic dikes were assigned to Acampamento Velho Fm. magmatism (Strieder and d'Ávila, 1985). However, dacitic dikes are not emplaced in circular structures around both LSIC and JGI, but in radial structures. Dacitic dikes did not produce high spatial frequency anomalies, even under varying direction of illumination. The high frequency and large amplitude magnetic anomalies represent shallow source structures (mafic dikes) displaying circular arrangement to both LSIC and JGI.

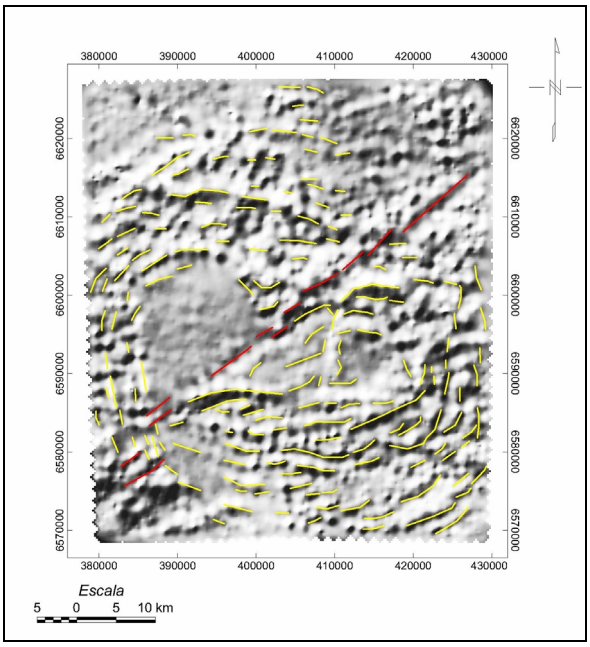

Figure 04 – Magnetic lineaments related to intrusions (LSIC and JGI), interpreted over 1st vertical derivative anomaly map in the Lavras do Sul region (RS, Brazil).

The main implication of the circular dikes circumscribing both LSIC and JGI is that, at some time during their emplacement history, they must have evolved as a single magma chamber. Circular and radial dikes also imply the development of a large caldera structure that must have evolved by multiple collapse episodes, from small (under LSIC) to wider (under LSIC + JGI) fracture sets. The development of a caldera structure is compatible to a ballooning type emplacement mechanism for LSIC and JGI (Roldão et al., 2000). A special geological investigation was designed in the soft meta-sediments of Palma Volcano-sedimentary Sequence to elucidate the emplacement mechanism and its relation to ore occurrences around LSIC and JGI (Roldão and Strieder, in prep.).

Acknowledgments

The authors thank **FAPERGS** (Proc. N° 96/0383-2) and **CNPq-PADCT** (Proc. N° 132047/1998-5) for research grants.

Bibliographic references

Andrade, M.S.; Strieder, A.J.; Gastal, M.C.P., 1998, Controle geotectônico, magamático e estrural das ococrrências minerais de Cu-Au na região de Lavras do Sul(RS): 40º Congresso Brasileiro de Geologia. Anais, BH, SBG-MG, pg 132.

Gastal, M.C.P., 1997, Suíte Saibro, RS: Avaliação de um modelo petrográfico: Curso de Pós-Graduação em Geociências Universidade Federal do Rio Grande do Sul, (Tese de Doutoramento). Porto Alegre, 365p.

Jackson, V.N., Ramos, V.A., Terry, S.A., and Zuzek, A.B., 1973, Projeto aerogeofísico Camaquã, Estado do Rio Grande do Sul: Texas Instruments, DNPM/CPRM/CENEN, Porto Alegre, 208p. (Inedited)

Lima, E.F, 1985, Petroquímica e Prospecção Litogeoquímica da Área da Merita, Região de Volta grande, Lavras do Sul, RS: Curso de Pó-Graduação em Geociências, Universidade Federal do Rio Grande do Sul, Dissertação (Mestrado), Porto Alegre, 162p.

Lima, E.F., 1995, Petrologia das Rochas Vulcânicas e Hipobissais da Associação Shoshonítica de Lavras do Sul-ASLS, RS: Curso de Pó-Graduação em Geociências, Universidade Federal do Rio Grande do Sul, Tese (Doutorado), Porto Alegre, 338p.

Roldão, D.G., 2000, Análise integrada de dados estruturais e geofísicos no controle de depósitos minerais na região oeste do Escudo Sul-riograndense (RS, Brasil): Dissertação de mestrado (PPGEM-EE-UFRGS), Porto Alegre, 133p.

Roldão, D.G. and Strieder, A.J., 2001, Structural geology of Palma region (RS, Brazil): Acta Geológica Leopoldensia. (in prep.)

Strieder, A.J. and d'Avila, R.S.F., 1985, Mapeamento geológico 1:25.000 da Folha Lagoa da Meia Lua, RS. Relatório da Faixa VIII, Projeto Lagoa da Meia Lua, IG-UFRGS, Porto Alegre, Trabalho de Graduação, 185p.

Application of airborne gamma-ray spectrometry in granitic intrusions map-ping: in the western of Sul-riograndense Shield (RS, Brasil)

Debora Grala Roldão and Adelir José Strieder, MODELAGE/DEMIN/UFRGS, Brazil

Abstract

Airborne gamma-ray spectrometry is a geophysical method very important in the geological mapping, because it is able to measure the chemical variation of radioactive elements (K, Th and U). This information can contribute significantly to an analysis and to an individualization of granitics intrusions. In this case, it was applied to granitic intrusions in the western part of Sul-riograndense Shield. The analysis of these geochemical informations derived from the gamma-ray spectrometry data permitted the discrimination of eight granitic intrusions (CSGC, SSGC, LSIC and Passo da Areia, Jaguari, Cerro das Marcas, Saibro and Passo das Chácaras granites). Granitic intrusions discriminated in airbone gamma-ray spectrometry maps displayed a compositional variation (tonal variation in K, U, Th and ternary maps). Tonal variation enabled the characterization of granitics bodies into calcium-alkaline, shoshonitic and alkaline granites.

Introduction

Gamma-rays are emitted during the decay of some naturally occurring elements in the Earth. Airborne gamma-ray spectrometry measures gamma radiation of radioelements during the process of decay. Naturally occurring elements that are able to emit radiation with sufficient energy to be measured in gamma-ray spectrometry surveys are potassium (K), thorium (Th) and uranium (U).

Gamma-ray spectrometry may be utilized as a geochemical instrument, because concentrations of radioelements vary according to the chemistry of emplacement lithological unit. Airborne gamma-ray spectrometry constitute an important element for explanation of the geological units (Dickson and Scott, 1997) and, eventually, for identification of structures that bound lithologic units. In this way, airbonegamma-ray spectrometry may be specifically important to discrimination and analysis of granitic bodies, little to non-deformed, in the west part of Sul-riograndense Shield.

Sul-riograndense Shield is located in the center-west of Rio Grande do Sul State. The western part is characterized by a complex litho-structural arrangement (e. g.: Almeida *et al.*, 1977; Silva Filho, 1991; Chemale Jr. *et al.*, 1995), where polydeformed rocks (gneiss and schist) are juxtaposed by poorly to non-deformed (volcano-sedimentary rocks and granitic intrusions, figure 1) units.

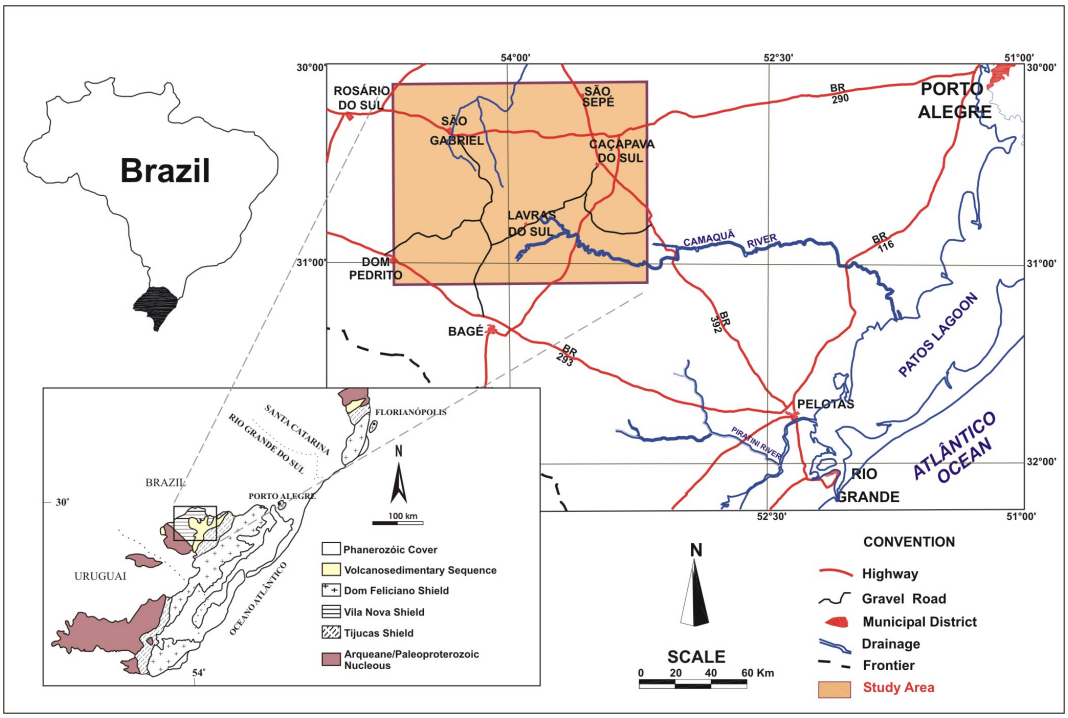

Figure 1 - Localization map of the studied area in Sul-riograndense Shield (RS, Brazil; modify by Roldão, 2000).

Granitic intrusions mapping

Geology of the western part of Sul-riograndense Shield

Sul-riograndense Shield is located in Meridional Segment of Mantiqueira Province (Almeida *et al.*, 1977). This province consists of archean and mesoproterozoic terrains, limited and intruded by Eopaleozoic and Neoproterozoic rocks. These rocks were formed during the Brasiliano Cycle and present a predominant NE-SW regional tectonic direction (Gastal, 1997). Main petrotectonic units that compose the west part of Sul-riograndense Shield may be grouped in:

1. paleoproterozoic terrains: consisting mainly of basic and acidic gneisses rocks (tonalites and trondhjemites), anortosites, ultramafites, meta-pelites and marbles. Lherzolites and pegmatites metamorphosed in granulite facies may also occur;
2. neoproterozoic terrains: consisting of mafic to ultramafic meta-volcano-sedimentary units, juxtaposed to gneissic units, mainly quartz-feldspatic;
3. intrusive granitic associations: granitic units vary from calcium-alkaline intrusions (monzonite, sienogranite and k-feldspate granite), to alkaline intrusions (biotite monzogranite and granodiorite). This magmatism represents the transition from post-orogenic environments to a probable stable environments;
4. Neoproterozoic/Eopaleozoic meta-volcano-sedimentary associations: composed by of sedimentary sequences inserted along felsic-to-intermediary volcanogenic sequences;
5. quaternary sediments: this unit consists of sandstone and pelites, with local levels of organic material and siltstone.

Processing of airborne gamma-ray spectrometry data

Airborne gamma-ray spectrometric data bank is derived from Camaquã Airborne Geophysics Project (Jackson *et al.*, 1973) and ceded by Companhia da Pesquias de Recursos Minerais (CPRM/RS). These data were taken in flight lines spaced of 1 Km apart and sampling interval in the flight lines is 127 m, in N45^{o}W direction. The flight mean height was of 125 m above the terrain.

Airborne gamma-ray spectrometric data bank of Camaquã Project was pre-processed by Jackson *et al.* (1973). These authors effectuated due corrections and calibrations. Pre-processing of airborne gamma-ray spectrometric data involved: (i) canal energy calibration; (ii) matrix reduction and pattern correction to spectrum of Th and U canals in White Mountains and in Haystack Mine, respectively; (iii) dead time normalization (cp2s); (vi) cosmic radiation correction; (v) background radiation correction; (vi) height correction and (vii) atmospheric radiation correction.

Processing of airborne gamma-ray spectrometric data of the studied area contain the subsequent stages: (i) statistical analysis of data; (ii) data filtering to eliminate artifacts and (iii) creation of radiometric maps (total counting, K, Th and U, figure 2). Figure 3 displays K/Th/U ratio map. This map displays the better visualization of granitic intrusions, as well as boundaries of these units and the relationship along them.

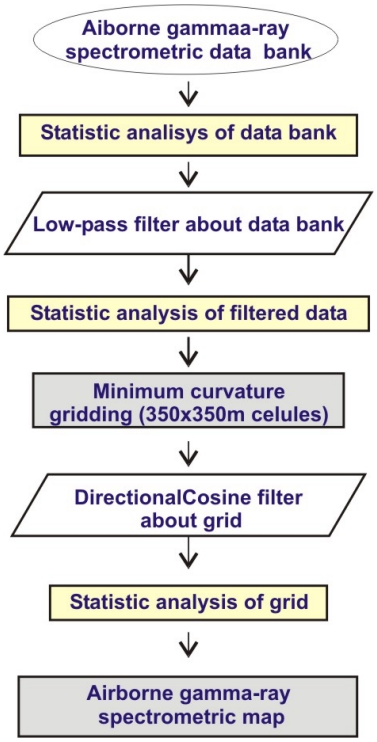

Figure 2 – Procedures applied for processing airborne gamma-ray spectrometric data.

Application of airborne gamma-ray spectrometric map in individualization and interpretation of gratinic bodies

Granitic intrusions of western part of Sul-riograndense Shield are emplaced in chemically contrasting lithologies (meta-volcano-sedimentary and gneiss rocks). This chemical contrast between intrusive units and their country rocks is reflected in airborne gamma-ray spectrometric maps and makes possible to individualize these units visually (figure 3).

Granitic intrusions mapping

Field mapping validated produced gamma-ray spectrometric maps. In this field mapping, it was verified that contacts correspond to geological reality. Initially, seven granitic bodies were discriminated: Caçapava do Sul Granitic Complex (CSGC), São Sepé Granitic Complex (SSGC, border and nucleus), Passo da Areia Granite, Jaguari Granite, Lavras do Sul Intrusive Complex (LSIC, border and nucleus), Cerro das Marcas Granite and Saibro Granite (border and nucleus; the latter is also named Cerro das Tunas Granite by Gastal, 1997).

The analysis of airborne gamma-ray spectrometric maps permits, yet, the chemical correlation along these seven granitic intrusions. Gastal (1997) classifies tardi- to post-tectonic granites in three magmatic suites: (i) high-K calcium-alkaline, (ii) shoshonitic and (iii) alkaline. In airborne gamma-ray spectrometric maps (mainly in ternary map, figure 3), it is possible to confirm this classification. CSGC and SSGC nuclea displayed a high-K concentration related to low-Th and –U concentration; this high-K concentration is typical of granites formed from evolved calcium-alkaline magmas. The calcium-alkaline granites display poor continental crust contribution during melting that explains the low-Th and –U concentration. LSIC and Saibro granite nucleus show high-K and –U concentrations. These high concentrations indicate that their magma received a higher crustal contribution during the fusion (more differentiated magma); high-K and –U concentration is common in shoshonitic magmas. The other granitic bodies (LSIC, SSGC and Saibro Granite borders and Passo da Areia, Jaguari and Cerro das Marcas granites) showed high concentration in three radioelements (K, Th and U), that defines alkaline affiliation (differentiated magma).

Upon airborne gamma-ray spectrometric maps and spectral signature characterization of tardi- to post-tectonic granites in western part of Sul-riograndense Shield, Iglesias (2000) conducted detailed field working that lead to the discovery of one new alkaline granitic intrusion in this region. It is located west to Saibro Granite and was named Passo da Chácara Granite by Iglesias (2000).

Conclusion

This paper showed that airborne gamma-ray spectrometry is a very important instrument on geological mapping, once it gives informations related to the chemistry of surface lithological units.

Analysis and interpretation of airborne gamma-ray spectrometric maps permitted adequate individualization of granitic intrusions in western part of Sul-riograndense Shield. It was possible to characterize a spectral geophysical signature (geochemical signature) of main intrusive units. In this paper, seven granitic intrusions were discriminated: CSGC, SSGC, LSIC and Passo da Areia, Jaguari, Cerro das Marcas and Saibro granites. The geochemical relationship between these units showed that granites might be grouped in to: calcium alkaline granites (CSGC and SSGC nucleus), alkaline granites (Jaguari, Passo da Areia and Cerro das Marcas granites and LSIC, SSGC and Saibro granite borders) and shoshonitic granites (LSIC and Saibro nucleus). The characterization of geochemical signature enabled the discrimination of one new granitic body, named of Passo das Chácaras Granite. Besides granitic intrusions, airborne gamma-ray spectrometric data may be also used to identify other lithologies, such as Neoproterozoic to Eopaleozoic volcanic units that are bright in ternary airborne gamma-ray spectrometric map.

References

Almeida, F.F.M., Hasui, H., Brito Neves, R.A., and Funk, R.A., 1977, Províncias Estruturais Brasileiras: In: Simpósio de Geologia do Nordeste, 38, Campina Grande. *Atlas*..., SBG, p.363-391.

Chemale Jr., F., Hartmann, and Silva, L.C. da, 1995, Stratigraphy and tectonism of Brasiliano Cyclo in Southern Brazil: Communications of the Geological Survey of Namibia, 10, 151-166.

Gastal, M.C., 1997, Suíte Intrusiva Saibro, RS: avaliação de um modelo petrológico: Tese de Doutorado, Curso Pós-grad. Geociências (IG-URFGS), Porto Alegre, 365p.

Iglesias, C. M. 2000, Análise integrada de dados geológicos e estruturais para a prospecção de ouro na região de Torquato Severo (RS): Dissertação de mestrado (PPGEM-EE-UFRGS), Porto Alegre, 103p.

Jackson, V.N., Ramos, V.A., Terry, S.A., and Zuzek, A.B., 1973, Projeto aerogeofísico Camaquã, Estado do Rio Grande do Sul: Texas Instruments, DNPM/CPRM/CENEN, Porto Alegre, 208p. (Inedited)

Silva Filho, B.C., 1991, Geology of the polyphase deformed precambrian terrain of the Vila Nova Region, state of Rio Grande do Sul, Southern Brazil. Part II: Structural sequence, Acta Geológica Leopoldensia, 14 (34):5-94.

Acknowledgments

Authors would like to thank CPRM, FAPERGS (Proc. N° 96/0383-2), CNPq-PADCT (Proc. N° 132047/1998-5) and CNPq-PADCT (Proc. N° 62.0155/97-3 GTM/UFPR) for research grants. I am also grateful to the colleague Geól[a]. Adriane Fischer for English revision and Prof. Francisco José Fonseca Ferreiras for the help in data processing.

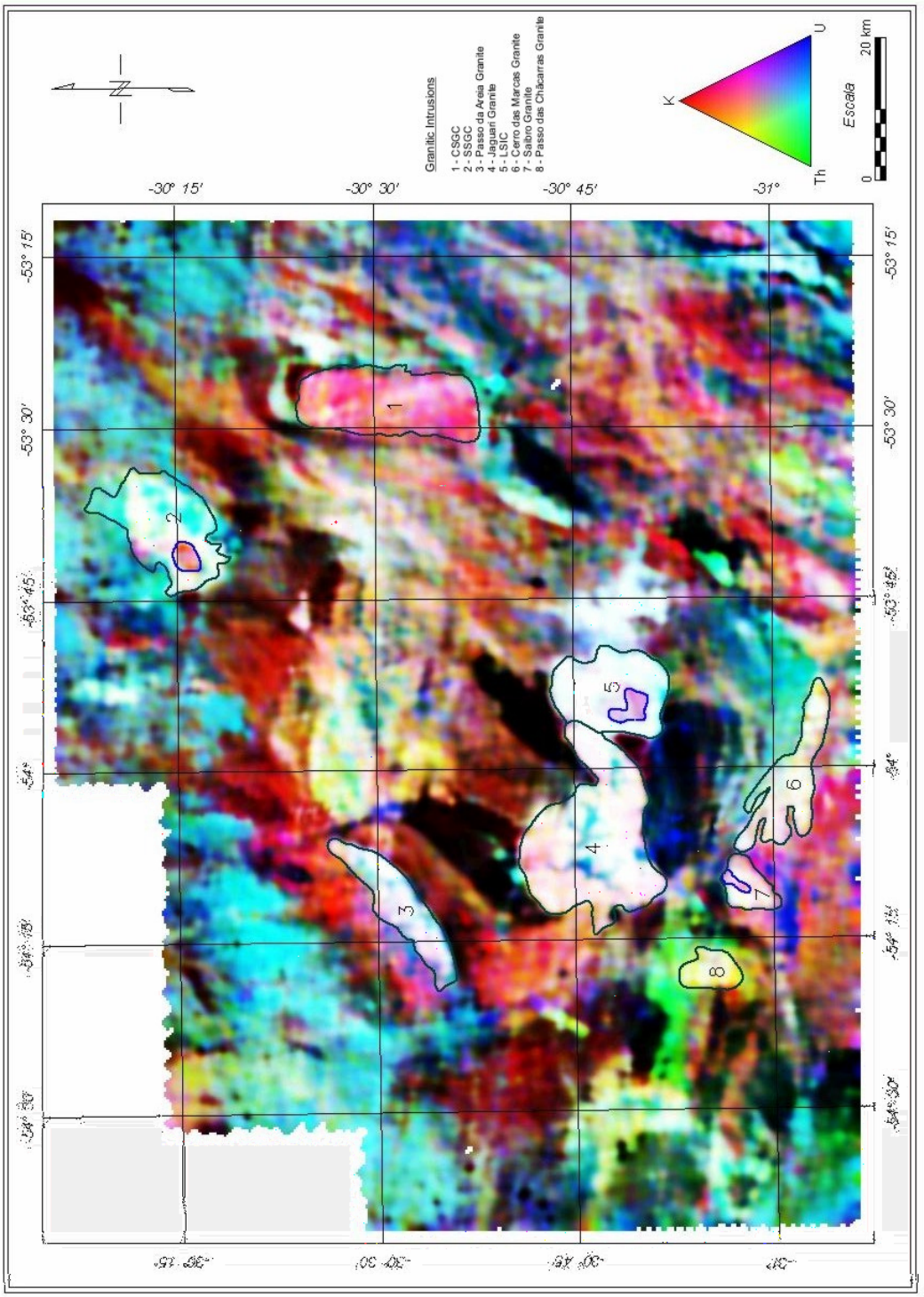

Figure 3 – Ternayr (K+Th+U) airborne gamma-ray spectrometric map with granitic intrusion, where lines in dark green is boundary and blue is nucleus.

Application of aeromagnetic surveys to structural mapping of the western part of Sul-riograndense Shield (Brazil)

Débora Grala Roldão and Adelir José Strieder, MODELAGE/DEMIN/UFRGS, Brazil

Abstract

Magnetic lineaments represent main magnetic traces identified in 1st vertical derivative aeromagnetic map (shallow source anomaly). These magnetic lineaments represent shallow level structural features that can be associated with deformational structures. Type-1 lineaments represent penetrative structures, such as: gneissic banding, schistose layers, foliation, sedimentary bedding, and other. Semi-detail cinematic analysis permitted to identify main paleostress directions for the western Sul-riograndense Shield. The integrated analysis of these informations (magnetic and type-1 lineaments and semi-detail cinematic analysis) enabled to characterize two deformational systems (sinistral and dextral). The sinistral system, also named Irapuá Duplex System, crosscut and is cut off by dextral system (mainly Ibaré Lineament). The deformational dynamic of western Sul-riograndense Shield makes possible to define a conjugated system as the last Neoproterozoic deformational phase.

Introduction

Aeromagnetic surveys consider geological informations in larger depth. These informations are intimately related with terrestrial magnetic field variations. These variations are typically associated with magnetic mineral and characteristic structures concentration of favorable areas to mineral deposits occurrence. The aim of this paper is to correlate magnetic and deformational structures in western part of Sul-riograndense Shield.

Sul-riograndense Shield is located in middle-west part of Rio Grande do Sul State (Brazil). The western area of Sul-riograndense Shield is characterized by litho-structural complexity (e.g.: Almeida *et al*., 1977; Silva Filho, 1991; Chemale Jr. *et al.*, 1995), where polydeformed rocks (gneiss and schist) are juxtaposed units not much deformed (volcano-sedimentary rocks and granitics intrusions, figure 1). Structural characterization of western part of Sul-riograndense Shield was determined upon lineaments maps. Magnetic lineaments were interpreted from aeromagnetometric maps. LANDSAT TM-5 images enabled identification and taking off penetrative lineaments, named of structural, or type-1, lineaments (Strieder and Amaro, 1997).

Processing of aeromagnetic data

Aeromagnetic data are from Camaquã Project (Jackson, 1973) and was gently made available by CPRM (Comp. Pesquisa de Recursos Minerais).

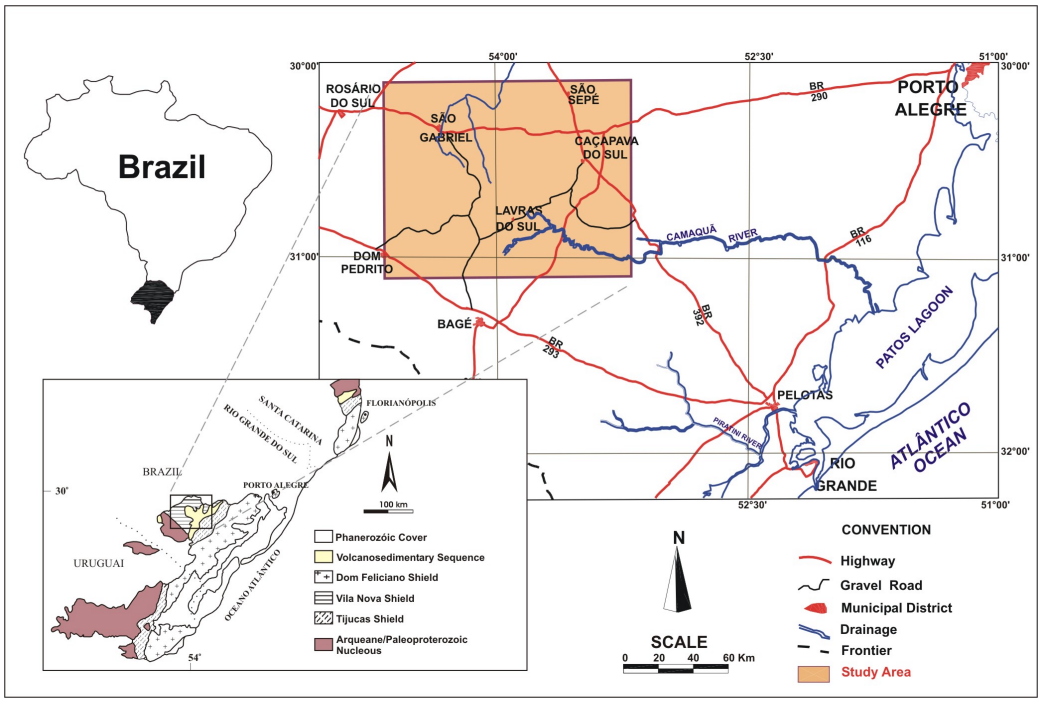

Figure 1 - Localization map of the studied area in Sul-riograndense Shield (RS, Brazil; modify by Roldão, 2000).

Flight lines are spaced 1000 m apart, and sampling interval in the flight lines is 127 m.

Aeromagnetic data bank of Camaquã Project was pre-processed by Jackson *et al.* (1973). In the pre-processing of airborne magnetic data, systematical errors were eliminated, such as: heading effects, removing diurnals, navigational effects, time variation in the magnetic field, aircraft effects and ground clearance variation.

Processing of aeromagnetic data included the subsequent steps: (i) statistical analysis of data; (ii) data filtering to eliminate artifacts, (iii) generation of total magnetic intensity map by minimum curvature gridding method, and (iv) application of filters of analytic signal and first vertical derivative over analytic signal filter (Figure 2). The 1st vertical derivative filter is used to point out short wavelength components (shallow source) and to eliminate deep source effect. The 1st vertical derivative is physically equivalent to measuring the magnetic field simultaneously at two points vertically above each other, subtracting the data and dividing the result by the vertical spatial separation of measurement points (Milligan and Gunn, 1997).

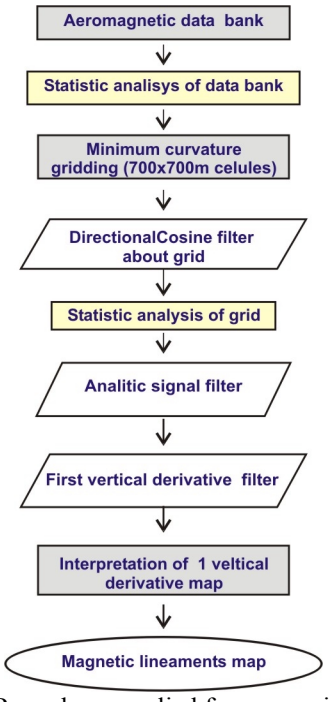

Figure 2 – Procedures applied for processing airborne magnetic data in western Sul-riograndense Shield (RS, Brazil).

Structural analysis of the western part of Sul-riograndense Shield

The structural analysis involves two investigation phases. First phase is related to investigations in regional scale, while the second phase is related to semi-detail scale. Regional scale investigation necessarily involves integrated analysis and interpretation of remotely sensed data (aeromagnetic map and satellite image). The investigation remotely sensed imaged does permit to select target areas for structural analysis in semi-detail scale.

Regional scale

Aeromagnetrometry is related to variations in magnetic minerals (magnetite, titanomagnetite, maghemita, pirrotita, etc) concentrations into geological structures. Magnetic lineaments map was made upon the first vertical derivative map. Magnetic lineaments map presents only lineaments that display large variation in magnetic amplitude. Magnetic lineaments were interpreted in the inflection point from high to low magnetic intensity. The interpretation of magnetic lineaments showed three characteristic patterns:

1. NE magnetic lineaments show a linear to slightly curvilinear character and materialize zones with a high magnetic intensity variation;
2. WSW magnetic lineaments show strongly curvilinear character, forming a sigmoidal pattern. The sigmoidal pattern is more intense close to NE magnetic lineaments, where WSW magnetic lineaments inflect in the NE magnetic lineaments direction;
3. WNW magnetic lineaments are restrict to ESE part of studied area and they are characterized by showing a rectilinear to light curvilinear character. These magnetic lineaments pattern shows a magnetic variation with smaller amplitude than WNW magnetic lineaments.

Type-1 lineaments are associated to penetrative structures. These lineaments developed parallel to positive and negative geomorphological features in a linear or curvilinear arrangement. Type-1 lineaments are composite lineaments, because they also show a tonal banding related to lithologies and structures (foliation, bedding, gneissic layering, …). Type-1 lineaments may structural delineate forms, such as folds and/or shear zones (Strieder and Amaro, 1997). The extraction of Type-1 lineaments was made upon LANDSAT TM-5, paper image (RGB, 3-4-5 composition; Roldão, 2000).

In western Sul-riograndense Shield, type-1 lineaments show a linear to curvilinear character. In

some cases, these lineaments show a circular to elliptic arrangement that define intrusive bodies. Structural lineaments also define rectilinear and slightly curvilinear bands with NE orientation. These bands show a high concentration of lineaments and have been characterized as high deformation zones. Where lineaments display a strong curvilinear arrangement, regional scale folds were defined.

Magnetic and type-1 lineaments relations show that: type-1 lineaments represent inter structural organization of lithologic units; while magnetic lineaments represent regional magnetic overprint that were originated mainly during the last deformational episodes is western Sul-riograndense Shield. This explains why some magnetic lineaments truncated Type-1 lineaments.

Semi-detail scale

In this investigation stage, a structural survey in target areas was proceeded. In the structural survey, geometric and cinematic features of deformational structures were characterized. Processing of structural data allowed cinematic analysis of the region, with the determination of paleotstress ellipsoids. On a general way, paleotstress directions show two main orientations in the western part of Sul-riograndense Shield. First orientation shows a NNW-SSE compression axis direction (σ_1); second orientation shows a WNW-ENE σ_1 direction (Figure 3b). Paleostress fields figure 3b display a poor variation in axes orientation, due to heterogeneities in rock and structures composition.

Conclusions

The cinematic analysis shows that last deformational episodes in Western Sul-riograndense Shield (Brazil) was characterized by two main deformational orientations (NNW-SSE and WNW-ESE compression). NNW-SSE compressional direction is responsible for the main actual distribution of structures, such as regional fault zones and post-tectonic granitic intrusions. However, WNW-ESE compressional direction plays an unclear role in the deformational history of Sul-riograndense Shield; in some places, it seems to be related to local structures, formed as consequence of stress-strain partitioning. Sinistral fault zones display NE-SW and NNE-SSW orientation and were named as Irapuá Duplex System (Roldão, 2000). Regional NW-SE dextral fault zone is mainly Ibaré Lineaments (located in NW part of area). Both systems show crosscutting relations and have the some stress axes orientation, what suggest they make part of a conjugated system. The fault propagation in this conjugated system controls geometry and emplacement of post-tectonic ganitic intrusions in western Sul-riograndense Shield.

References

Almeida, F.F.M., Hasui, H., Brito Neves, R.A., and Funk, R.A., 1977, Províncias Estruturais Brasileiras: In: Simpósio de Geologia do Nordeste, 38, Campina Grande. *Atlas*..., SBG, p.363-391.

Chemale Jr., F., Hartmann, and Silva, L.C. da, 1995, Stratigraphy and tectonism of Brasiliano Cyclo in Southern Brazil: Communications of the Geological Survey of Namibia, 10, 151-166.

Jackson, V.N., Ramos, V.A., Terry, S.A., and Zuzek, A.B., 1973, Projeto aerogeofísico Camaquã, Estado do Rio Grande do Sul: Texas Instruments, DNPM/CPRM/CENEN, Porto Alegre, 208p. (Inedited)

Milligan, P.R., and Gunn, P.J., 1997, Enhancement and presentation of airborne geophysical data: AGSO Journal of Autralian Geology and Geophisics, 17(2): 77-82.

Roldão, D.G., 2000, Análise integrada de dados estruturais e geofísicos no controle de depósitos minerais na região oeste do Escudo Sul-riograndense (RS, Brasil): Dissertação de mestrado (PPGEM-EE-UFRGS), Porto Alegre, 133p

Silva Filho, B.C., 1991, Geology of the polyphase deformed precambrian terrain of the Vila Nova Region, state of Rio Grande do Sul, Southern Brazil. Part II: Structural sequence, Acta Geológica Leopoldensia, 14 (34):5-94.

Strieder, A.J., and Amaro, V.E., 1997, Structural patterns removed from remotely sensed lineaments: Revista da Escola de Engenharia – EGATEA, 25(4):109-117.

Acknowledgments

Authors would like to thank CPRM, FAPERGS (Proc. N° 96/0383-2), CNPq-PADCT (Proc. N° 132047/1998-5) and CNPq-PADCT (Proc. N° 62.0155/97-3 GTM/UFPR) for research grants. I am also grateful to the Geól[a]. Adriane Fischer for English revision and Prof. Francisco José Fonseca Ferreiras for the help in data processing.

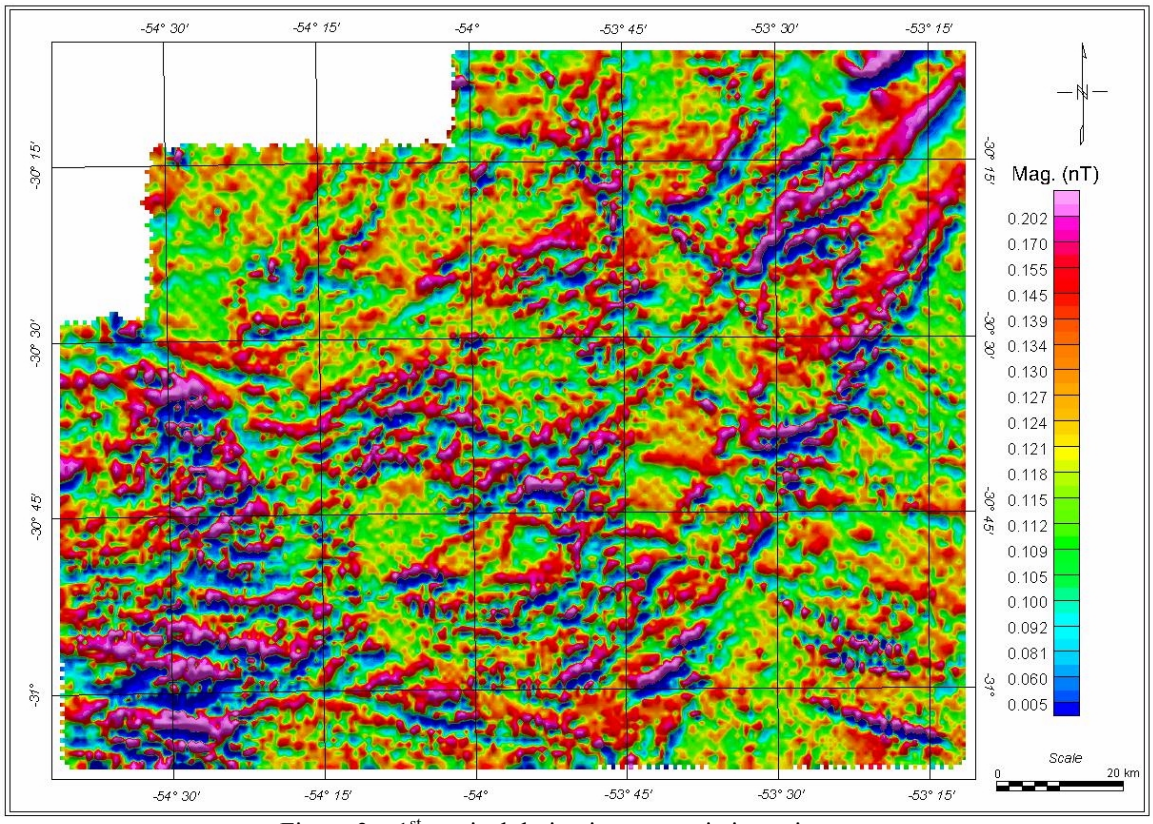

Figure 3 – 1st vertical derivative magnetic intensity map.

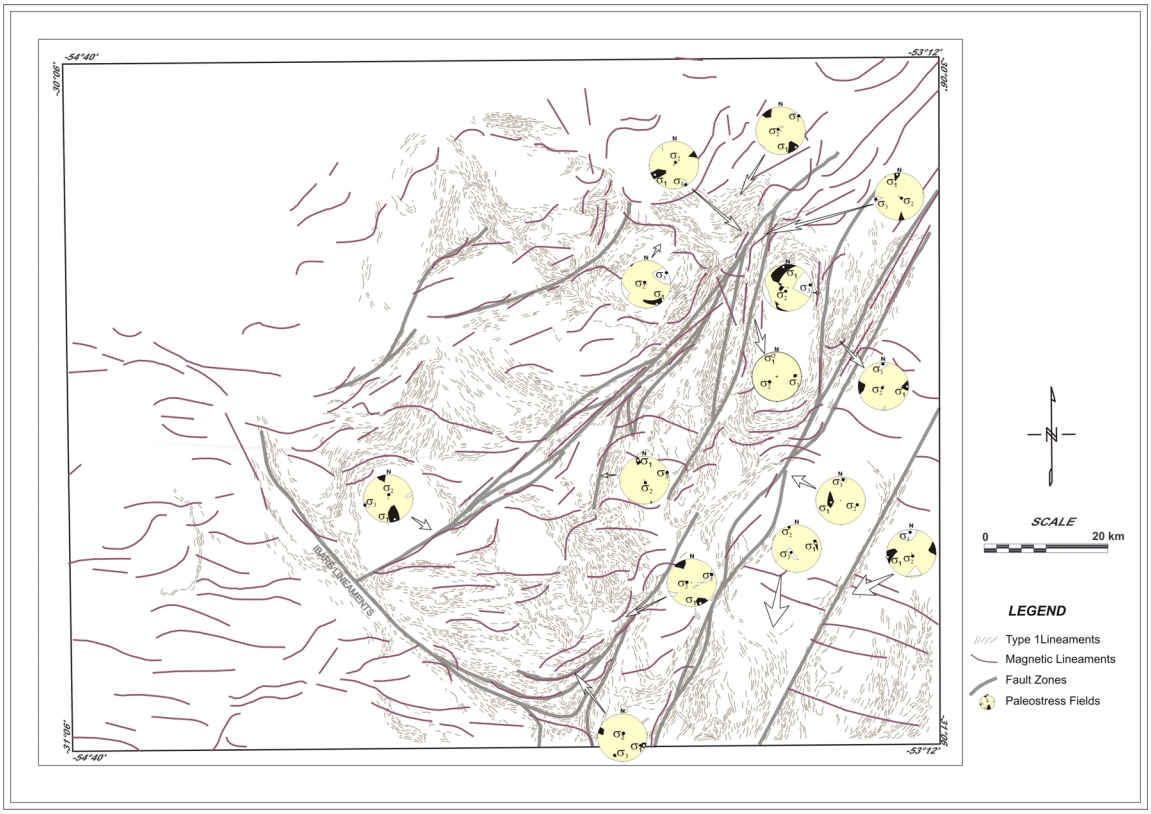

Figure 3 – Magnetic and Type-1 lineaments integrated map, with interpretative sketch.

Comparação entre Granitóides de parte da Serra do Mar no Estado do Paraná através da Aerogamaespectrometria

Carlos Vieira Portela Filho [1,2]; Francisco José Fonseca Ferreira [1]; Eduardo Salamuni [3]; Juliana Bahniuk [4]
[1] Laboratório de Pesquisas em Geofísica Aplicada, LPGA/UFPR; [2] Curso de Pós-Graduação em Geologia, UFPR; [3] Departamento de Geologia, UFPR; [4] Curso de Graduação em Geologia- UFPR, Bolsista PIBIC/CNPq

Abstract

This paper make use of gamma-ray spectometric data to compare two geological unities with granitoid composition from Serra do Mar Suite and Paranaguá Domain, southeast of Paraná state. This rocks presents different evolution during late Proterozoic. The obtained results shows that the images of eTh, K and eTh/eU ratio and the parameter F=K*eTh/eU, correspond to gechemical indicator of magmatic differentiation, alcalinity and a avaliation of the radionuclides mobility on the terrain, which permit show the differences between the mentioned rocks.

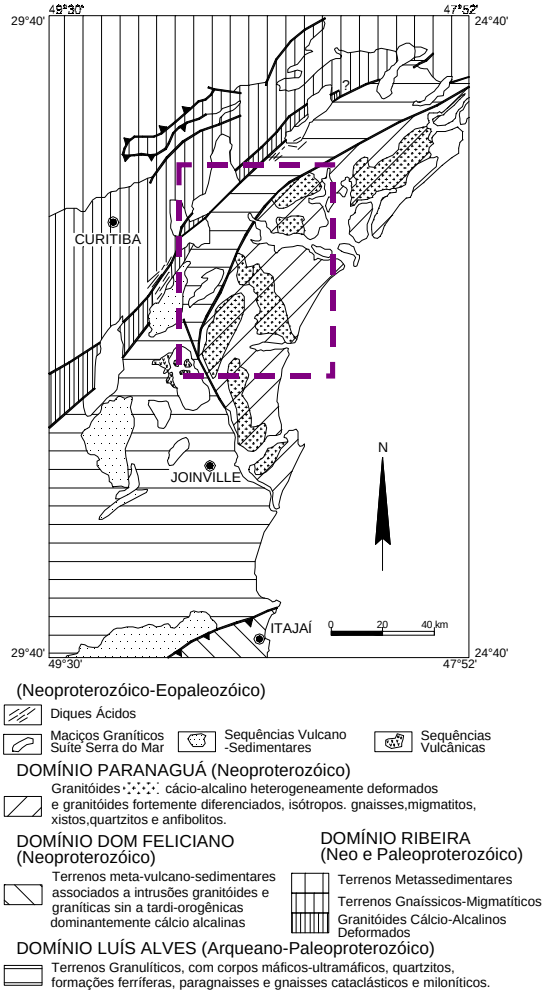

Figura 1 – Compartimentação tectônica do sudeste do Paraná e nordeste de Santa Catarina (mod. de Kaul, 1997) indicando a área estudada.

Introdução

A área estudada localiza-se à sudeste do primeiro planalto paranaense, entre as coordenadas geográficas 26º00' - 25º15' W e 49º 00' - 48º30' S, a qual corresponde às regiões da Serra do Mar e da planície costeira em quase toda sua extensão no estado do Paraná.

Neste trabalho serão abordados os granitóides do Maciço Granítico Suíte Serra do Mar e do Domínio Tectônico Paranaguá (Siga Jr., 1995), gerados durante o Proterozóico Superior, devido a eventos pós-colisionais ocorridos no final da consolidação do Gondwana (Kaul, 1997). Utilizando dados do Projeto Aerogeofísico Serra do Mar Sul (BARMP, 1997), foram gerados mapas de contorno de K e eTh, além de razões eTh/eU e do parâmetro F (F=K*eU/eTh). O objetivo desta pesquisa é comparar os mencionados granitóides, com base nas suas assinaturas gamaespectrométricas.

Contexto Geológico

Os granitóides do Maciço Granítico Suíte Serra do Mar, estão localizados sobre o cráton Luís Alves e em parte no Cinturão Ribeira. São representados na área pelos granitos Graciosa, Anhangava, Marumbi, Serra da Igreja e Morro Redondo (figuras 1 e 2). Esses granitóides representam a transição de um magmatismo cálcio-alcalino (tardi-orogênico) à alcalino (anorogênico, tipo A), de acordo com Kaul & Cordani (2000).

Os granitóides do Domínio Paranaguá constituem corpos alongados que balizam o contato oeste deste domínio com os gnaisses granulíticos do Domínio Luís Alves. Na área esses granitóides foram diferenciados por Lopes (1987), que identificou cinco variedades graníticas denominadas de Morro Inglês, Rio Canasvieiras, Cubatãozinho, Rio do Poço e Estrela (figuras 1 e 2), os quais apresentam afinidades com as séries cálcio-alcalina de alto K (Siga Jr., 1995). Este autor determinou que o intervalo de idades K-Ar, para os maciços graníticos da Suíte Serra do Mar, é de 585-520Ma, enquanto para os granitóides do Domínio Paranaguá é de 560-480Ma.

Comparação entre Granitóides por Aerogamaespectrometria

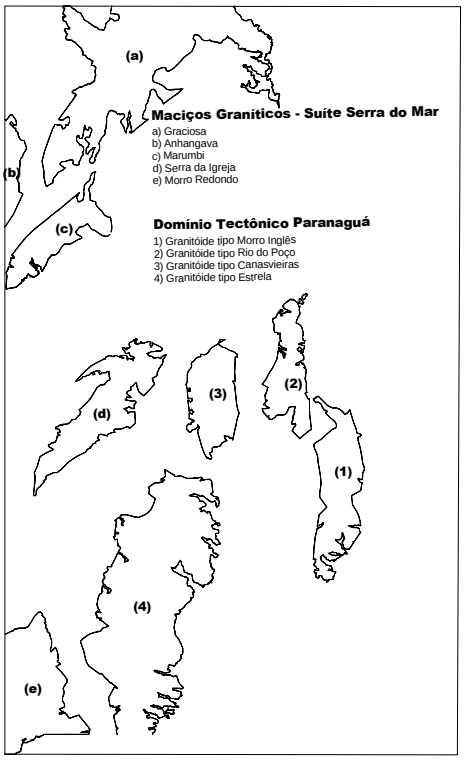

Figura 2 – Localiação dos granitóides da área de estudo.

Métodos

O método adotado consistiu da análise crítica das variáveis gamaespectrométricas (K, eTh, eU) contidas no banco de dados do Projeto Aerogeofísico Serra do Mar Sul (CPRM, 1978), cujos dados originais em contagens por segundo (cps) foram recentemente transformados em % e ppm, respectivamente, pelo *Brazil Airborne Radiometric Mapping Project* (BARMP, 1997). A partir daí foram geradas as razões Th/U, U/K, Th/K e o parâmetro F = K*U/Th (Gnojek & Prichystal, 1985). O aerolevantamento foi realizado a uma altura média sobre o terreno de 120m, espaçamento em torno de 1.000m entre as linhas de vôo e um interevalo de amostragem de 56m ao longo delas. O processamento dos dados para a geração de malhas regulares de 500x500m, foi realizado no pacote *Geosoftä (4.3),* através do método da mínima curvatura. Em seguida todas as malhas foram exportadas para o pacote *ER Mapperä* (*6.1*), onde foram transformadas em imagens e sobrepostas a um modelo digital de terreno (MDT), construído a partir da digitalização de curvas de nível e pontos cotados das cartas plani-altimétricas, e aos contatos geológicos dos principais maciços granitóides da área estudada. De posse destes produtos, a comparação entre os maciços foi norteada por indicadores litogeoquímicos, como alcalinidade e diferenciação magmática, e também pela migração dos radionuclídeos na paisagem considerando a evolução pedogenética/geomorfológica da área.

Diferenciação Magmática

Em função das rochas ígneas concentrarem Th e U na medida que se diferenciam do manto, as relações do tipo eTh/eU podem medir o grau de diferenciação magmática. Desta maneira quando esta relação se aproxima da igualdade, o grau de diferenciação magmática é maior.

O mapa da razão eTh/eU (Figura 3), mostra que os granitóides do Domínio Paranaguá, apresentam uma razão mais próxima da igualdade do que as rochas da Suíte Serra do Mar, sugerindo uma maior diferenciação no Domínio Paranaguá.

Esta interpretação parece coerente, quando comparada com a informação cronológica dessas rochas. Segundo Siga Jr. (1995), enquanto os Maciços Graníticos da Suíte Serra do Mar encontravam-se relativamente frios, as rochas do Domínio Paranaguá permaneciam em isotermas superiores a 300^{o}C, significando uma maior diferenciação magmática deste último domínio.

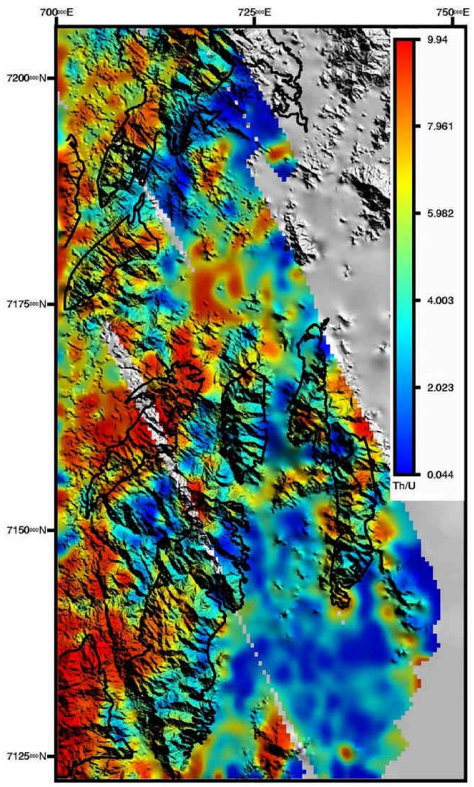

Figura 3 – Mapa da Razão Th/U

Alcalinidade

Lipski & Vasconcellos (1998) comparam dados de análises geoquímicas do granito Anhangava com dados gamaespectrométricos. Estes autores observaram uma relação de incremento do tório com as fácies mais alcalinas do granito. Quimicamente, o tório possui afinidade com as associações minerais de rochas alcalinas, a exemplo dos carbonatitos.

Dessa maneira o mapa de anomalias do tório (Figura 4), sugere um aumento da alcalinidade em direção aos granitóides da Suíte Serra do Mar. No Domínio Paranaguá também observa-se anomalias internas, que podem ser um indicativo da complexidade faciológica desses corpos.

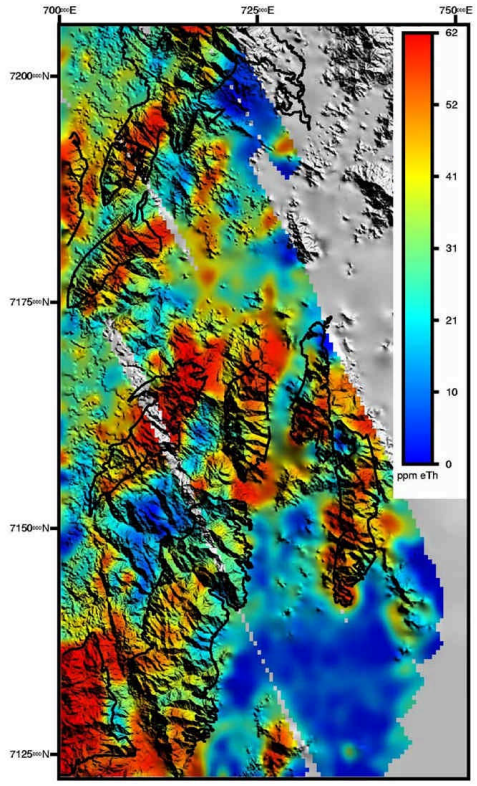

Figura 4 – Mapa de Anomalias do Tório

Da mesma forma que a diferenciação magmática, a interpretação da alcalinidade é fortalecida com dados geoquímicos. Neste caso, Siga Jr. (1995), determinou para o granitóide tipo Rio do Poço uma tendência mais alcalina.

Considerando que as rochas do Domínio Paranaguá são mais diferenciadas, conseqüentemente são menos alcalinas devido ao enriquecimento em sílica.

Mobilidade dos Radionuclídeos na Paisagem

Para avaliar o grau de mobilidade dos radionuclídeos solúveis (principalmente K e U), oriundos dessas rochas, foram gerados os mapas do potássio e do parâmetro F (figuras 5 e 6).

A análise do relevo mostrou que as duas principais unidades granitóides distribuem-se numa mesma superfície de aplainamento, o que teoricamente representaria uma mobilidade semelhante para os radionuclídeos. No entanto, uma avaliação mais acurada mostrou que os granitóides da Suíte Serra do Mar apresentam-se mais dissecados, onde as anomalias a eles relacionadas encontram-se também próximas dos limites desses corpos, concentrando-se nas zonas de colúvio dispostas ao sopé das serras, denotando mobilidade dos radioelementos (vide maciços Marumbi e Graciosa, Figuras 5). Em contraste, o Domínio Paranaguá apresenta-se menos dissecado, com as anomalias de K e do parâmetro F circunscritas aos maciços, portanto com uma mobilidade menor, a exemplo do granitóide tipo Cubatãozinho (figuras 5 e 6).

Analisando o problema do ponto de vista geológico, pode-se supor um vetor de origem neotectônica, dado pela reativação de falhas antigas no contato do Domínio Paranaguá com o cráton Luis Alves. Evidências de reativação de falhas nesta região também foram observadas em campo (Portela Fº., 2000).

Com relação ao comportamento das anomalias do parâmetro F, observa-se que normalmente elas estão localizadas nas áreas de maior declividade (zonas de colúvio) e junto à alinhamentos estruturais de direção NE e NW.

Discussão

A gamaespectrometria, associada à informações geológicas e geoquímicas, demonstrou ser uma importante ferramenta na caracterização dos granitos desta área, assim como na distribuição espacial dos radionuclídeos.

As relações entre os dados geológicos, geoquímicos e geofísicos podem ser aplicadas em outras áreas, devendo-se levar em conta as características das escalas lcal e regional.

Recomenda-se testar as relações de alcalinidade e de diferenciação magmática, para uma série de amostras de granitos de diferentes quimismos e idades, afim de comprovar a eficiência do método.

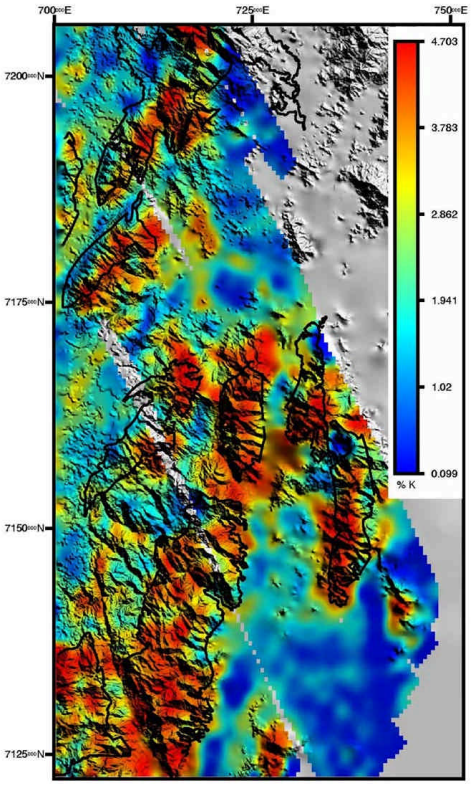

Figura 5 – Mapa de Anomalias do Potássio

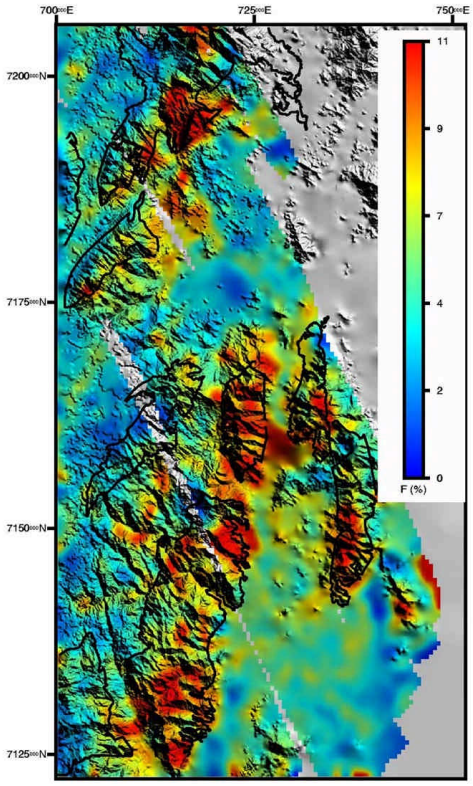

Figura 6 – Mapa do Parâmetro F (F=K*U/Th)

Agradecimentos

Os autores agradecem às colegas Josiane A. Silva e Silvana B. Riffel pelos seus incentivos, e à professora Eleonora M. G. Vasconcellos (UFPR) pelas discussões durante o andamento do trabalho e ao Projeto Geofísica Aplicada CNPq/PADCT, contrato no. 62.0155/97-3, pelo apoio para a realização da pesquisa.

Referências

BARMP 1997. Brazil Airbone Radiometric Mapping Project. Technical Report and Survey Atlas. A collaboration between PGW-CPRM, RJ.

Ferreira, F.J.F. & SOUZA, J.L de,. 2000. Gamaespectrometria: Fundamentos, Geoquímica e Distribuição dos Radioelementos em Rochas e Solos. Curso de Graduação em Geologia, Disciplina Geofísica Aplicada, 65p. (apostila)

Kaul, P.F.T. 1997. O magmatismo na Serra do Mar e Adjacências (Sul do Brasil) no final do Neoproterozóico e seus condicionantes tectônicos. Inst. de Geociências, Universidade de São Paulo, São Paulo, Tese de Doutorado, 293p.

Kaul, P.F.T. & Cordani, U.G. 2000. Geochemistry of the Serra do Mar Granitoid Magmatism and Tectonics Implications, Southern Brazil In: Revista Brasileira de Geociências. v. 30 número 1; p.115-119

Lipski, M. & Vasconcellos, E.M.G. 1998. Caracterização de fácies do granito Anhangava (PR) utilizando dados aerogamaespectrométricos. In: XL Congresso Brasileiro de Geologia, Belo Horizonte, SBG-MG, Anais, p. 383

Lopes, O.F., 1987a; Zoneamento Metamórfico da Formação Rio das Cobras do Pré-Cambriano do Estado do Paraná. In: III Simpósio Sul-Brasileiro de Geologia, Curitiba. Atas. Curitiba, SBG, v.1, p. 303-312.

Portela Fº, C.V., 2000. Análise da Tectônica Rúptil e Paleotensões em rochas do embasamento da Bacia de Curitiba e porções adjacentes da Serra do Mar (II): continuidade dos estudos estruturais. *In*: Anais do VIII Evento de Iniciação Científica, Curitiba.

Siga JR, O. (1995) Domínios Tectônicos do Sudeste do Paraná e Nordeste de Santa Catarina: Geocronologia e Evolução Crustal. São Paulo, 212 p. (Tese de Doutorado Apresentado ao Instituto de Geociências da Universidade de São Paulo).

Deformación del Mioceno en la Región del Sur–Este de México

Ronquillo Jarillo, Gerardo [1], Valencia Islas, Juan [2] ,
Lozada Zumaeta, Manuel [3]
Instituto Mexicano del Petróleo [1,2,3]
FIES D-791
Programa de Yacimientos Carbonatados naturalmente Fracturados.
Eje Central Norte Lázaro Cárdenas 152
07730 México, D.F

Resumen

El estudio consistió en delimitar estructuras en la litosfera del Sur - este de México, con base en la interpretación de las cartas de anomalías gravimétricas, la de interfaz corteza manto, la de los gradientes horizontales y la de distribución de la sísmicidad y mecanismos focales para hacer una comparación con estructuras reconocidas en superficie.

Con estos estudios se deduce que algunas estructuras superficiales que afectan a las cuencas del Sur - este se profundizan y están ligadas con la deformación de estas cuencas sedimentarias Terciarias.

Se propone un modelo de deformación donde hay una ruptura de la placa continental y la de Cocos afines del Oligoceno provocando la deformación de las cuencas terciarias y el volcanismo de los Tuxtlas. Esta interpretación complementaría ayuda al entendimiento de los modelos de evolución global propuesta por varios autores para la evolución del SE de México.

Introducción

El área de estudio se localiza entre los meridianos 92° 00'- 98° 00' de longitud Oeste y los paralelos 14° 00' y 20° 00' de latitud Norte Figura .1

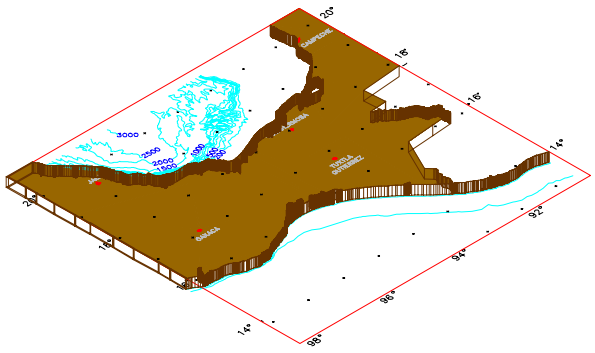

Fig. 1. Localización del área de estudio del Sur – este de México.

Existe una gran polémica sobre las causas de la deformación en el Mioceno del Sureste de México. Recientemente, los avances en los estudios de geología superficial, sísmicidad, anomalías magnéticas y gravimétricas, perfiles sísmico profundos de refracción y análisis geoquímicos de elementos mayores y trazas en rocas volcánicas, han establecido una variedad de modelos de la deformación de las rocas sedimentarias y de la profundidad, estructura y evolución de la litosfera.

Carfantan en 1986 hace una síntesis de la mayoría de los trabajos realizados hasta esta fecha; además propone una evolución tectónica desde el Paleozoico hasta el Terciario, observando una fase extensiva Triásica- Jurásica, un evento compresivo al final del Senoniense responsable del levantamiento de la Sierra de Chiapas, para el fin del Cretácico y principios del Paleogeno interpreta una fase transpresiva asociada al movimiento de la falla Motagua - Polochic. Posteriormente Delgado y Carballido 1990 proponen un cambio de orientación del sistema Polochic, respecto a los lineamientos del área del Istmo de Tehuantepec, ocasionando el desarrollo de una Cuenca Marginal entre Puerto Angel - Macuspana.

Castro ,R, (1980). Propone un modelo de la corteza terrestre para el sur de México, empleando sismos profundos. Singh y Montera en (1991) hacen una reconstrucción de la subducción de la placa de Cocos comenzando hace 20 M.A y al oeste de Chiapas, el más prominente desarrollo tectónico de la cordillera de Tehuantepepec , la cual actua como una zona de transición en la morfologia de la Trinchera de Centro América.

En recientes trabajos de Cecilio J. Rebollar etal 1999) ,definieron la geometría de la zobna Wadati - Benioff bajo Chiapas , así como la distribución de los esfuerzos principales en la placa subducida. La placa de Cocos buza aproximadamente 25° en Oaxaca , 30° bajo el Golfo de Tehuantepec y 40° hacia el sudeste.

Lineamientos Regionales

Principalmente se analizaran dos lineamientos en superficie que fueron interpretados con imágenes de satélite, mapas geológicos y mormogeologicos ; que por métodos geofísicos se observó que tienen una continuidad hasta el manto. El primer lineamiento denominado en la figura 2. como A-A', que corresponde en superficie al frente de la Sierra de Zongólica y Juárez, limita la planicie costera del golfo en las regiones de Veracruz y Oaxaca; nombrado por AMOCO-PEMEX-IMP (1994) como Falla Novillero Víbora Chachalacas y tiene una orientación NW SE.

El otro N-S que va de la región de los Tuxtlas al golfo de Tehuantepec, se marca como B-B' y correspondería a la falla del Istmo (Meneses 1980). Por ultimo el lineamiento C- C' Sierra de Chiapas.

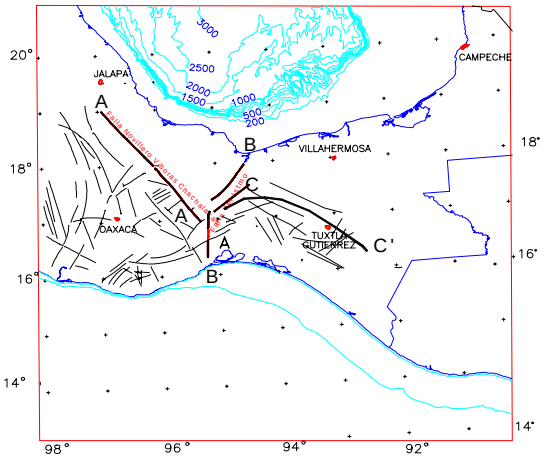

Fig. 2. Mapa simplificado de lineamientos del sur este de México.

Análisis de la Litosfera del Sur este de México

Los trabajos Singh y Moret (1991) de la configurción de la profundidad de la placa muestran que hace 20 Ma. cerca de la trinchera, la placa alcanzaba 27 km. de profundidad mientras que en el borde continental ésta llegaba a los 30 Km. Para la parte central de Oaxaca se profundiza a 40 Km. Para la configuración de la placa en la región del Istmo y hacia el Golfo estos autores han calculado profundidades entre los 80 y 200 Km en forma lateral.

Spranger (1994) con los estudios de refracción profunda propone un modelo de perfil sísmico de la corteza integrado con la anomalía de Bouguer, de Puerto Escondido a Alvarado, con un ángulo de subducción de 12° a 14° y profundidades cerca de la trinchera de 17 Km. En la región de Alvarado Veracruz esta zona alcanza hasta los 100 Km.

Ronquillo *et. al.* (1996) calculan la profundidad del contacto corteza - manto y sus gradientes horizontales usando el modelo de compensación de Airy Heiskanen´s (Jachens 1989) en la cual considera una densidad constante de la corteza de 2.67 gr/cm^3 , densidad del manto de 3.27 gr/cm^3. Para estos cálculos se empleó el mapa topográfico de la National Geographic Center con una relación de muestreo de 4 Km. Posteriormente determinan el efecto isostático en tercera dimensión en el dominio de la frecuencia con el algoritmo Parker´s (1973) usando el paquete interactivo de interpretación del sistema de análisis LCT.

La configuración resultante Figura 3a. muestra que el borde continental de este contacto alcanza las profundidades de 30 Km. y progresivamente en la parte central de Oaxaca llega hasta valores de 40 Km. En la planicie disminuye a 31 Km. Se deduce que hay un gradiente principal que corresponde al lineamiento B-B' (falla de Istmo) con profundidades promedio de 31 Km que marca una perturbación a nivel del manto.
El lineamiento A-A' es el límite occidental de la planicie costera y coincide con el gradiente horizontal de 31 Km de profundidad Figura 3b. También se interpretan gradientes horizontales de importancia que serían los limites entre la Sierra de Chiapas con las Cuencas del Sureste.

a

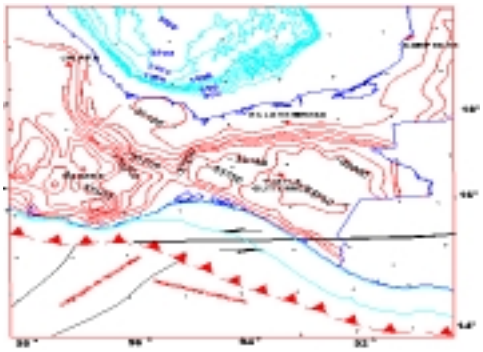

b

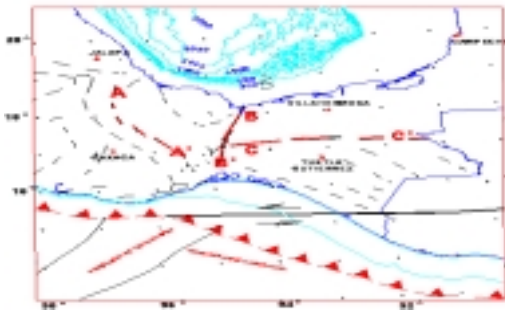

Fig.3. a. Profundidad de la interfaz corteza manto. b. Gradientes Horizontales de la interfaz corteza manto.

Sísmicidad

Al analizar el mapa de sísmicidad del Servicio Sismológico Nacional hasta 1996 se observo que algunos los focos sísmicos coinciden con algunos de los lineamientos superficiales principales AA´ ,B B´ y CC´ propuestos en el análisis de la geología superficial, por lo que se confirma que estos corresponden a accidentes que se profundizan y están relacionados con el movimiento de las placas.

Por lo tanto, en el lineamento B B´, que es de interés, se tiene sismos con magnitudes del orden de 4.2 a 7.4 , sin embargo los mas representativos son los de magnitud de 4.2 a 5.4, con profundidades que oscilan de 0 a 300 km.

Lo referente al análisis de los mecanismos focales Los autores de (Cecilio J. Rebollar et al.1999 concluyen que se tiene un cambio fuerte en el buzamiento de la placa de Cocos en la intersección de la cordillera de Tehuantepec y la Trinchera de Centro América. La sísmicidad en esta zona es difusa hasta profundidades de 200 km. Deduciendo un incremento gradual del buzamiento de la placa de Cocos de Oaxaca a Chiapas .

Interpretación de la Tectónica Profunda

Tomando en cuenta todos los análisis geológicos, geoquímicos, sísmicos y modelos geofísicos realizados en presente trabajo, así como los modelos evolución geológica propuestos en la apertura del Golfo de México por Coney (1983) ,Padilla y Sanchez (1986) Guzman Speziale (1989) se observan las siguientes relaciones.

Durante el Triásico y Jurásico Tardio, el bloque Yucatán migra del Norte hacia el Sur a través del lineamiento A-A' descrito en este estudio y reconocido por Pindel (1985). Esta falla de movimiento lateral derecho y que se extiende hasta el basamento explicaría para el Terciario la diferencia que hay entre el volcanismo del Eje neovolcánico y el volcanismo alcalino interpretado en la costa del Golfo de México.

El movimiento colocaría al bloque Yucatán en el Sur de México a través del lineamiento que nosotros hemos denominado B-B' o falla del Istmo, este fenómeno integra a la placa continental en una serie de bloques que sus limites suturan para formar una gran placa.

Mientras sucedía este fenómeno en la región pacifica se tenía la actividad magmática representada por un arco volcánico, producto de la subducción de la placa de Kula en el límite de Guerrero y del desplazamiento lateral del bloque Chortis .

A principios del Cretácico el bloque de Honduras y Nicaragua fue integrado al Sur de México. Posteriormente a este fenómeno el área se fue estable tectónicamente que vino a constituir como una porción de la placa continental de norte América.

Durante el Cretácico tardío y principios del Terciario temprano existen algunas referencias de movimientos tectónicos en el área de estudio, hacia la parte norte y central de México se desarrollaba la orogenia laramide; que para Coney (1981) fue el resultado de la acreción de los arcos volcánicos que se localizaban en el occidente de México.

Mientras esto ocurría en el sur de México el movimiento del sistema de Fallas Motagua Polochic daba fenómenos de Transpresión.

Por lo que se propone un modelo para Mioceno figura 4, donde la Subducción diferencial de la placa de Cocos provoca un movimiento lateral izquierdo en la falla del Istmo (lineamiento B-B'); y esta Subducción diferencial da origen a una fusión de la placa dando lugar al emplazamiento del Vulcanismo de los Tuxtlas.

Además del movimiento lateral en la región de la falla del Istmo de Tehuantepec y la subducción da un vector de fuerza de tipo compresivo con dirección NE-SW que deforma los sedimentos de las cuencas Terciarias. Bajo este esquema la falla del Istmo sería un límite de placas formada por una sutura originada en el Jurásico debida al emplazamiento del bloque Yucatán.

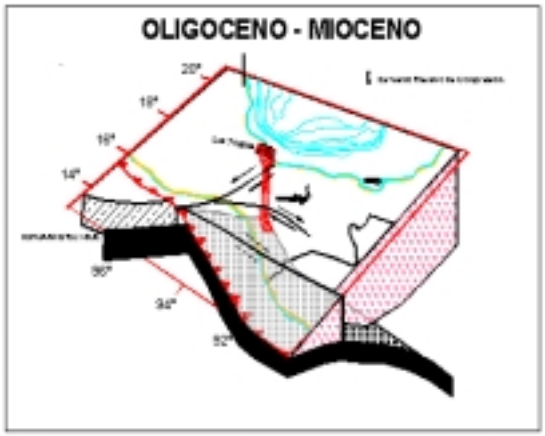

Fig.4. Modelo de deformación del Sur este de México para el Mioceno.

Conclusiones

Con estos estudios se deduce que las estructuras que se interpretan en superficie se profundizan y afectan a la interfaz corteza manto. Tomando en cuenta los modelos de evolución global propuesta por varios autores para la apertura del golfo de México se puede concluir que la deformación Tectónica esta ligada a la evolución de un límite de placas que se reconoció en este sector del país. Por lo tanto, el modelo de deformación propuesto, donde se tiene una ruptura de la placa continental y la de Cocos afínales del Oligo-

ceno provocando la deformación de las cuencas terciarias y el volcanismo de los Tuxtlas. Esta interpretación complementaría ayuda al entendimiento de los modelos de evolución global propuesta por varios autores para la evolución del SE de México.

Referencias

Carfatan ,J.Ch. 1986. Du Systeme Cordillerain Nord-Americain au domaine Caraibe- Etude geologique du Mexique meridional. Universitde Savoie, Departement des Sciencies de la Terre, Band 1 u.2.558 S.

Castro – Escamilla ,R., 1980. Un modelo de la corteza terrestre para el sur de Méxco mediante el uso de sismos profunds . Tesis de Licenciatura, ,Facultad de Ingeniería,UNAM.

Delgado - Argote, L.A., y Carballido-Sánchez, E,A., 1990. Análisis tectónico del Sistema Transpresivo Neogénico entre Macuspana, Tabasco, y Puerto 4-Ángel, Oaxaca,México. Rev. Inst. Geología,UNAM, v.9, No1, pp. 21-32

Cecilio j. Rebollar, Victor H. Espíndla, Antonio Uribe , Antono Mendoza and Arturo Pérez-Vertti , 1999,vol.38,num.2, pp. 95-106

Coney, P. J., 1983. UN modelo tectonico de México y sus relaciones con América del Norte, América del Sur y el Caribe; Revista del Instituto Mexicano del Petróleo. V.15(1), p.6-15

Coney, P.J. 1981. Accretionary Tectonics in Western North America, in W.R Dickinson and W.d Payne eds. Relations of Tectonics to Ore Depositsin the Southern Cordillera Arizona , Geol. Soc. Digest. Vol.14,pp23-37

Guzmán –Speziale, M., W. D. Pennington and T. Matumoto,1989. 1989. The triple junction of the North America, Cocos , and Caribbean plates.Seism. Tect., 8, 981 – 997.

Jachens, R. C., and R. W, Simpson., 1989. Isostatic residual gravity and crustal geology of the United States Pakiser, L. C y W. O., Geophysical Framework of the continental United States. Geological Society of America Memoir 172., 405-424 pp.

Jacobo Albarrán J., 1997 *Studio geologico e petrologico del complesso vulcanico di los Tuxtlas, stato di Veracruz, Messico.* Tesis de Doctorado Universita degli Studi di Pisa.

Parker R, 1973. The rapid calculation of potencial anomalies. Geophysics. J. Roy Astr.Soc.31, pp447-455.

Pindell (1985).Alleghenian reconstruction and subsequente evolution of the Gulf of Mexico, Bahamas and Proto – Caribbean : Tectonics V. 4 p 1-39.

Ronquillo, J. G., López G. G., Lozada Z. M., y Valencia Islas J. 1996. Gradientes Horizontales Correlacionados con la Tectónica y Evolución de Cuencas. Asociación Mexicana de Geofísicos de Exploración , A:C., Memorias del VII Simposio de Geofísica y Exposición .Veracruz, México, p259-266.

R. J. Padilla., Sánchez., 1986. Post-Paleozoic Tectonics of Northeast Mexico and its role in the evolution of the Gulf of Mexico, Geof. Int. Vol. 25-1, 157-206 pp.

Singh, S.*K and F.Mortera,,1991. Source time funtionsof large Mexican Subduction earthquakes,morphology of the Benioff zone, age of the olate, and their tectotonic implications. J. Geophys. Res. 96,487-502*

Spranger, M., 1994. Eine erste Geotraverse durch Sudmexiku. Auswerturg desrefraktionsseismishen Profils. Universitat zu kiel. Dissertation.

Estudos geofísicos no contexto geológico estrutural da Faixa Apiaí no sudoeste de São Paulo, Brasil.

M.J.T.Rosales; mario@iag.usp.br
W. Shukowsky, wladimir@iag.usp.br
M.S. M. Mantovani, marta@iag.usp.br
Instituto Astronômico e Geofísico-USP. Brasil

Abstract

A Faixa Apiaí (Sistema de Dobramentos Apiaí) ocupa a região centro-oeste e norte do Escudo Atlântico no Paraná ingressando no extremo SW deste escudo em São Paulo, sendo constituída por complexas associações metasedimentares subordinadamente metavulcânicas, estruturadas como nappes com transporte tectônico para SW, afetadas por intrusões batolíticas de granitóides diversos (Batólitos Cunhaporanga, Três Córregos e Agudos Grandes) e de stocks graníticos, e localmente cobertas por depósitos molássicos (e. g., Formação Camarinha e Grupo Castro), sendo o conjunto seccionado por grandes falhas transcorrentes dextrais de direções próximas a NE–SW, destacando-se o Lineamento Lancinha.

O presente trabalho trata sobre a aplicação do método gravimétrico visando complementar o mapeamento geológico existente da porção sudeste do Cinturão Ribeira, definida por Faixa Apiaí, e nesta direção tentar integrar os resultados da interpretação dos dados gravimétricos num contexto geológico-tectónico-estrutural com o intuito de obter uma visão detalhada e esclarecedora da estruturação geológica profunda da região, compreendida aproximadamente entre as latitudes 23º 30' S - 25º 30' S e as longitudes 50º 00 W - 47º 30' W.

Os resultados obtidos conforme a interpretação dos dados gravimétricos, permitiram correlacionar contatos ou falhas verificadas no campo com o comportamento da anomalia Bouguer, assim como revelar zonas de importantes descontinuidades crustais tais como o Lineamento Lancinha, a Falha Morretes e o Alinhamento Guapiara.

Introdução

O Cinturão Ribeira é a unidade tectônica exposta ao longo da faixa ENE-WSW da borda leste da bacia do Paraná, compreendendo o cinturão dobrado Apiaí, composto por rochas vulcano-sedimentares de médio e baixo grau, intrudido por granitos sin e pós-tectônicos do Ciclo Brasiliano e cavalga na direção SE sobre a microplaca de Curitiba (Hasui et al. 1975).

O Domínio Apiaí neste contexto é referido a porção sudeste do Cinturão Ribeira.
Os estudos gravimétricos realizados na região da Faixa Apiaí permitiram obter resultados proeminentes enquanto a busca de nexos de caráter geológico que permitam dar uma explicação geofísico-estrutural a todo um conjunto de lineamentos gravimétricos regionais orientados segundo duas direções preferenciais: uma primeira NE-SW concordante com a direção das principais estruturas geológicas regionais de idade Precambriana e uma segunda aproximadamente N45ºW que corta em sentido transversal o "trend" geológico regional da Faixa Apiaí e que de alguma maneira estes lineamentos posicionam-se paralelamente a os dois alinhamentos estruturais mais importantes conhecidos na região que são o Alinhamento de Guapiara e o Alinhamento de São Jerônimo-Curiúva, orientados ambos segundo NW (Ferreira et al. (1981).

Arcabouço Geológico-Tectônico Regional

O mapa geológico da Fig. 1, compreende a região de estudo localizada aproximadamente a 150 km ao sudoeste da cidade de São Paulo, delimitada pelas coordenadas 50º 00 W - 47º 30' W e 23º 30' S - 25º 30' S. Refere-se à porção sudeste do Cinturão Ribeira nomeada por Faixa Apiaí ou Sistema de Dobramentos Apiaí (Hasui et al., 1975).

A geologia da região é caracterizada por um conjunto de rochas supracrustais, de grau metamórfico fraco e médio, classicamente denominado de Grupo de Açunguí.
O embasamento dessas supracrustais é constituído por um conjunto de rochas gnáissico-migmatíticas, com alguns núcleos charnockíticos maiores, e intercalações variadas de metassedimentos. Ocorre principalmente a sul, e localizadamente em alguns núcleos antiformais em meio ao Grupo Açunguí.
Geologicamente a região encontra-se limitada na porção norte pelo Lineamento Taxaquara e ao sul próximo da cidade de Curitiba pela Falha Morretes.
O padrão estrutural regional é caracterizado por um grande número de intrusões granitóides múltiplas, de idades e características diversas, afetando tanto as

supracrustais como o embasamento gnáissico-migmatítico. Esse conjunto é afetado por um denso sistema anastomosado de zonas de cisalhamento transcorrentes de idade Precambriana, com caráter predominantemente dúctil e dúctil-rúptil.

De maior importância regional, tanto em extensão e continuidade, como na delimitação de blocos tectônicos, são o Lineamento da Lancinha- Itapeúna, que se junta ao Lineamento Ribeira para formar o Lineamento Cubatão, e os Lineamentos de Morro Agudo, Quarenta–Oitava e Figueira, que parecem ser ramos divergentes do Ribeira; e o Lineamento Itapirapuã, situado mais ao norte. Neste contexto a Falha Morretes localizada ao sul, próximo de Curitiba, apresenta fortes evidencias de ser uma importante descontinuidade crustal que separaria as rochas pertencentes ao Domínio Curitiba do Domínio Luís Alves (Siga Jr., 1995).

Anomalia Bouguer

O mapa de anomalia Bouguer para a região da Faixa Apiaí (Fig. 3) mostra-se ainda inconsistente do ponto de vista de complementar o mapeamento geológico existente da região em escala aproximada de 1:1.000000 (Mapa geológico da Fig. 1).

De maneira geral pode-se observar uma faixa de anomalias positivas Bouguer bordejando toda a costa sudeste em direção a cidade de São Paulo. Esta faixa anômala regional encontra-se limitada na região central da Sistema Apiaí pelo Lineamento Lancinha-Itapeuna–Cubatão.

Revela-se como um limite importante na região, um lineamento localizado ao nordeste da cidade de Curitiba, que estes autores interpretam como uma possível continuação da Falha Morretes (Siga Jr, 1995), em direção ao Estado de São Paulo.

Interpretação dos dados gravimétricos

A interpretação dos dados gravimétricos dos perfis C-C', F-F', G-G' e J-J', tem caráter qualitativo/semiquantitativo. Temos selecionado estes perfis por estar localizados nas áreas mais centrais da Faixa Apiaí, de maneira que cortam as principais unidades litoestratigráficas da região, no caso do perfil C-C' (Fig. 4), localiza-se próximo do perfil geológico ABCD interpretado por Campanha & Sadowski (1999) mostrado na Fig. 2.

Integração dos dados geofísicos e geológicos

Com o intuito de ter uma visão do comportamento do campo de anomalia Bouguer em toda a região da Faixa Apiaí, e tentar correlacionar com aquelas zonas de importantes descontinuidades crustais que separam as principais unidades litoestratigráficas definidas por Campanha & Sadowski. (1999), foi confeccionado um mapa geológico-geofísico da porção sudeste do Cinturão Ribeira (Fig. 5). Os elementos mais importantes a destacar são os seguintes:

- No extremo sudeste do mapa quase seguindo a direção da linha da costa observa-se um lineamento gravimétrico vindo dos domínios tectonicos-estratigráficos do nordeste de Santa Catarina definidos por Siga Jr., (1995); nessa região ao SW da cidade de Curitiba essas rochas foram agrupadas no Domínio Paranaguá, o qual segundo mostram as evidencias gravimétricas poderia ter continuidade em direção NE até o interior do Estado de São Paulo. Esse lineamento gravimétrico poderia associar-se a um considerável adelgaçamento crustal resultado da justaposição de Paranaguá, que deu origem a uma expressiva granitogênese de natureza alcalina-peralcalina.
- De ser confirmado a continuidade do Domínio Paranaguá em direção NE paralelo a linha da costa, parece ser que ele limita ao norte com o Lineamento Serra Negra, o qual constituiria o limite sul do Domínio Luís Alves de Siga Jr., (1995).
- Na parte norte do lineamento Lancinha aparece um outro lineamento gravimétrico de caráter regional localizado entre os lineamentos Itapirapuã e Ribeira, vindo da porção oeste da Faixa Apiaí, ao sul da cidade de Castro, observa-se que este lineamento gravimétrico estende-se em direção NE até entrar na Área I, nas proximidades da cidade de Apiaí, onde possivelmente uma ramificação do mesmo continua mais ao norte na direção da cidade de Nova Campina na Folha de Ribeirão Branco.
- Dois lineamentos gravimétricos importantes também são revelados na direção NW-SE, transversais ao "trend" regional das principais unidades da Faixa Apiaí: 1) Localizado ao NE da cidade de Curitiba e associado ao Alinhamento São Jerônimo-Curiúva, 2) Localizado ao SW da cidade de Iguape e associado ao Alinhamento de Guapiara.

Conclusões

Os estudos gravimétricos realizados na região da Faixa Apiaí permitiram estabelecer as seguintes considerações:

- A atual distribuição e densidade das estações de gravidade na região mostra-se de maneira geral inconsistente para a confecção de um mapa de anomalia Bouguer que complemente o mapeamento geológico existente (Escala 1:1.000000, Campanha & Sadowski., 1999).
- A interpretação dos perfis gravimétricos C-C', F-F', G-G' e J-J' (interpolados pontualmente), permitiu correlacionar contatos ou falhas verificadas no campo com o comportamento da anomalia Bouguer, assim como revelar zonas de importantes descontinuidades crustais tais como o Lineamento Lancinha, a Falha Morretes e o Alinhamento Guapiara.
- Segundo interpretação dos dados gravimétricos os domínios litoestratigráficos estabelecidos por Siga Jr (1995) no nordeste de Santa Catarina tais como os Domínios Luís Alves, Curitiba e Paranaguá poderiam ter continuidade na direção NE até o interior do Estado de São Paulo.
- Os lineamentos gravimétricos regionais orientados segundo NW-SE dispostos paralelamente aos Alinhamentos de Guapiara e São Jerônimo-Curiúva permitem inferir a origem profunda destas estruturas.

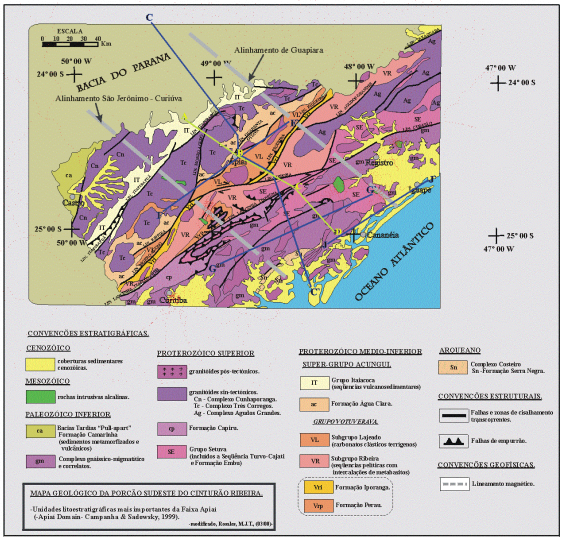

Fig. 1 Mapa geológico da porção sudeste do Cinturão Ribeira, mostrando a localização do Perfil geológico A-B-C-D, interpretado por Campanha & Sadowski (1999). Mostra-se a localização dos perfis gravimétricos que foram objeto de interpretação neste trabalho.

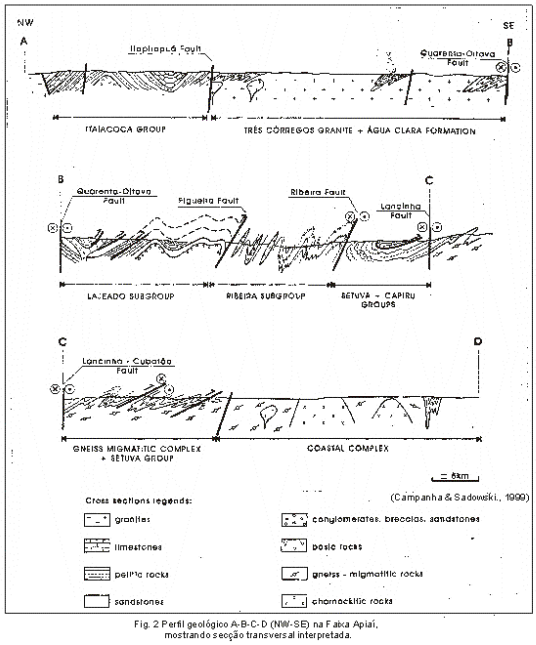

Fig. 2 Perfil geológico A-B-C-D (NW-SE) na Faixa Apiaí, mostrando seção transversal interpretada.

Referências

CAMPANHA, G. A. da C.; SADOWSKY, G. R. (1999). –Tectonics of the southern portion of the Ribeira Belt (Apiaí Domain). In: Precambrian Research N0: 98: 31-51. Elsevier Science B. V., (1999).

FERREIRA, F. J. P. et al. (1981). Constribuição ao estudo do alinhamento estrutural de Guapiara. In: SIMPOSIO REGIONAL DE GEOLOGIA, 3, Curitiba. Atas São Paulo, SBG, v.1, pp 226-240.

HASUI, Y.; CARNEIRO, C.D.R.; COIMBRA, A.M., (1975). The Ribeira Folded Belt. Revista Brasileira de Geociências, São Paulo, SBG 5 (4): 257-262.

SIGA Jr, O. (1995). Domínios Tectônicos do Sudeste do Paraná e Nordeste de Santa Catarina: Geocronologia e Evolução crustal. Tese de Doutoramento, Instituto de Geociências-USP., p.212, 1995.

Agradecimentos

Nossos agradecimentos pessoais ao CAPES pelo apoio financiero na execução dos trabalhos de campo gravimétricos e ao grupo de pesquisa GEOLIT do Departamento de Geofísica do IAG - USP.

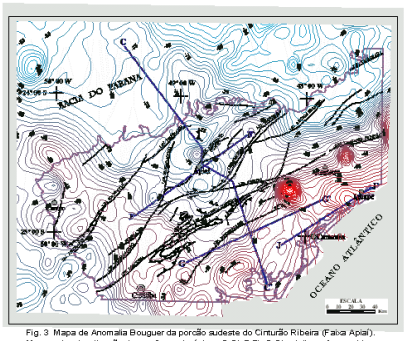

Fig. 3 Mapa de Anomalia Bouguer da porção sudeste do Cinturão Ribeira (Faixa Apiaí). Mostrando a localização dos perfis gravimétricos C-C', F-F', G-G' e J-J' que foram objeto de interpretação, e um arcabouço tectônico da Faixa Apiaí com as principais zonas de cisalhamento transcorrente de idade Precambriana.

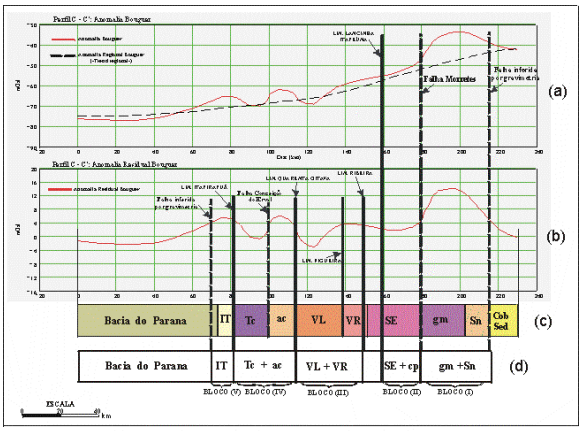

Fig. 4 Perfil gravimétrico C-C'. (a) Anomalia Bouguer, "Trend" regional; (b) Anomalia Residual Bouguer; (c) Unidades litoestratigráficas expostas na Faixa Apiaí; (d) Compartimentação em Blocos geofísicos- estruturais.

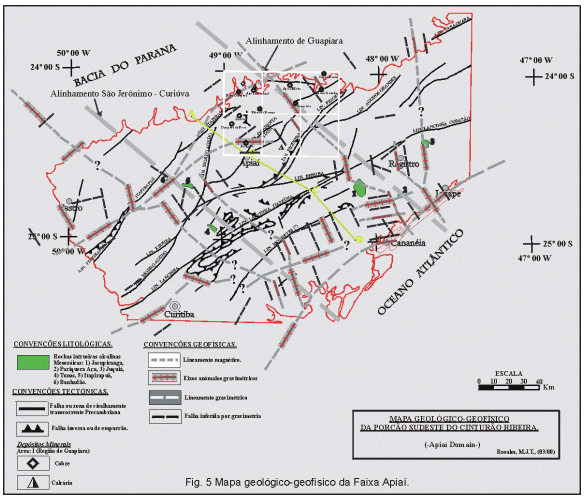

Fig. 5 Mapa geológico-geofísico da Faixa Apiaí.

Gamaespectrometria do Granito Serra do Carambeí – PR

Francisco José Fonseca Ferreira [(1)]; Silvana Bressan Riffel [(1,2)]; Maximilian Forlin [(1)]; Gilson Burigo Guimarães [(3)]
[(1)] Laboratório de Pesquisas em Geofísica Aplicada, LPGA/UFPR;[(2)] Curso de Graduação em Geologia-UFPR, Bolsista PIBIC/CNPq; [(3)] Universidade Estadual de Ponta Grossa, UEPG-PR

Abstract

The present study involves the ground gamma-ray spectrometric mapping of the uraniferous alkali granite Serra do Carambeí - PR (9,9 ppm U_3O_8) placed at the Carambeí, PR. It was observed a good correlation between the ground gamma-ray spectrometric data, obtained in the field, and the airborne gamma-ray spectrometric data of the Serra do Mar Sul project. The field observations corroborated, as well the uranium anomalies of the felsic dykes. Through thorium element grades, it was possible to delimitate the alkali granite Serra do Carambeí and distinguish it from the calcio-alkaline host rocks, Cunhaporanga Granitic Complex.

Introdução

O presente estudo envolve o mapeamento gamaespectrómetrico terrestre do granito uranífero Serra do Carambeí–PR (9,9 ppm de U_3O_8). Um dos objetivos do trabalho, além de identificar áreas radioanômalas enriquecidas em urânio, em correspondência com dados geológicos (Pinto-Coelho, 1986), foi comparar os dados obtidos com aqueles oriundos do Projeto Aerogeofísico Serra do Mar Sul (CPRM, 1978), recentemente transformados de contagens por segundo (cps) para % de K e ppm de eTh e eU pelo *Brazil Airborne Radiometric Mapping Project* (BARMP, 1997).

Geologia do Granito Serra do Carambeí

O Granito Serra do Carambeí-PR, situado no município homônimo, dista cerca de 140 km à noroeste de Curitiba e está compreendido entre as coordenadas 25º00' e 24º21' de latitude sul e 50º02' e 49º52' de longitude oeste. Posicionado no Pré-Cambriano Superior e relacionado às rochas granitóides intrusivas pós-tectônicas, está totalmente circunscrito pelo Complexo Granítico Cunhaporanga (sin a tardi-tectônico). Constitui um *stock* estruturalmente homogêneo e alongado, com direção N30E, ocupando uma área aproximada de 33 km^2 (Pinto-Coelho, 1986).

O mapa geológico de Pinto-Coelho (1986), mostra que os contatos do maciço com o Complexo Granítico Cunhaporanga e os diques máficos mesozóicos do Arco de Ponta Grossa são tectônicos, enquanto com a Formação Furnas são litológicos. A intrusão da Serra do Carambeí é classificada como um álcali-feldspato granito com um quimismo predominantemente alcalino em contraste com sua encaixante cálcio-alcalina. Uma das particularidades do corpo é a presença de diques félsicos (*elvans*) de pequenas espessuras (máximo de 25 cm), enriquecidos em urânio e dispostos nas porções nordeste e sudoeste (Pinto-Coelho, 1986).

Aquisição dos dados terrestres

A aquisição dos dados terrestres foi realizada através de um gamaespectrômetro de 512 canais (GS-512, fabricado pela Scintrex/Geofyzika). Foram levantados 138 pontos, espaçados entre 250 e 500 m, distribuídos ao longo de estradas, preferencialmente no *stock* granítico mas também nas suas encaixantes imediatas. O posicionamento das estações foi realizado por um *GPS* (Magellan Trailblazer XL), apoiado por fotografias aéreas de 1980, em escala 1:25.000, cedidas pela Minerais do Paraná S.A. (Mineropar).

As leituras gamaespectrométricas foram tomadas em contagens por segundo (cps) e automaticamente transformadas em concentrações de K em % e de eU e eTh em ppm, com base em procedimento de calibração realizado no Instituto de Radioproteção e Dosimetria – IRD, da Comissão Nacional de Energia Nuclear – CNEN. Diariamente obteve-se os teores do *background* atmosférico para posterior correção dos dados de campo. A medição da radiação cósmica foi realizada na represa dos Alagados, utilizando um barco de madeira sobre uma lâmina d'água com profundidade superior a 2 m. As medidas foram tomadas com tempo de integração de três minutos. Para maior representatividade das leituras, as medições foram repetidas três vezes, posteriormente tomando-se a média. Os valores observados situaram-se próximos de zero ou negativos, sendo aqui desconsiderados.

Dados aéreos utilizados

Os dados aerogeofísicos utilizados (K em %, e eTh e eU em ppm) são provenientes do *Brazil Airborne Radiometric Mapping Project* (BARMP, 1997), gentilmente cedidos à UFPR/LPGA pelo Serviço Geológico do Brasil (CPRM). Os dados originais foram coletados a uma altura média sobre o terreno de 120 m, segundo linhas de vôo orientadas na direção preferencial N30W e separadas de aproximadamente 1 km.

Gamaespectrometria do Granito Serra do Carambeí-PR

Processamento dos dados geofísicos e geográficos

Os dados geofísicos aéreos e terrestres foram processados no pacote *Geosoft OASIS Montaj* ^{TM} (*4.3*), interpolados pelo método da mínima curvatura e contornados a partir de células de 500 m. Para facilitar a comparação entre ambos os conjuntos de dados, delimitou-se uma mesma área e foram gerados mapas dos radioelementos K, eTh e eU. Os dados aéreos da contagem total foram transformados em dose (taxa de exposição em R/h) por BARMP (1997), enquanto para os terrestres utilizou-se a expressão recomendada por Barreto *et al*. (1986).

Para avaliar a eventual migração dos radionuclídeos na paisagem, foi gerado um modelo digital de elevação do terreno (MDE) a partir da digitalização em *Autocad* (*14*) das curvas de nível e dos pontos cotados oriundos das cartas planialtimétricas da área. Posteriormente, através do pacote *ER Mapper* (*6.1*), as imagens gamaespectrométricas ternárias foram sobrepostas ao relevo.

Resultados obtidos e discussão

Os mapas de contorno das figuras 1 a 3 representam os dados radiométricos aéreos, enquanto os das figuras 4 a 6 exibem os terrestres. Nas figuras 1, 2, 4 e 5 são também observados os diques "riolíticos", as anomalias cintilométricas e os limites do corpo, extraídos de Pinto-Coelho (1986). Já nas figuras 3 e 6 observa-se a distribuição espacial dos dados aéreos e terrestres, respectivamente. Nota-se, em geral, nestas ilustrações, que o corpo granítico é bem diferenciado de suas encaixantes imediatas, principalmente pelos elevados teores de eU e eTh, refletindo o contraste alcalino/cálcio-alcalino.

Observa-se, sobretudo nas figuras 1 e 4, que a porção mais elevada que sustenta a Serra do Carambeí é depletada em potássio como função dos processos pedogenéticos de lixiviação do K, em espessa cobertura de solos. Nestes e nos demais mapas, nota-se que as anomalias de K, eU e eTh são maiores nas extremidades NE e SW do corpo, refletindo tratos de exposição de blocos e lajes graníticas, além dos diques "riolíticos" e das anomalias cintilométricas anteriormente referidas.

Os mapas das figuras 1 a 6 mostram uma certa correlação entre os dados gamaespectrométricos aéreos e terrestres. Com o objetivo de quantificar esta comparação, foram procedidas as médias entre os teores das variáveis K, eTh,, eU dos respectivos bancos de dados, as quais são apresentadas na Gráfico 1.

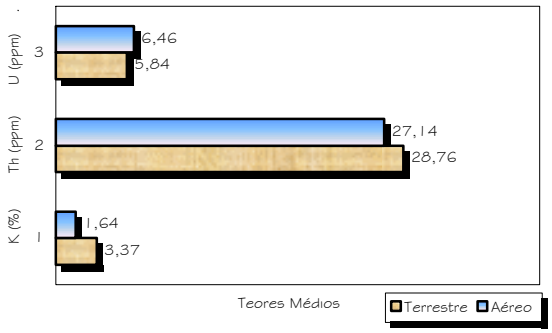

Gráfico 1 – Comparação entre as médias (K,eTh,eU).

Como pode-se notar no Gráfico 1, os teores de potássio e de tório terrestres são maiores do que os aéreos, em cerca de 51 % e 6 %, respectivamente. Porém, o teor médio do urânio aéreo é em torno de 10 % superior ao terrestre. Tais discrepâncias devem-se às diferentes formas de aquisição dos dados. No levantamento aéreo, a informação de cada ponto de leitura representa uma determinada área, a qual é função da altura de vôo (Grasty, 1976). Já o dado terrestre reflete apenas o ponto de medição, dificultando, assim, a correlação espacial e estatística.

Uma outra alternativa de comparação entre os dados aéreos e terrestres pode ser visualizada nas figuras 7 e 8, respectivamente, representativas da sobreposição de imagens ternárias de K(R)-eTh(G)-eU(B) ao MDE. Na Figura 7, nota-se claramente a delimitação do granito alcalino da Serra do Carambeí, através do enriquecimento em eTh, em contraste com as encaixantes cálcio-alcalinas, mais enriquecidas relativamente em K e eU, do Complexo Granítico Cunhaporanga. Por outro lado, na Figura 8, pode-se diferenciar as porções enriquecidas em eU, nos extremos NE e SW do corpo principal, as quais estão relacionadas aos diques félsicos, enquanto as encaixantes são mais enriquecidas em K, como esperado.

Os dados de contagem total (CT) convertidos para dose (R/h) também foram comparados, porém só no contexto do *stock* granítico da Serra do Carambeí (figuras 9 e 10). Apesar de uma certa correlacão visual, os dados estatísticos mostram grandes discrepâncias como pode-se apreciar na Tabela 1.

	CT aérea	CT terrestre
Valor mínimo	2,85	10,12
Valor máximo	13,96	49,04
Valor médio	7,35	18,30

Tabela 1 – Comparação entre os dados de CT.

Gamaespectrometria do Granito Serra do Carambeí-PR

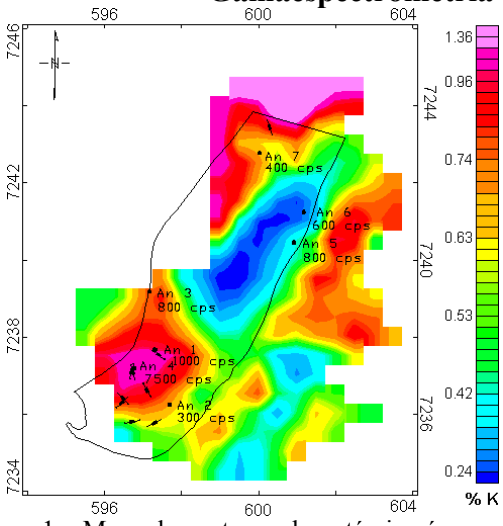

Figura 1 – Mapa de contorno do potássio aéreo.

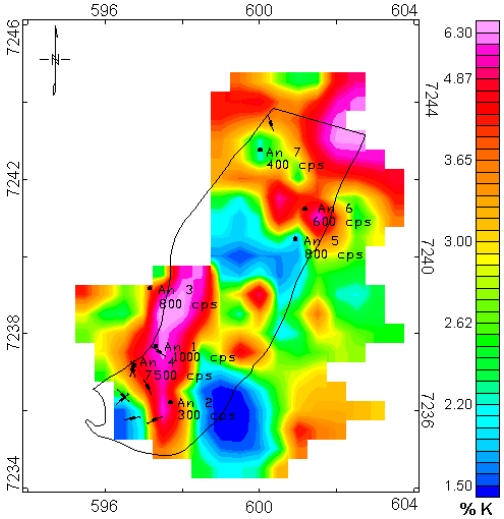

Figura 4 – Mapa de contorno do potássio terrestre.

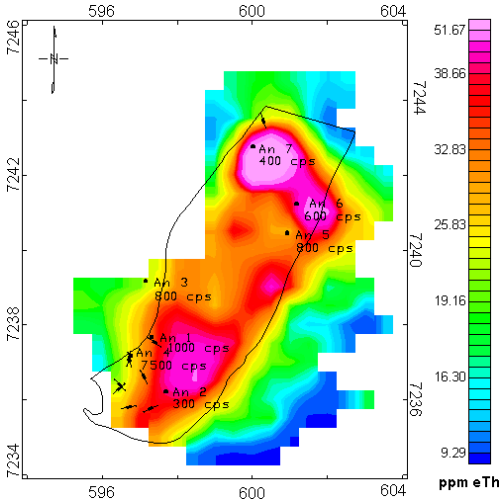

Figura 2 – Mapa de contorno do tório aéreo.

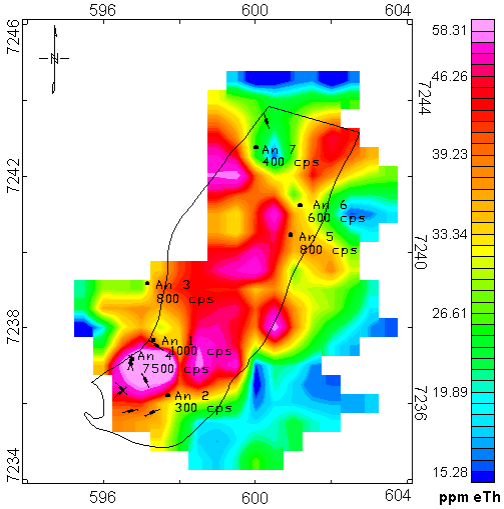

Figura 5 – Mapa de contorno do tório terrestre.

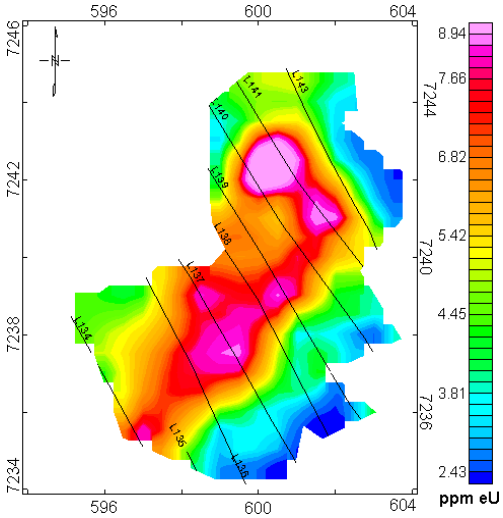

Figura 3 – Mapa de contorno do urânio aéreo.

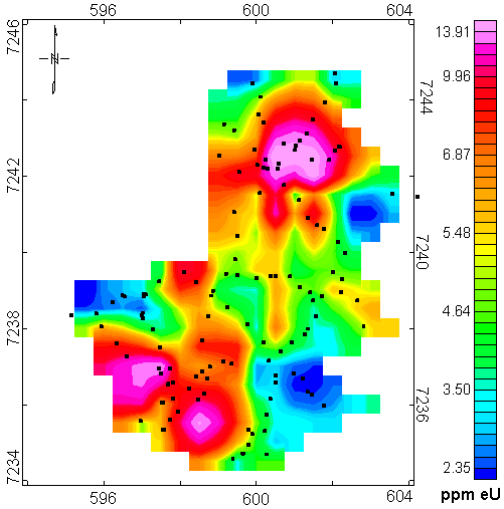

Figura 6 – Mapa de contorno do urânio terrestre.

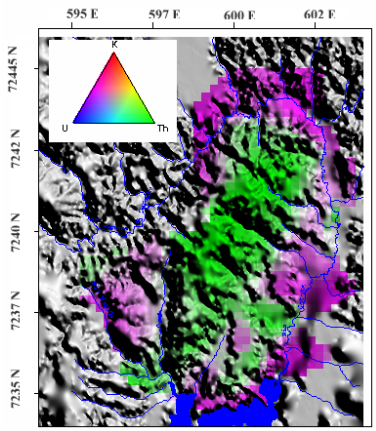

Figura 7 – Imagem RGB aérea sobreposta ao MDE.

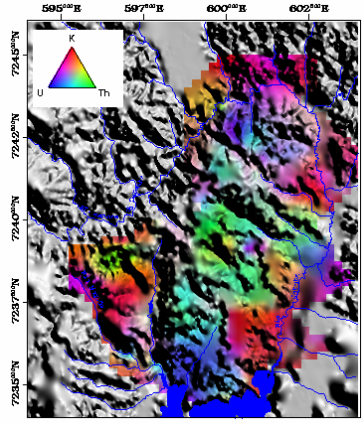

Figura 8 – Imagem RGB terrestre sobreposta ao MDE

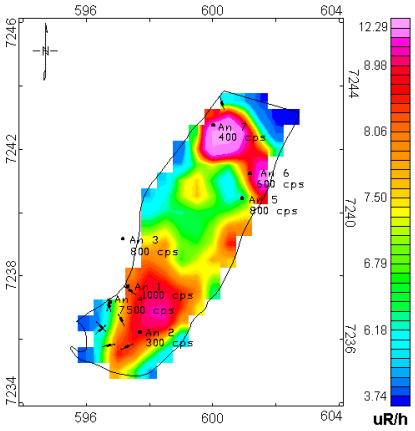

Figura 9 – Mapa da contagem total aéreo.

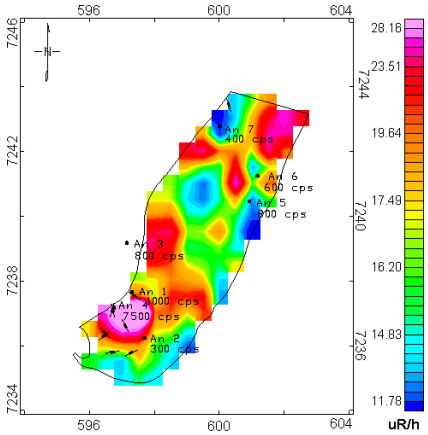

Figura 10 – Mapa da contagem total terrestre.

Conclusões

Observou-se boa correlação entre os dados gamaespectrométricos aéreos e terrestres. Os dados de campo confirmaram as anomalias de urânio em áreas de afloramento de diques "félsicos" uraníferos nas extremidades NE e SW do corpo.

O método radiométrico possibilitou a distinção e a delimitação do granitóide alcalino da Serra do Carambeí de sua encaixante cálcio-alcalina, representada pelo Complexo Granítico Cunhaporanga, em função do enriquecimento em eTh do primeiro. A sobreposição das imagens ternárias geofísicas ao modelo digital de elevação, possibilitou verificar a migração dos radionuclídeos na paisagem.

A partir dos dados de contagem total transformados em dose, estima-se que o corpo não ultrapasse o índice máximo admissível para o ser humano (300 mR/semana, Telford *et al*., 1990).

.

Referências Bibliográficas

BARMP, 1997. Brazil Airbone Radiometric Mapping Project. Technical Report and Survey Atlas. A collaboration between PGW-CPRM, RJ.

Barreto, P.M.C.; Austerlitz, C.; Malheiros, T.; Lovborg, L. 1986. Radioactive concret sources at IRD/CNEN, Brazil, for the calibration of uranium exploration and environmental field instruments. IRD/DEX-3/CNEN, 66 p. (inédito).

Grasty, R. L. 1976. The circle of investigation of airoborne gamma-ray surveys; *In: Report of activities, Part B, Geol. Survey. Can. Paper 76-1B*, p. 77-79.

Pinto-Coelho, C.V. 1986. O granito Serra do Carambeí-PR e as anomalias uraníferas associadas, Brasília. Dissertação (Mestrado), Departamento de Geociências, Universidade de Brasília, 308f.

Telford, W. M., Geldart, L. P., Sheriff, R. E. 1990. Applied Geophysics. New York: Cambridge University, 770p.

Integração de Dados Aerogamaespectrométricos e Geológicos para a Individualização de Maciços Graníticos na Região da Serra da Graciosa (PR)

Guilherme A. R. Gualda [(1)]; Francisco José Fonseca Ferreira [(2)]; Carlos V. Portela Filho [(2)]; Sílvio R. F. Vlach [(1)]
[(1)] Instituto de Geociências, USP; [(2)] Laboratório de Pesquisas em Geofísica Aplicada, LPGA/UFPR

Abstract

The granites of the Serra da Graciosa Area (Paraná State, South Brazil) are important representatives of the post-collisional magmatism that formed the Serra do Mar Province along the final stages of the Brasiliano Cicle (ca. 600-580 Ma). These granites are still poorly studied mostly due to the difficulty of access to the area. Geological and airborne gamma-ray spectrometric data have been integrated in order to identify and delimitate the granitic bodies.Five occurrences have been identified; each one with sizes between 40 and 100 km^2. They support the highest mountains of the region and are characterized by positive anomalies of K, eU and eTh in comparison to the basement gneisses and amphibolites. These results point to the necessity of defining five independent massifs in the Serra da Graciosa Area.

Introdução

A região da Serra da Graciosa, no Estado do Paraná, concentra ocorrências expressivas de granitos da Província Serra do Mar, formada por intenso magmatismo pós-colisional ao final do Ciclo Brasiliano (*ca*. 600-580 Ma). Estes granitos têm sido estudados em caráter principalmente regional e pouco se conhece das características geológicas, estruturais e petrológicas de cada uma das ocorrências.

O relevo bastante acidentado, a escassez de vias de acesso e, em especial, a cobertura vegetal muito densa da Mata Atlântica, são importantes restrições a estudos detalhados, de forma que os dados obtidos *in situ* são em geral em pequeno número e mal distribuídos. Neste panorama, ferramentas de sensoriamento remoto podem ser importantes para o mapeamento adequado destas ocorrências graníticas.

Neste trabalho, dados aerogamaespectrométricos do *Brazil Airborne Radiometric Mapping Project* (BARMP, 1997) são integrados a informações geológicas de campo para fundamentar a compartimentação dos granitos da região da Serra da Graciosa em maciços individuais.

Contexto geológico regional

Os maciços da Província Serra do Mar são constituídos por rochas graníticas e sieníticas e ocorrem isolados ou associados a bacias vulcano-sedimentares; distribuem-se ao longo da Serra do Mar, paralelamente ao litoral atlântico, desde a região nordeste de Santa Catarina até o sudeste de São Paulo. São intrusivos em rochas arqueanas do Cráton Luiz Alves e neoproterozóicas da Microplaca Curitiba. (Kaul, 1984; Siga Jr. *et al.*, 1993).

O Cráton Luiz Alves é formado por granulitos de composição tonalítica a granodiorítica, com intercalações de granulitos máficos, com idades arqueanas (2.700-2.600 Ma) ou transamazônicas (2.250-1.850 Ma). Para leste, no Cinturão Granitóide Costeiro, predominam granitóides cálcio-alcalinos porfiríticos de idades brasilianas (615-570 Ma, *cf*. Siga Jr. *et al.*, 1993). A Microplaca Curitiba é composta por gnaisses bandados e anfibolitos transamazônicos (2.150-1.800 Ma), variavelmente migmatizados no Ciclo Brasiliano (620-550 Ma).. Monzogranitos deformados brasilianos (720 Ma – U-Pb em zircão; 580 Ma – Rb-Sr em rocha total) afloram em diversas áreas.

Os maciços da Província Serra do Mar afloram paralelamente ao contato entre o Cráton Luiz Alves e o Cinturão Granitóide Costeiro, e a sua origem é atribuída ao rearranjo crustal decorrente da colisão do Cinturão Granitóide Costeiro com as Microplacas Curitiba e Luiz Alves, em ambiente tipicamente pós-colisional. (Siga Jr. *et al.*, 1994).

Geologia local

A região enfocada neste trabalho situa-se a cerca de 40 km a leste da cidade de Curitiba, alongada na direção SSW-NNE e com dimensões aproximadas de 50 x 17 km. Morfologicamente, é marcada por cinco serras principais: Capivari, Órgãos, Graciosa/Farinha Seca, Marumbi e Baitaca/Boa Vista (Figura 1).

O reconhecimento das rochas graníticas na região deve-se a Maack (1961), que reuniu os granitos das serras da Graciosa e dos Órgãos sob a denominação de *complexos de granitos alcalinos*, salientando que estes são separados por rochas gnáissicas do embasamento e por *diques do vulcanismo gondwânico*. Os granitos da Serra do Marumbi foram mapeados como uma unidade independente, inferindo-se também a ocorrência de *granitos alcalinos* na Serra do Capivari.

Os primeiros mapeamentos sistemáticos são devidos a Cordani e Girardi (1967) e Fuck *et al*. (1970), que definem o Maciço Graciosa (*ca*. 300 km^2), incluindo nele as ocorrências das serras do Capivari, Órgãos e Graciosa/Farinha Seca, além do Maciço Marumbi, este com área de ocorrência semelhante à descrita por Maack (1961). À oeste,

Fuck (1966) define o Maciço Anhangava, que sustenta a Serra da Baitaca/Boa Vista.

Materiais e métodos

Os trabalhos de campo incluiram perfís geológicos ao longo de estradas, trilhas e/ou drenagens, que permitiram (1) reconhecer as fácies graníticas presentes; (2) coletar amostras representativas e (3) identificar as relações entre os granitos e encaixantes.

Um modelo digital de terreno (MDT) foi construído para a área, com base em malha regular de pontos espaçados de 500 m, cujas altitudes foram extraídas de folhas topográficas 1:50 000 (Figura 2).

Os mapas aerogamaespectrométricos foram obtidos através de interpolação dos dados do Projeto Aerogeofísico Serra do Mar Sul (CPRM, 1978), cujas contagens (cps) de K, eTh e eU foram convertidas em % e/ou ppm pelo *Brazil Airborne Radiometric Mapping Project* (BARMP, 1997). Silva e Mantovani (1994) discutem em detalhe a metodologia utilizada e a qualidade dos dados originais disponíveis. Após análise crítica das variáveis K, eTh, eU, foram gerados mapas de distribuição elemental, das razões eU/K, eU/eTh, eTh/K, do parâmetro F = K*eU/eTh (Gnojek & Prichystal, 1985) e de composições ternárias K(R)-eU(G)-eTh(B) e eU/K(R)-eU/Th(G)-eTh/K(B).

Resultados e discussão

A ocorrência dos granitos como feições evidentemente destacadas do relevo, bem como os teores elevados de eTh, eU e K em relação às rochas gnáissicas e anfibolíticas encaixantes, tornam possível identificar os corpos graníticos nas imagens disponíveis (*cf.* Figuras 2, 3 e 4).

Nos mapas aerogamaespectrométricos, os corpos graníticos destacam-se pelos elevados teores de K, eTh e eU, separados por porções com valores mais baixos (Figuras 3 e 4), característicos do embasamento. Em geral, é marcante a coincidência dessas áreas com os tratos de maior altitude, mostrando que as rochas graníticas sustentam as principais serras da região (Figura 2).

Entretanto, algumas áreas adjacentes àquelas de maior altitude, sobretudo a leste da vertente da Serra do Mar, mostram importantes anomalias dos radionuclídeos. As características naturais da região permitem sugerir pelo menos dois tipos de mecanismos capazes de promover a migração de radionuclídeos em direção à cotas mais baixas. Os acentuados desníveis de relevo levam, por um lado, a intensa movimentação recente de blocos; por outro lado, é possível que processos pedogenéticos tenham conduzido à mobilização e transporte de radionuclídeos, sobretudo K e U (Dickson & Scott, 1997; Wilford *et. al*., 1997). Uma avaliação mais detalhada permite identificar indícios de cada um desses processos.

Os mapas aerogamaespectrométricos mostram fortes anomalias na região central da Serra dos Órgãos (Figuras 3 e 4). Na porção sudeste o padrão é mais complexo, com teores menores acompanhando uma importante drenagem (*cf.* Figura 3), sugestivos de processos de remoção seletiva de radionuclídeos. Na área da Serra da Graciosa/Farinha Seca, as respostas são mais homogêneas, com anomalias marcadas para K, eU e eTh. As imagens mostram anomalias também à leste da vertente da Serra do Mar. Entretanto, a composição K-U-Th (Figura 4) exibe diferenças sutis de tonalidade entre estas áreas, o que, aliado à constatação da ocorrência de encaixantes próximo à base da serra, indica que a extensão oriental da anomalia deva também resultar da migração de radioelementos..

Já na porção nordeste da Serra do Marumbi, os granitos *in situ* sustentam vertentes subverticais da Serra do Mar e blocos decamétricos de granito são observados a grandes distâncias dos contatos, sobre áreas de afloramento das encaixantes. Em conseqüência, as anomalias aerogamaespectrométricas se estendem por distâncias bem superiores às observadas em outras áreas, sem alteração da assinatura espectral (*cf.* Figura 4). É interessante ainda notar que os mapas mostram dois centros com teores mais altos de radionuclídeos, um em cada extremo do maciço (Figura 3). Ainda assim, devido à amostragem geológica restrita, não é possível inferir uma compartimentação interna para este maciço, uma vez que os tipos petrográficos observados nestas áreas são petrográfica e mineralogicamente muito semelhantes.

Na área da Serra da Baitaca/Boa Vista, as observações de campo mostram que a ocorrência de granitos é também coincidente com as áreas de maior altitude. Entretanto, os mapas indicam uma resposta espectral heterogênea e pouco acentuada (Figuras 3 e 4). Na porção oriental, a composição K-U-Th exibe assinatura similar àquela das outras serras (Figura 4); mas, na porção ocidental, esta composição mostra um padrão diferenciado, sem análogos nas demais áreas estudadas. Aflora nesta área uma grande variedade de tipos graníticos e sieníticos, o que poderia, pelo menos em princípio, explicar a distribuição heterogênea dos elementos radioativos. Contudo, as anomalias menos acentuadas observadas, são incompatíveis com estas rochas, o que sugere mobilização importante de radionuclídeos.

Conclusões

A integração de informações geológicas com dados aerogamaespectrométricos para a região da Serra da Graciosa, Serra do Mar, no Estado do Paraná, permite indicar pelo menos cinco áreas de ocorrência de rochas graníticas, cada uma delas circunscrita por rochas do embasamento. Esta conclusão está de acordo com os contrastes petrográficos bem marcados observados em cada uma destas serras (Gualda, em preparação).

Além disso, granitos e sienitos de caráter pós-colisional, como os estudados, afloram em geral na forma de maciços de geometria circunscrita, com áreas raramente superiores a *ca*. 80-100 km^2,

Torna-se evidente, portanto, a necessidade de serem individualizados pelo menos cinco maciços independentes na região, como sugerido na Figura 4.

Agradecimentos

Agradecemos ao Prof. Dr. W. Shukowski (IAG-USP), pela disponibilização de dados para modelagem digital de terreno, à FAPESP (Proc. 98/15656-7) e ao Projeto Geofísica Aplicada LPGA-UFPR-PADCT/CNPq (62.0155/97-3 GTM).

Referências Bibliográficas

BARMP 1997. *Brazil Airborne Radiometric Mapping Project. Technical report and survey atlas*. A collaboration between Paterson, Grant & Watson Limited (PGW), Companhia de Pesquisa de Recursos Minerais (CPRM) and Geological Survey of Canada (GSC), Rio de Janeiro, RJ.

Basei, M.A.S.; Siga Jr., O.; Machiavelli, A.; Mancini, F. 1992. Evolução tectônica dos terrenos entre os cinturões Ribeira e Dom Feliciano (PR-SC). *Revista Brasileira de Geociências*, **22**: 216-221.

Cordani, U.G.; Girardi, V.A.V. 1967. Geologia da Folha de Morretes. *Boletim da Universidade Federal do Paraná, Geologia*, **26**:1-40.

CPRM 1978. Projeto Aerogeofísico Serra do Mar Sul. Companhia de Pesquisa de Recursos Minerais – CPRM. Relatório Final (inédito).

Dickson, B.L. & Scott, K.M. 1997. Interpretation of aerial gamma-ray surveys – adding the geochemical factors. *In*: Airborne Magnetic and Radiometric Surveys, *Journal of Australian Geology & Geophysics*, **17**: 187-200.

Fuck, R.A. 1966. Geologia da Folha Piraquara. *Boletim da Universidade Federal do Paraná, Geologia* (inédito).

Fuck, R.A.; Muratori, A.; Trein, E.; Bertoldo, A.; Hausen, J. 1970. *Rio Capivari*: folha geológica 1:70.000. Comissão da Carta Geológica do Paraná.

Gnojek, I. & Prichystal, A. 1985. A new zinc mineralization detected by airborne gamma-ray spectrometry in Northern Moravia (Czechoslovakia). *Geoexploration*, **23**(4): 491-502

Hasui, Y.; Carneiro, C.D.R.; Coimbra, A.M. 1975. The Ribeira Folded Belt. *Revista Brasileira de Geociências.*, **5**: 257-266.

Kaul, P.F.T. 1984. Significado dos granitos anorogênicos da Suíte Intrusiva Serra do Mar na evolução da crosta do sul-sudeste do Brasil, no âmbito das folhas SG-22, Curitiba e SG-23, Iguape. *In*: CONGR. BRAS. GEOL., 33. Rio de Janeiro. SBG. *Anais…*, **6**: 2815-2825.

Kaul, P.F.T. 1997. O magmatismo na Serra do Mar e adjacências (sul do Brasil) no final do Neoproterozóico e seus condicionantes tectônicos. Tese de Doutoramento. IG-USP. 293 p. (inédito).

Lopes, A.P.; Soares, A.P.; Lipski, M.; Vesely, F.F.; Vasconcellos, E.M.G. 1998. Análise faciológica do granito Anhangava (PR) a partir de dados petrográficos e geoquímicos. *In:* CONGR. BRAS. GEOL., 40. Belo Horizonte. SBG. *Anais…*, 497.

Maack, R. (1961) Sobre a ocorrência de granitos alcalinos no Estado do Paraná e sua posição dentro das fases orogenéticas algonquianas. *Boletim da Universidade Federal do Paraná, Geologia*, **4**:1-52.

Misener, D.J.; Sinclair, R.; Mourão, L.M.F. (1997)A new Brazil radiometric database generation and application. *In:* CONGR. INTERN. SOC. BRAS. GEOF., 5. São Paulo. SBGf. *Expanded Abstracts…*, **1**: 564.

Siga Jr., O (1995) Domínios tectônicos do sudeste do Paraná e nordeste de Santa Catarina: geocronologia e evolução crustal. Tese de Doutoramento. IG-USP. Inédita. 164 p.

Siga Jr., O.; Basei, M.A.S.; Machiavelli, A. (1993) Evolução geotectônica da porção NE de Santa Catarina e SE do Paraná, com base em interpretações geocronológicas. *Revista Brasileira de Geociências*, **23**(3): 215-223.

Siga Jr. *et al.* (1994) Maciços Graníticos da porção Sudeste do Paraná e Nordeste de Santa Catarina: geocronologia e implicações tectônicas. *In:* CONGR. BRAS. GEOL., 38. Camboriú. SBG. *Anais…*, 400-401.

Wilford, J.R.; Bierwirth, P.N.; Craig, M.A. 1997. Application of airborne gamma-ray spectrometry in soil/regolith mapping and applied geomorphology. *In*: Airborne Magnetic and Radiometric Surveys, *Journal of Australian Geology & Geophysics*, **17**(2): 201-216.

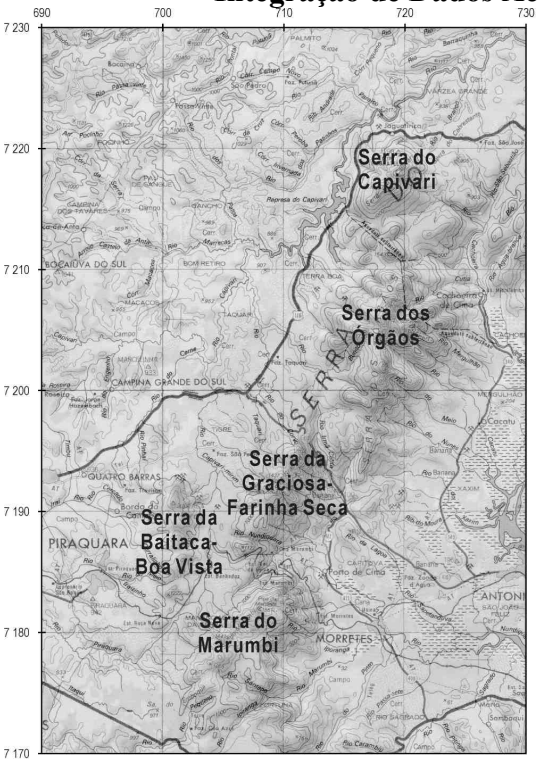

Figura 1 – Toponímia da região da Serra da Graciosa. Fonte: Folha Curitiba (1:250.000).

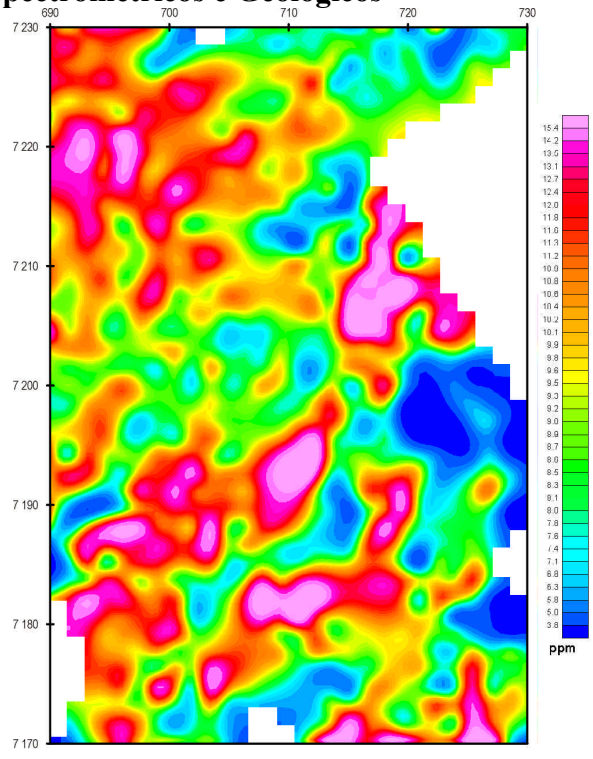

Figura 2 – Mapa de contorno do tório (Th).

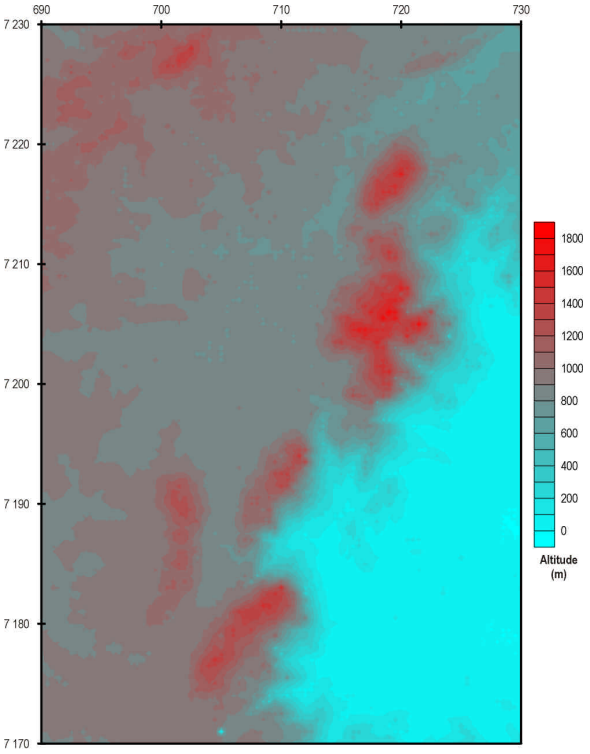

Figura 2 – Modelo digital de terreno (MDT) da região da Serra da Graciosa – PR.

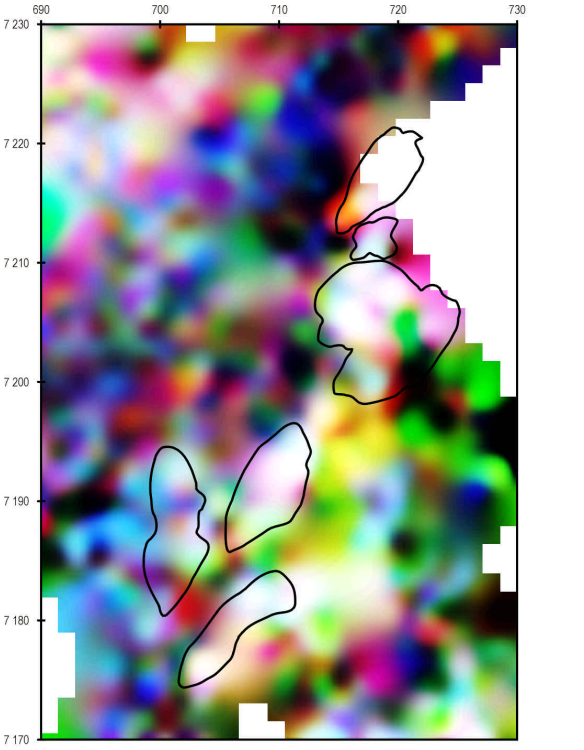

Figura 4. Mapa de composição ternária K(R)-U(G)-Th(B). Em preto, contatos geológicos sugeridos por Gualda (2001, em preparação).

INTEGRAÇÃO DE DADOS GEOFÍSICOS DA PORÇÃO CONTINENTAL DA BACIA DE CAMPOS

Georges Pavie, LENEP-UENF/Macaé-RJ, georges@lenep.uenf.br
Abel Carrasquilla, LENEP-UENF/Macaé-RJ, abel@lenep.uenf.br
Marco Ceia, LENEP-UENF/Macaé-RJ, marco@lenep.uenf.br

Abstract

This work consists in the interpretation of existing data of the continental portion of Campos Basin, referring to gravity, magnetic and magnetoteluric (MT) geophysical methods. The gravity data were obtained by PETROBRAS during forty years, and, the magnetic ones resulted of airborne surveys performed by CPRM in 1978, which covered almost all Rio de Janeiro State. On the other hand, MT data were collected by LENEP/UENF and National Observatory (ON/MCT) in 1998, through a profile between Farol de São Tomé County and Campos dos Goytacazes City. After an adequate processing, a bidimensional inverse interpretation (2D) of each data set was made through the WINGLINK™ software. These interpretations show a good agreement in the determination of the regional basement depth (gneiss, basalt and amphibolite) and the thickness of the package sedimentary (clays, conglomerates, shales and sands). In the meantime, only the magnetic interpretation was able to show clearly the rift process of the basin.

Introdução

A Bacia de Campos é limitada pelos arcos de Vitória (N) e Cabo Frio (S), por um sistema de falhas que põe os sedimentos em contato com o embasamento (W), e, pela crosta oceânica no talude da plataforma continental (E) (Figura 1). A sua área sedimentar engloba uma superfície de 30.000 km^2, com apenas 600 km^2 na parte terrestre. O mapa geológico regional mostra a predominância de rochas pré-cambrianas na região, constituídas por uma associação de biotitas, gnaisse, granitos, porfiroblastos, migmatitos, etc. (*Peçanha et al.*, 1998). Quanto à estratigrafia, na parte terrestre as formações sedimentares gradam para uma delgada seção de aluviões continentais vermelhos, designados como Fácies São Tomé. Estes clásticos apresentam uma idade quaternária e pertencem à fase *drift*, formados basicamente por depósitos progradacionais do sistema deltaico do rio Paraíba do Sul. Suas relações estratigráficas com a Formação Barreiras do terciário são ainda pouco conhecidas, a qual apresenta uma litologia constituída de arenitos (argilosos finos, grossos e conglomeráticos, quartzosos ou feldspáticos, com cimento limonítico), siltitos, camadas argilosas e bauxíticas. O esboço estrutural da bacia mostra um sistema binário de lineamentos estruturais regionais que afetam embasamento e sedimentos, com os mais proeminentes na direção SW-NE e os mais suaves na direção NW-SE*(Dias et al., 1990)*. Por outro lado, em 1958, a PETROBRAS começou a usar métodos geofísicos na área, com levantamentos de sísmica marinha e gravimétrico terrestre. Em 1959 foi perfurado o poço estratigráfico 2-CST-1-RJ no Farol de São Tomé, que mostrou 1963 m de sedimentos (intercalações de arenitos, folhelhos, argilas e conglomerados) sobre 625 m de basaltos, assentados diretamente sobre o embasamento gnáissico, sem a presença de óleo ou gás *(Munis,* 1993).

Metodologia

Na região estudada, a CPRM realizou em 1978 levantamentos aéreos (magnéticos e gamaespectrométricos), cobrindo quase a totalidade do Estado do Rio de Janeiro na direção N-S. Os dados magnéticos desses levantamentos foram utilizados neste estudo (*Mourão*, 1995). Por outro lado, os dados gravimétricos foram digitalizados a partir do mapa *Bouguer* da área, no qual foi interpolado o perfil Farol de São Tomé – Campos dos Goytacazes (*Schaller,* 1973). Os dados MT, entretanto, foram obtidos numa campanha terrestre realizada em 1998 entre o ON/MCT e o LENEP/UENF nesse mesmo perfil, consistindo de três sondagens. No processamento dos dados magnéticos, os mapas de contorno apresentavam-se com problemas originados no próprio levantamento aéreo. Este tipo de erro aparece por causa da existência de comprimentos de onda nas direções paralela e perpendicular ao levantamento, com valores de até duas vezes o espaçamento entre as linhas de vôo. O erro foi diminuído através do micro - nivelamento dos dados, com o uso da técnica proposta por *Minty* (1991), que consiste de filtragens passa baixa e alta, seguidas de convolução. Uma vez contornado este problema, os dados foram representados na forma de mapa através do *software* GEOSOFT, de onde foi selecionado o perfil Farol - Campos. Posteriormente, com base na malha do campo magnético, foi feita uma continuação para baixo, para fazer uma comparação com a interpretação dos outros métodos à nível da superfície do terreno. O sinal analítico dos dados também foi calculado, afim de realçar as estruturas geológicas presentes, mostrando as mudanças laterais relacionadas com as bordas dos corpos no subsolo. Os dados MT, por outro lado, receberam seu usual tratamento, transformando as séries temporais medidas para o domínio da freqüência, através da transformada de *Fourier*, e calculando os valores da resistivida-

Geological Context

The precambrian area of Jaguaribe-SE sheet (Figure 1) is constituted for parts of Cearense, Rio Grande do Norte and Transversal tectonic domains. Those domains are limited by neoproterozoic expressive shear zones and subdivided into several tectonostratigraphics terranes (Santos et al., 1999). The Patos shear zone represent a first order boundary confirmed by geochronologic and geophysical data, separating two major crustal segments. The northern composed by a complex neoproterozoic thrust-and-fold belt, overthrusting Archean to Early Proterozoic terranes, comprising the Cearense domain; and the Rio Grande do Norte domain, characterised by a Brasiliano belt, implanted over Archean-Early Proterozoic terranes. The southern composed mainly by Meso-Neoproterozoic meta-volcanosedimentary terranes accreted to adjacent northern edge of the São Francisco craton.

Data Processing

By means of Oasis Montaj 5.0 (Geosoft), a grid of magnetic total field has been processed and filtered. The shallow (< 5 km) and deeper (> 5 km) sources maps have been performed by spectral analyses. Analytic signal and analytic signal phase techniques obtained enhancement of particular trends and magnetic bodies. Sources tops depths have been determined by means of Euler 3D deconvolution, for models (structural index) of contact, dike, sphere and cylinder. Airborne gamma-ray spectrometric grids have been stacked for generation of a ternary map distribution (U, Th and K). The gravity profiles have been interpreted by qualitative and semiquantitatives means (Talwani's algorithm).

The geological, magnetic and gamma-ray spectrometric data have been correlated with the Gold, Iron, Copper, Asbestos, Graphite, Vermiculite, Lead, Manganese, Scheelite and Emerald mineralizations. Also with geochemical anomalies of Gold, Iron, Nickel and Titanium.

Interpretation and Tectonic Correlation

a) Aeromagnetic Data

The interpretation and correlation were executed with basis in the tectonostratigraphic terranes framework (Ferreira & Santos, 2000) The data was analysed in the sense of verifying the geophysics validity of this framework and characterising your limits and/or sutures (Figure 2).

The Rio Piranhas terrane is characterised for anomalies with axis lengthened in the NE-SW direction. The wavelengths change between 10 and 25 km and amplitudes between 50 and 150 nT. Those anomalies are correlated with a big volume of acid orthoderived rocks. Gabroic rocks are correlated with elliptical anomalies (wavelength about 10 km) in the centre-east portion. At the Caicó (RN) city surrounding occurs a wide area (55-width km) with non-magnetic orthogneiss. This area is limited by strong magnetic alignments correlated with shear zones. In the Portalegre shear zone have some emerald and ruby mineralizations.

The Granjeiro terrane has a highly magnetisation zone, expressed in negative anomalous axis guided in the E-W direction. These anomalies have amplitudes of up to 200 nT, produced for a basic orthoderived rocks and a great volume of meta-volcanosedimentary supracrustal rocks. The limits between Patos and Malta shear zones are marked by abrupt magnetic contrasts with the adjacent terranes.

The Seridó belt has a highly magnetic substratum. This basement is expressed by anomalies with magnetic axis guided in the NE-SW direction. The limits are defined for shear zones related with abrupt magnetic contrasts, regarding the adjacent terranes. At the Cruzeta's city (RN) surrounding, a wide positive axis lengthened in the NE-SW direction, corresponds to thick packages of non-magnetic and of low grade metamorphic supracrustal rocks. This terrane is characterised by a number of scheelite mines.

The São José do Campestre terrane has small amplitudes anomalous magnetic axis (<50 nT) guided in the NE-SW and ENE-WSW directions. Those magnetic signatures correspond to Neoproterozoic sheared granite rocks. Elliptic anomalies with wavelength lower than 10 km and smaller amplitudes than 100 nT occurs at the inner part this terrane.

The Alto Moxotó terrane is marked by the presence of elliptic highly magnetic cores (negative axis with amplitudes of up to 200 nT). Those magnetic anomalies are related with relict of high-pressure granulitic to eclogitic facies rocks, preserved in mafic-ultramafic rocks along terrane boundary. Those rocks can represent a disperse suture, remnant of a mesoproterozoic oceanic crust. They form a belt in the NE-SW direction; limited in the south-east by Congo/Cruzeiro do Nordeste shear zone.

The Rio Capibaribe terrane is characterised by positive axis that reflect non-magnetic ortho and paraderived rocks. Locally occur lengthened anomalies, with amplitudes lower than 100 nT, correlated with low magnetisation lithologic bodies.

The Alto Pajeú terrane has two distinct aeromagnetic contexts. The first is a positive axis belt reflecting non-magnetic thick supracrustal package. The other is

a lengthened and sigmoidal magnetic anomaly belt in a NE-SW direction, correlated with outcrop of alkaline plutonic rocks (Syenitoid Line). Those anomalies have maximum amplitudes of 100 nT and wavelengths lower than 15 km. The Alto Pajeú terrane has many gold mineralization in shear zones controlled structures.

The Piancó-Alto Brígida terrane also has two distinct aeromagnetic contexts. At south-east, a wide positive axis belt is related with the outcrop of a non-magnetic thick low metamorphic degree supracrustal rocks sequence. This sequence is interleaving with non-magnetic stocks and batholiths of neoproterozoic granitic rocks. Other belt, located to north-west, is limited by Patos shear zone. Granites and migmatite rocks outcrops are magnetically defined by positive and negative axis pairs, with amplitudes lower than 100 nT and wavelengths about 15 km.

b) Airborne Gamma-Ray Spectrometry Data

The gamma-ray spectrometry data analysis indicates that the potassium distribution has a clear contrast marked by Patos shear zone. In the north, it's observes a homogeneous distribution, with contents higher than 3,5%. This signature is caused by a great volume of calc-alkaline granites, porphiritic granites and granodiorites intrusions. This pattern is interleaving for low potassium areas, associates to the sedimentary coverage and gabro-dioritic rocks. Regarding to the adjacent units, shear zones are marked by trends of potassium or by abrupt fall contents.

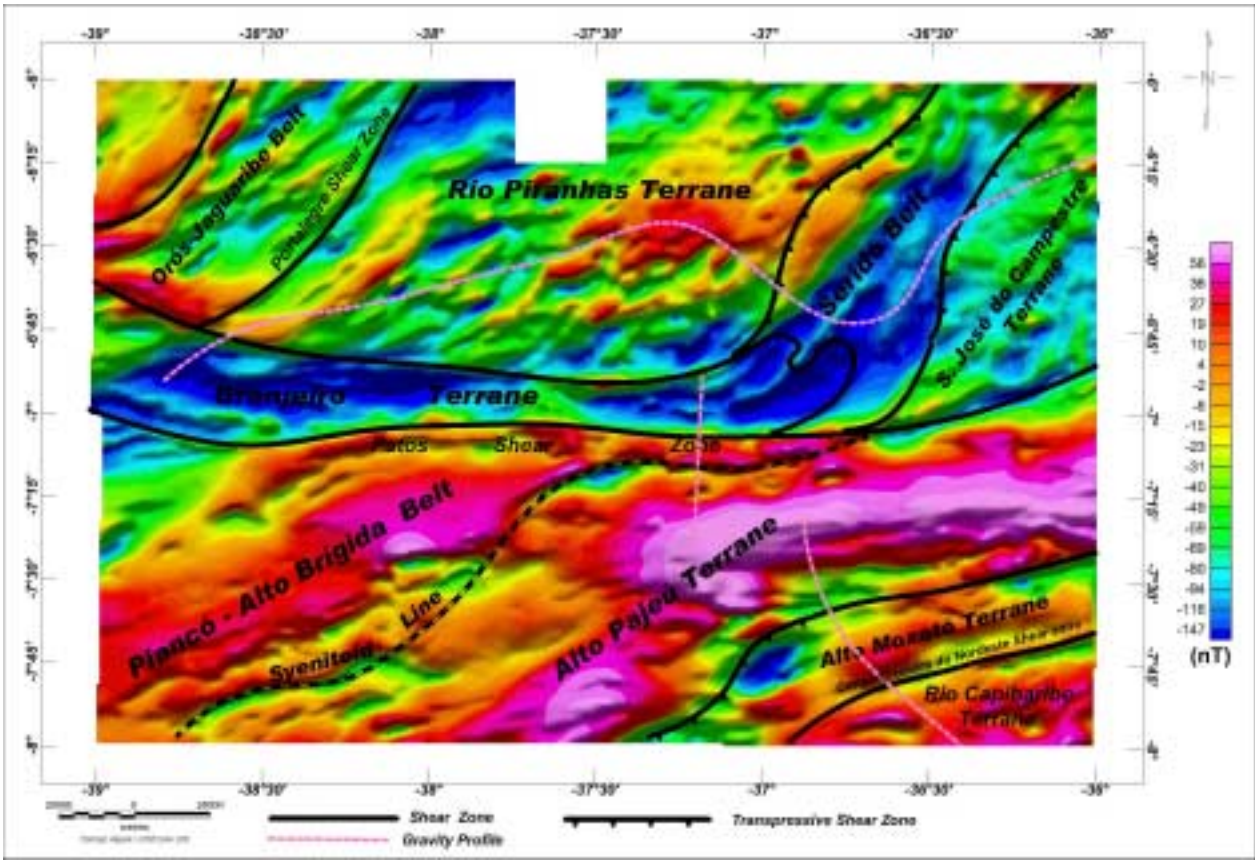

Figure 2 - Colourful shaded total field magnetic anomaly map with shear zones and tectonostratigraphic terranes.

At the south of the Patos shear zone, the potassium distribution is less homogeneous. Apparently that reflects a less intense level of granitization. Elevated contents (>3%) concentrate in trends related with tectonic limits, shear zones or batholiths and isolated syenitic intrusions.

This potassium distribution pattern doesn't repeat in the uranium map. In this case, it's concentrate in

related trends shear zones and in the innermost parts of the batholiths.
The thorium distribution has similar aspects of the uranium, however concentrating inside the bodies and geological structures limits.

c) Gravity Data and Tectonic Limits

The Patos shear zone importance as a deeper crustal limit is confirmed by a bipolar gravity signature (positive-negative) and by geochronologic data.
Two distinct gravity tendencies, separated by a highly horizontal gradient, have been detected in the gravity profile that crosses the Patos shear zone. The positive tendency corresponds to the terranes located at the north of shear zone and negative tendency zone is located at the south. Beyond those main tendencies, have been identified small positive and negative residual amplitudes, related to granitic rocks and metasedimentary units.
In the aeromagnetic data, the Patos shear zone is associated with a negative axis belt. The magnetic regional signal is clearly distinct from north to south of that shear zone. Deeper magnetised bodies (up to 20 km) dominate at the north. Low magnetisation bodies, related with thick bands of supracrustals and intensely granitized rocks, dominate at the south.
A long gravity profile allows the qualitative interpretation of five crustal blocks in the central region of study area. Their limits correspond to positive horizontal gradient stretches. Gravity Bouguer anomalies with maximum amplitudes of 20 mGal are correlated with upper crust structures. Three blocks are constituted for dense upper crust and two for very granitized upper crust. The blocks represented by a dense upper crust are Granjeiro terrane, the east part of Rio Piranhas terrane/Seridó belt (there are no possibility to separate these two terrane by gravity) and internal nucleus of the São José do Campestre terrane. This lasts one with 3.5 Ga archeans rocks. Granitized upper crust occurs in the west part of Rio Piranhas terrane and in the west margin of São José do Campestre terrane.
At the southern of study area, a gravity profile depicted a positive-negative anomalous pair, with amplitude of 40 mGal (peak to peak). The highly horizontal gradient corresponds to the limit between Alto Moxotó and Rio Capibaribe terranes. The profile contains a long wavelength component (about 150 km) that represents the regional gravity field. This signature is related with crustal thickening that increases gradually from north-west to south-east. The apex of this thickening corresponds to central region of the Rio Capibaribe terrane. The residual anomalies (amplitudes between 2 to 15 mGal) overlapped to this regional are related with upper crust heterogeneity. Consequently, has been separated three different crustal compartments. Tow of very granitized upper crust and one of dense upper crust. The compartments that represent very granitized upper crust correspond to the south margins of Alto Pajeú and Rio Capibaribe terranes. The compartment that represents dense upper crust corresponds to the Alto Moxotó terrane.

Conclusions

Correlation of magnetic, gamma-ray spectrometry and gravity data with geological data of Jaguaribe-SE sheet demonstrate to be a useful tool in the study of tectonic compartments and composition of the precambrian crust. The magnetic patterns and alignments present a good correlation with known tectonostratigraphic terranes and faults boundaries. Magnetic, gravity and geochronologic data confirm a deeper crustal limit at the Patos shear zone. Moreover, it's possible to localise unknown terranes and shear zones.

References

Ferreira, C. A. & Santos E. J., 2000. Programa Levantamento Geológico Básicos do Brasil: carta geológica, carta metalogenética previsional (folha Jaguaribe SE, SB.24-Z, escala 1:500.000). CPRM, Recife. (In press).

GETECH & PGW, 1996. South American Magnetic Mapping Project. Technical Report and Survey Atlas. 111 p.

PGW; CPRM; GSC, 1997. Brazil Airborne Radiometric Mapping Project. Technical Report and Survey Atlas. 30 p.

Santos, E.J.; Van Schmus, W. R.; Brito Neves, B. B.; Oliveira, R. G.; Medeiros, V. C., 1999. Terranes and their boundaries in The Proterozoic Borborema Province, Northeast Brazil. VII SNET, Lençóis, Bahia, Brasil, Anais, Sessão 2, p. 121-124.

Acknowledgements

I would like to thank CPRM-Geological Survey of Brazil for permission to publish this work.

Integrated Gravity, Magnetic and Seismic Study Offshore Brazil

Guy Flanagan, Phillips Petroleum Company, gflanag@ppco.com,
Charles L. Campbell, ACCEL Services Inc., campbell@neosoft.com,
Bill Kilsdonk, Phillips Petroleum Company, mvkilsd@ppco.com,
Michael O. Maler, Phillips Petroleum Company, momaler@ppco.com,
Dale E. Bird, Bird Geophysical, dale@birdgeo.com,
Kari L. Kirkham, Phillips Petroleum Company, klkirkh@ppco.com

Summary

Seismic data quality in the area of the Campos, Santos, and Espirito Santos Basins is limited at depth due to the presence of significant amounts of salt. We used classic gravity and magnetic interpretation integrated with regional seismic and geology to study the regional tectonics, basin architecture, thermal history and salt distribution in offshore Brazil. Analysis of high quality regional gravity and magnetic data improved our understanding crustal thinning, definition of the pre-salt basement depth and architecture, and distribution of salt canopies. Our analysis included regional and detailed 2D gravity and magnetic models, automated depth to basement analysis, and key enhancements of the mapped data. A key to the success of the project has been the integration of the seismic interpretation through remote access and a close working relationship with the project team including contractors, through regular working visits and reviews. Results were integrated continuously with the project team and focused on: 1) interpretation of deep structure, salt thickness and extent; and 2) evaluating source rock potential, thermal history, and migration pathways on both a regional and block specific basis.

Introduction

Our interpretation used a classic approach to gravity and magnetic interpretation.

1. Generate and qualitatively interpret the basic and residual gravity and magnetic maps.

2. Correlate residual gravity profiles and seismic.

3. Generate a regional depth to magnetic basement surface.

4. Integrate two-dimensional seismic, structural, and gravity models.

5. Interact closely with contractors and project teams.

Qualitative Map Interpretation

We generated a series of basic and residual maps from the gravity and magnetic data to use in the qualitative analysis. These consisted of:

1. Bathymetry

2. Gravity
   a. Freeair gravity including a regional merge with the satellite gravity data
   b. Bouguer gravity
   c. Highpass and bandpass filtered Bouguer gravity
   d. Azimuth of the horizontal gradient of the Bouguer gravity
   e. Upward continuation of the Bouguer gravity

3. Magnetics
   a. Reduction to the magnetic pole
   b. First vertical derivative of the RTP magnetics
   c. Highpass and bandpass filtered RTP magnetics
   d. Azimuth of the horizontal gradient of the pseudogravity of the magnetics

The anomaly enhancement and isolation processing highlighted information available from the gravity and magnetic data. This was especially true for the signal associated with the sedimentary section and basement surface. Although many variations of these techniques were applied, only a subset considered most were used in the analysis.

Key products of this analysis were the azimuth maps. One of the key elements of gravity and magnetic interpretation is the identification of lineaments due to structural or lithologic changes. Thus, techniques that highlight these gradients are particularly useful in potential field analysis. One simple method to identify such gradients is to calculate the magnitude of the horizontal gradient. This results in closed maxima over the highest gradients. Then, we calculate the azimuth of this gradient map and key the azimuth to the 360-degree color wheel (figure 1).

This displays the gradient boundaries as sharp contacts without influence from the anomaly amplitude.

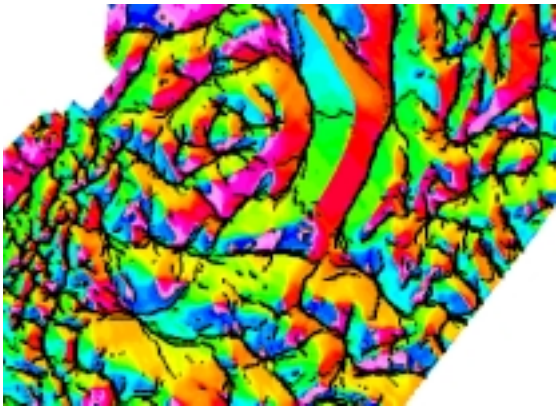

Figure 1. Example of Azimuth Display.

Secondary key products were: 1) an upward continuation that highlighted the more regional basement features; as well as, 2) using the residual of the upward continuation (the difference between the Bouguer gravity and the upward continued Bouguer) that highlighted salt anomalies. Additional gradient (azimuth) analysis of upward continued Bouguer maps correlated onshore geologic fault fabrics with offshore basement lineaments. The residual of the upward continued Bouguer was key to the seismic interpretation of the salt.

Seismic/Gravity Correlation

As an aid to seismic based salt interpretation the 1 km upward continued gravity residual was back interpolated onto seismic locations, scaled, and loaded as a horizon in Seisworks. A line-by-line correlation then highlighted areas where the seismic salt interpretation agreed with the residual gravity. For example, where the first pass seismic interpretation showed massive salt and a residual gravity low was observed the correlation was considered good. However, areas with seismically interpreted massive salt but without a distinct gravity residual anomaly indicated the possibility of a salt canopy, quickly identifying areas where the seismic interpretation should be reexamined (figure 2).

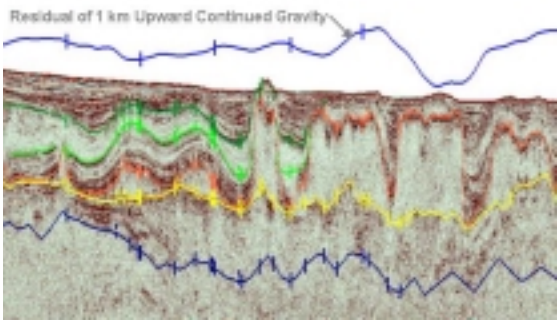

Figure 2. Correlation of Seismic and Gravity Residual

Depth to Magnetic Basement

Depth to magnetic basement calculations were performed using 2 techniques: profile based Werner deconvolution and as a regional check grid based Euler deconvolution. The resultant depth to basement surface (figure 3) was then used as input and integrated into the 2D gravity and magnetic modeling.

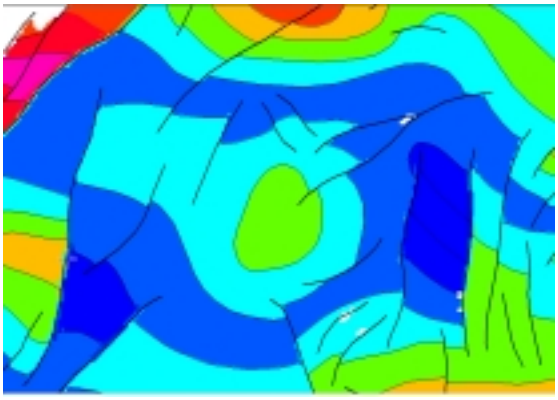

Figure 3. Example of Depth to Basement Map (blues-low, reds/oranges-highs)

Integrated 2D Seismic, Structural, Gravity Modeling

We generated a series of regional geoseismic x-sections as a baseline for detailed analysis of the gravity and magnetic data. Depth converted structural and stratigraphic interpretations of the seismic data were input to 2D gravity models. Basement horizons were added from the regional depth to basement analysis and a first pass lower crust and Moho contact were drawn at approximately 20 and 35 km depth.

An observed long wavelength major regional gradient was removed by adjusting the Moho surface prior to more detailed modeling of the salt. Results of the depth to Moho from the modeling were extrapolated between lines to yield a regional Moho grid which when combined with the regional depth to basement allowed calculation of the stretching factor (Beta) for basin modeling. The 3D basement interpretation was continuously refined and updated using results from the 2D models.

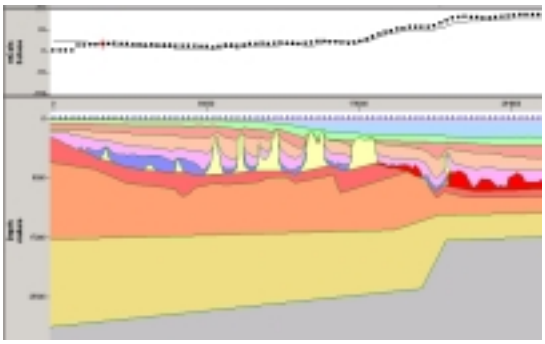

Figure 4. Modeling Example

Interaction with the Contractors and Project Team

One of the key elements contributing to the success of this project was the close interaction between the outside contractors, Brazil project team and the gravity and magnetic interpreter. Contractor work was focused on a particular product such as depth to basement or generation of initial 2D gravity models with regular interaction and reviews with the project team and in-house specialist. Remote access to seismic and gravity programs allowed staff in different locations to exchange maps, models and results in a timely and efficient manner.

Conclusions

Results of this project have and continue to greatly enhanced our understanding of the Brazilian margin petroleum system in many ways including:

1. Source – regional depth to basement has identified possible pre-salt depocenters.

2. Maturation- identification of relative depth of burial and crustal thickness.

3. Migration- identification of shape of pre-salt depocenters and possible migration pathways (basement highs, salt welds, etc.).

4. Identification of major basement elements, volcanics, salt, etc.

Acknowledgements

Gravity and magnetic data courtesy of Austin Exploration Inc and ARK Geophysics Ltd.

LA TRANSFORMADA ONDICULAR APLICADA Al ANÁLISIS SÍSMICOS DE REFLEXIÓN.

Manuel Lozada Z. [1] y Gerardo Ronquillo J. [2]
Instituto Mexicano del Petróleo
Programa de Yacimientos Carbonatados naturalmente Fracturados.
Eje Central Norte Lázaro Cárdenas 152
07730 México, D.F

[1] *mlozada @ imp.mx*; [2] *gronqui @ imp.mx*

Resumen.

Se presentará de una manera orientada el análisis tiempo-frecuencia y aplicará la transformada ondicular, como herramienta de procesamiento, análisis y evaluación de datos sísmicos de reflexión.

Las aplicaciones en el campo de la Geofísica del análisis Tiempo-Frecuencia (tiempo-escala o distancia-escala), comprenden, la compresión de datos, filtrado de ondas de tubo y análisis de señales sísmicas y más restringidamente aplicaciones en métodos potenciales (gravimetría y magnetometría). La teoría de la transformada ondicular en particular, se ha desarrollado aceleradamente en los últimos años en diversas especialidades y aplicado en la compresión y procesamiento de imágenes y filtrado óptimo de señales, entre otras.

2. Introducción.

La transformada ondicular ha despertado la atención de geofísicos en particular e ingenieros y matemáticos en general. Constituye una poderosa herramienta en disciplinas asociadas al análisis de señales transitorias y en el procesamiento digital de imágenes (Cody, 1992; Strang, 1989, 1995; Keyser, 1994; Foufoula and Kumar, 1994).

Considerablemente más eficiente, principalmente desarrollada por la comunidad involucrada con el procesamiento de señales, resultó la transformada ondicular discreta (DWT) basada en la codificación en sub-bandas. La conexión entre ondículas y codificación en sub-bandas fue puesta en evidencia por Mallat (1989).

Recientemente, algunos autores han aplicado las técnicas ondiculares en el procesamiento de datos potenciales. Estas aplicaciones incluyen la solución de problemas inversos de escalas considerables (Li and Oldengurg, 1997) y la interpretación de perfiles (Chapin, 1997; Chapin and Mosher, 1997), en la reducción y análisis de datos magnetométricos (Ridsdill-Smith and Dentith, 1999).

El análisis de ondícula se ha convertido en una herramienta utilizada frecuentemente para analizar variaciones localizadas de espectros de potencia que eventualmente pueden estar presentes en una serie de tiempo. Al descomponer una serie temporal en el espacio tiempo-frecuencia, es posible determinar tanto la variabilidad de los modos dominantes así como la forma como estos modos varian en el tiempo. La transformada ondicular es utilizada para analizar series de tiempo que contienen espectros de potencias no estacionarias a numerosas y diversas frecuencias.

En la primera fase de este trabajo se presentan los aspectos básicos relacionados con la transformada de ondícula con especial orientación hacia la geofísica y con énfasis a la sísmica de exploración. En la segunda parte se presentarán las aplicaciones, de esta herramienta relativamente nueva y poderosa, al análisis y procesamiento de datos de sísmica de reflexión.

2. **Localización tiempo-frecuencia.**

La transformada de Fourier de una función o señal estacionaria, puede verse como una combinación lineal de ondas senos y cosenos, esto es en términos de funciones armónicas. Estas funciones base tienen un soporte infinito en el dominio del tiempo y una localización perfecta en el dominio de las frecuencias, por consiguiente las funciones senosoidales están muy bien localizadas en el dominio de las frecuencias pero no lo están en el dominio del tiempo, ya que su soporte es de longitud infinita como consecuencia de su periodicidad. La transformada de Fourier proporciona la representación en el dominio de las frecuencias (número de onda) de procesos temporales, de señales o funciones que están definidas exclusivamente en el tiempo (espacio).

La magnitud del espectro de una señal, a una frecuencia particular, se obtiene de la distribuciones de las amplitudes presentes durante el intervalo total de existencia de la señal o durante uno o algunos periodos seleccionados, en contraposición a la transformada ondicular, la cual tiene la característica de efectuar la descomposición local tiempo-frecuencia y que permite estimar las variaciones dependientes del tiempo de las frecuencias instantáneas contenidas en señales no estacionarias, señales que quedan expresadas como una combinación lineal de ondículas.

3. Aplicaciones sísmicas.

En la Figura 3.1 se ilustra una perturbación sísmica y su correspondiente espectro de amplitud. Esta figura nos permite observar algunas características sobresalientes. No tiene una escala respecto a la cual

esta función esté definida. Esto es debido a que coeficientes significativos ocurren a muchas frecuencias.

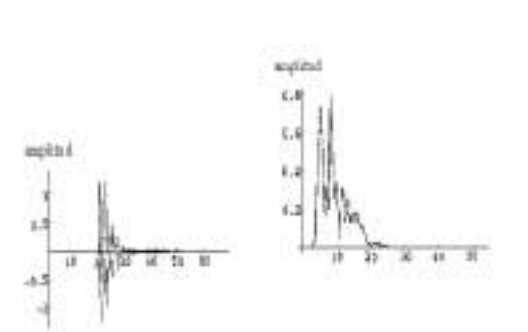

Figura 3.1: Perturbación sísmica y su espectro de Fourier.

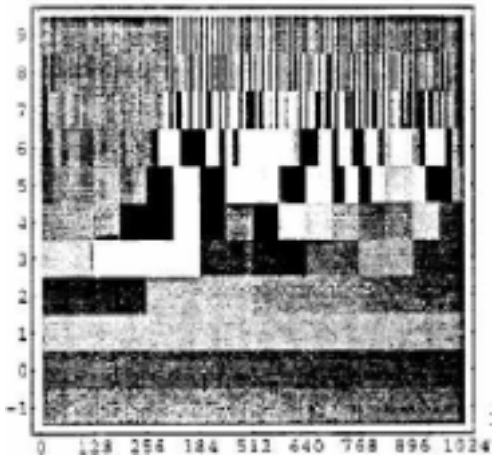

Figura 3.2: Densidad espectral (plano tiempo-frecuencia).

En la Figura 3.1 se ilustra el espectro o densidad espectral en el plano tiempo-frecuencia de la transformada ondicular del pulso sísmico y cuyo espectro de Fourier se ilustran en la Figura 3.2.

El punto más importante es el efecto de altas frecuencias que están predominantemente presentes a pequeñas traslaciones espaciales (respecto al origen) y los términos de baja frecuencia a grandes traslaciones espaciales. Sin embargo ésta información no está contenida en el espectro de Fourier. La gráfica de densidad espectral del pulso sísmico ilustra éstas características. Los coeficientes ondiculares se muestran en la gráfica de densidad espectral en el plano tiempo-frecuencia. El eje vertical representa la escala o resolución de la descomposición. Es análogo a la frecuencia. Por ejemplo, un valor de nueve en el eje vertical se refiere a una escala de resolución de 2^{-9} de la longitud total del conjunto de datos o números de datos. El eje horizontal representa la localización espacial. En este caso, el conjunto es muestreado a 1024 puntos, de aquí que sean 1024 posibles localizaciones. Notamos, sensiblemente, que a resoluciones bajas los bloques son más grandes. Los coeficientes se distribuyen en una escala de grises, indicados en tonalidades de grises; los negros corresponden a magnitudes menores que las tonalidades claras. Cada bloque representa un coeficiente ondicular del desarrollo.

Reconsiderando la ecuación, $h_{a,b}(x) = \sqrt{|a|}\; h_0\left(\frac{(x-b)}{a}\right)$ observamos que las translación están cubiertas por el parámetro b y las dilataciones por el parámetro a. Para pequeños valores de a $(a<1)$ la ondícula es una versión expandida de la función $\phi_{a,b}(x)$, que permite analizar los aspectos de las bajas frecuencias a cierta localización b. Para grandes valores de a $(a>1)$, la ondícula es una versión comprimida de la función $\phi_{a,b}(x)$, por lo cual permite analizar los aspectos de bajas frecuencias alrededor de la localización b. El parámetro de dilatación a permite amplificar los aspectos de altas frecuencias locales.

En las Figuras 3.3 y 3.4 respectivamente, perteneciente a este contexto, se presenta una sección sísmica sintética a profundidad y su correspondiente proyección en el sub-espacio de nivel de resolución 3. La capacidad de representación del contenido de altas frecuencias queda ilustrado. En la Figura 3.5 presentamos una traza sísmica con su representación ondicular en 7 niveles de resolución.

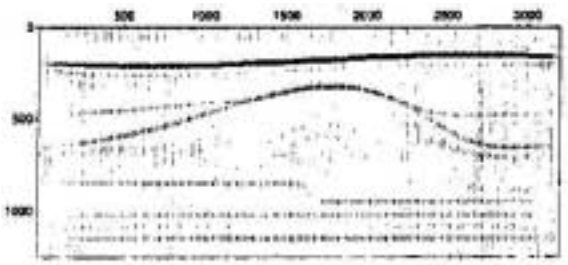

Figura 3.3: Sección sísmica sintética a profundidad.

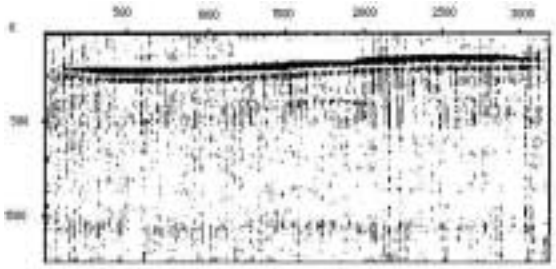

Figura 3.4: Proyección de la sección sísmica sintética a profundidad en el sub-espacio de nivel de resolución 3

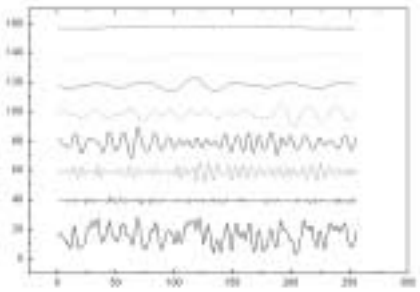

Figura 3.5: Traza sísmica y siete niveles de resolución.

En la Figura 3.6 presentamos la representación gráfica de una perturbación sísmica y la descomposición del mismo a los niveles de resolución 2 y 3 respectivamente.

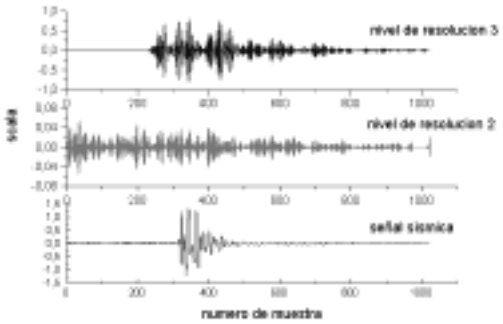

Figura 3.6: Perturbación sísmica y su descomposición a los niveles de resolución 2 y 3 respectivamente.

La aplicación de la transformada ondicular y del análisis de multiresolución en el pre-procesamiento y análisis de datos sísmico de reflexión cubre diversas aplicaciones. El antecedente directo de esta parte del trabajo está relacionado a Faqui et al. (1995) quien aplicó la transforma ondicular en procesos de filtrado antes y después del apilado, como también en la representación de la señal sísmica en el dominio tiempo-frecuencia y en los trabajos de Cohen, et al. (1993), como también Lozada M. y Ronquillo (1997a, 1997b), Ronquillo Jarillo, G. y Lozada Zumaeta, M.,(1997a, 1997b). En la Figura 3.7 se presenta una de una ventana perteneciente a una sección sísmica apilada y como consecuencia de la aplicación del análisis de multiresolución, la misma ventana sísmica al nivel de resolución 4.

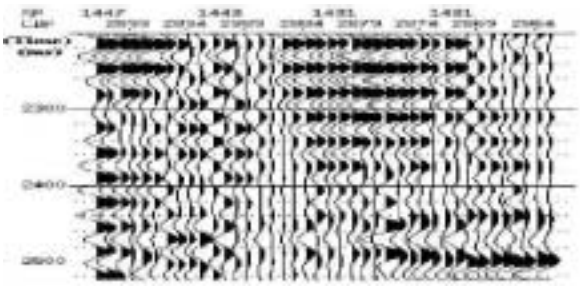

Figura 3-7:Análisis de Multiresolución. Descomposición de los datos al nivel de resolución 4.

4. Concluciones.

Las ondículas o representación ondicular tiene su propio campo de aplicación en el procesamiento digital de señales e imágenes. Puede utilizarse independiente o complementariamente a los métodos tradicionales del Análisis de Fourier.

Dado que las señales sísmicas en general son de carácter transitorios y oscilatorias por naturaleza, pueden ser eficientemente representarse por bases ondiculares.

5. Referencias y bibliografía.

Cody, Mac A., (April 1992), The Fast Wavelet Transform, Dr. Dobb's Magazine.

Cohen, J.K. and Chen, T. (1993), Fundamentals of the wavelet transform for seismic data processing, Tech. Rep. CWP-130, Center for Wave Phenomena, Colorado School of Mines.

Chapin, D., (1997), Wavelete transforms: A new paradigm for interpreting gravity and magnetics data: 67th Ann. Internt. Mtg., Soc. Expl. Geophys., Expanded Abstracts, 486-489.

Chapin, D., and Mosher, C., (1997), Method and appartus for identifying geological structures using wavelet analysis of potential fields: U.S. Patent 5 673 191.

Faqui, L., Nurul Kabir, M. M. and Verschuur, D. J., (1995), Seismic processing using the wavelet transform and the Radon transform: Journal of seismsic exploration, 4, 375-390.

Foufoula-Georgiou, E. and Kumar, E., (1994), (Eds.). Wavelets in Geophysicis. Academic Press.
Keyser, G., (1994), A Friendly Guide to Wavelets (Birkhauser), Boston.

Li, Y., and Oldenburg, D., (1997), Fast inversion of large scale magnetic data using wavelets: 67th Ann. Internat. Mtg., Soc. Expl. Geophys., Expanded Abstracts, 490-493.

Lozada Zumaeta M., y Ronquillo Jarillo, G., (1997a), Aplicaciones de la Transformada Ondicular en la determinación de atributos sísmicos en sismología de Reflexión. Resúmenes de la Reunión Anual de la UGM, Puerto Vallarta, Jalisco, México.

Lozada Zumaeta, M., y Ronquillo Jarillo, G., (1997b), Maximización de la relación señal/ruido en el dominio de la transformada ondicular. Resúmenes de la Reunión Anual de la UGM, Puerto Vallarta, Jalisco, México.

Lozada M., Ronquillo G., (1997c), Wavelet Transform and Seismic Attribute, International Geoscience Conference, Moscow.

Mallat, S., (1989), A theory for multeresolution signal decomposition, IEEE Trans. Pattern Anal. Machine Intell., 11, pp. 674-693

Ridsdill-Smith, T.A., Dentith, M. C. (1999), The wavelet transform in aeromagnetic processing, Geophysics, 64, 1003-1013.

Ronquillo Jarillo, G. y Lozada Zumaeta, M. (1997a), Atributos sísmicos y análisis de multiresolución aplicado a la delimitación de un yacimiento de Gas. Resúmenes de la Reunión Anual de la UGM, Puerto Vallarta, Jalisco, México.

Ronquillo, G., Lozada M., Navarro M., and Alcega H. (1997b), Seismic Attribute Applied to a Gas Reservoir in Sand, International Geoscience Conference Moscow.

Strang, G., and Nguyen, T., (1996), Wavelets and filter banks: Wellesley-Cambridge Press.

Ronquillo Jarillo, G. y Lozada Zumaeta, M., (1997a) Atributos sísmicos y análisis de multiresolución aplicado a la delimitación de un yacimiento de Gas. Resúmenes de la Reunión Anual de la UGM, Puerto Vallarta, Jalisco, México.

Ronquillo, G., Lozada M., Navarro M., and Alcega H. (1997b), Seismic Attribute Applied to a Gas Reservoir in Sand, International Geoscience Conference Moscow.

Magnetic, Gravity and Gamma-Ray Spectrometry Responses of Tectonostratigraphic Terranes in the Jaguaribe-SE sheet (SB.24-Z), Northeastern-Brazil

Roberto Gusmão de Oliveira, CPRM-Geological Survey of Brazil
Edilton José dos Santos, CPRM-Geological Survey of Brazil
José Maria Ferreira da Silva Júnior, CPRM-Geological Survey of Brazil
Carlos Alberto Cavalcanti Lins, CPRM-Geological Survey of Brazil

Abstract

A total field anomaly-magnetic grid, gamma-ray spectrometry data and gravity profiles have been correlated with geological data in the Jaguaribe-SE sheet (SB.24-Z, scale 1:500.000). Two major crustal segments characterise the precambrian area of Jaguaribe-SE sheet. The Patos shear zone limits this compartments as a first order boundary. Geophysical data has been confirmed the importance this shear zone as a crustal structure. Also, this correlation demonstrates that several shear zones; lithologic boundaries and tectonostratigraphic terranes have strong affinity with magnetic patterns and U, Th and K distribution. As a result of this integrated study, a consistent tectonic framework of this area has been constructed, as a tool for terrane analysis and metallogenic researches.

Introduction

This communication relates the results obtained from the integration of geophysical, geological, geochemical and mineral resources data of Jaguaribe-SE sheet (scale 1:500.000, Figure 1). The interpretation includes quantitative and semiquantitative geophysical modelling of geological bodies from airborne magnetic and gravity data. This Interpretation can be a useful tool for new information about rock units and reveal shallow and deep structures, as well as, supply regional geologists with 3-dimensional shape of the geological bodies and tectonic compartments.

Used Data

Geological: geological map of Jaguaribe-SE (SB.24-Z) sheet (Figure 1) in scale 1:500.000 (Ferreira & Santos, 2000).
Geophysical: magnetic grid (1x1 km) from South American Magnetic Mapping Project (GETECH & PGW, 1996); b) U, Th and K gamma-ray spectrometric grids (1x1 km) from Brazil Airborne Radiometric Mapping Project (PGW; CPRM & GSC, 1997); c) gravity profiles surveyed by CPRM during regional geological mapping (PLGB).
Geochemical: CPRM's databases (SEAG) of surveys performed since 70' years and analysed by optical emission spectrography.
Mineral Resources: CPRM´s databases of mineral occurrences (META) performed since 70' years.

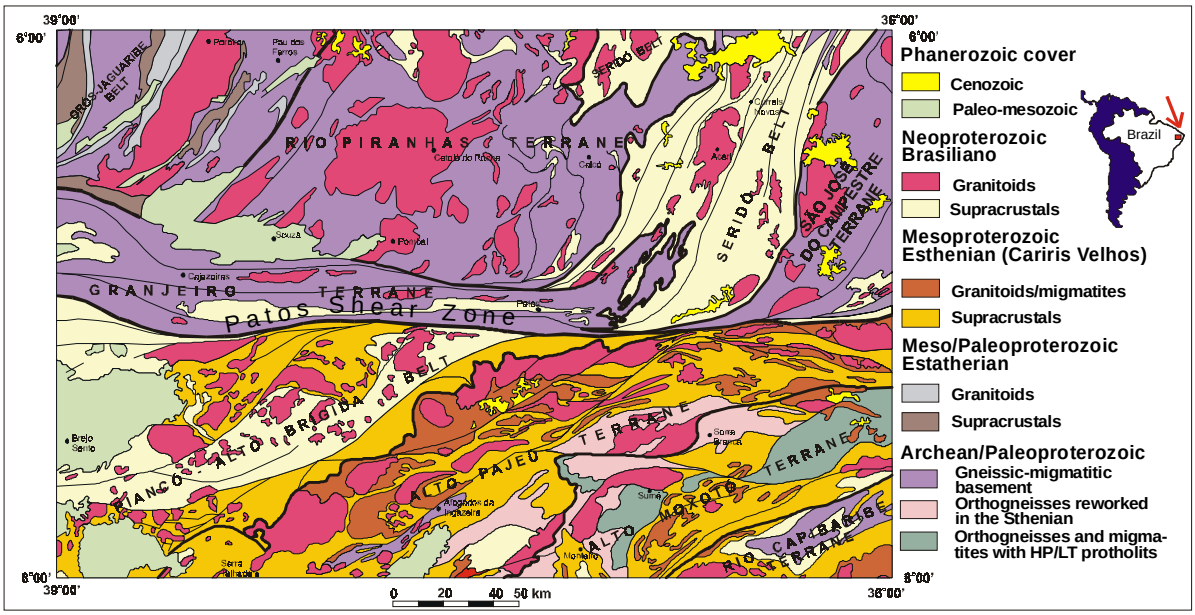

Figure 1 - Simply geological map of the Jaguaribe-SE sheet (SB.24-Z)

Geological Context

The precambrian area of Jaguaribe-SE sheet (Figure 1) is constituted for parts of Cearense, Rio Grande do Norte and Transversal tectonic domains. Those domains are limited by neoproterozoic expressive shear zones and subdivided into several tectonostratigraphics terranes (Santos et al., 1999). The Patos shear zone represent a first order boundary confirmed by geochronologic and geophysical data, separating two major crustal segments. The northern composed by a complex neoproterozoic thrust-and-fold belt, overthrusting Archean to Early Proterozoic terranes, comprising the Cearense domain; and the Rio Grande do Norte domain, characterised by a Brasiliano belt, implanted over Archean-Early Proterozoic terranes. The southern composed mainly by Meso-Neoproterozoic meta-volcanosedimentary terranes accreted to adjacent northern edge of the São Francisco craton.

Data Processing

By means of Oasis Montaj 5.0 (Geosoft), a grid of magnetic total field has been processed and filtered. The shallow (< 5 km) and deeper (> 5 km) sources maps have been performed by spectral analyses. Analytic signal and analytic signal phase techniques obtained enhancement of particular trends and magnetic bodies. Sources tops depths have been determined by means of Euler 3D deconvolution, for models (structural index) of contact, dike, sphere and cylinder. Airborne gamma-ray spectrometric grids have been stacked for generation of a ternary map distribution (U, Th and K). The gravity profiles have been interpreted by qualitative and semiquantitatives means (Talwani's algorithm).

The geological, magnetic and gamma-ray spectrometric data have been correlated with the Gold, Iron, Copper, Asbestos, Graphite, Vermiculite, Lead, Manganese, Scheelite and Emerald mineralizations. Also with geochemical anomalies of Gold, Iron, Nickel and Titanium.

Interpretation and Tectonic Correlation

a) Aeromagnetic Data

The interpretation and correlation were executed with basis in the tectonostratigraphic terranes framework (Ferreira & Santos, 2000) The data was analysed in the sense of verifying the geophysics validity of this framework and characterising your limits and/or sutures (Figure 2).

The Rio Piranhas terrane is characterised for anomalies with axis lengthened in the NE-SW direction. The wavelengths change between 10 and 25 km and amplitudes between 50 and 150 nT. Those anomalies are correlated with a big volume of acid orthoderived rocks. Gabroic rocks are correlated with elliptical anomalies (wavelength about 10 km) in the centre-east portion. At the Caicó (RN) city surrounding occurs a wide area (55-width km) with non-magnetic orthogneiss. This area is limited by strong magnetic alignments correlated with shear zones. In the Portalegre shear zone have some emerald and ruby mineralizations.

The Granjeiro terrane has a highly magnetisation zone, expressed in negative anomalous axis guided in the E-W direction. These anomalies have amplitudes of up to 200 nT, produced for a basic orthoderived rocks and a great volume of meta-volcanosedimentary supracrustal rocks. The limits between Patos and Malta shear zones are marked by abrupt magnetic contrasts with the adjacent terranes.

The Seridó belt has a highly magnetic substratum. This basement is expressed by anomalies with magnetic axis guided in the NE-SW direction. The limits are defined for shear zones related with abrupt magnetic contrasts, regarding the adjacent terranes. At the Cruzeta's city (RN) surrounding, a wide positive axis lengthened in the NE-SW direction, corresponds to thick packages of non-magnetic and of low grade metamorphic supracrustal rocks. This terrane is characterised by a number of scheelite mines.

The São José do Campestre terrane has small amplitudes anomalous magnetic axis (<50 nT) guided in the NE-SW and ENE-WSW directions. Those magnetic signatures correspond to Neoproterozoic sheared granite rocks. Elliptic anomalies with wavelength lower than 10 km and smaller amplitudes than 100 nT occurs at the inner part this terrane.

The Alto Moxotó terrane is marked by the presence of elliptic highly magnetic cores (negative axis with amplitudes of up to 200 nT). Those magnetic anomalies are related with relict of high-pressure granulitic to eclogitic facies rocks, preserved in mafic-ultramafic rocks along terrane boundary. Those rocks can represent a disperse suture, remnant of a mesoproterozoic oceanic crust. They form a belt in the NE-SW direction; limited in the south-east by Congo/Cruzeiro do Nordeste shear zone.

The Rio Capibaribe terrane is characterised by positive axis that reflect non-magnetic ortho and paraderived rocks. Locally occur lengthened anomalies, with amplitudes lower than 100 nT, correlated with low magnetisation lithologic bodies.

The Alto Pajeú terrane has two distinct aeromagnetic contexts. The first is a positive axis belt reflecting non-magnetic thick supracrustal package. The other is

a lengthened and sigmoidal magnetic anomaly belt in a NE-SW direction, correlated with outcrop of alkaline plutonic rocks (Syenitoid Line). Those anomalies have maximum amplitudes of 100 nT and wavelengths lower than 15 km. The Alto Pajeú terrane has many gold mineralization in shear zones controlled structures.

The Piancó-Alto Brígida terrane also has two distinct aeromagnetic contexts. At south-east, a wide positive axis belt is related with the outcrop of a non-magnetic thick low metamorphic degree supracrustal rocks sequence. This sequence is interleaving with non-magnetic stocks and batholiths of neoproterozoic granitic rocks. Other belt, located to north-west, is limited by Patos shear zone. Granites and migmatite rocks outcrops are magnetically defined by positive and negative axis pairs, with amplitudes lower than 100 nT and wavelengths about 15 km.

b) Airborne Gamma-Ray Spectrometry Data

The gamma-ray spectrometry data analysis indicates that the potassium distribution has a clear contrast marked by Patos shear zone. In the north, it's observes a homogeneous distribution, with contents higher than 3,5%. This signature is caused by a great volume of calc-alkaline granites, porphiritic granites and granodiorites intrusions. This pattern is interleaving for low potassium areas, associates to the sedimentary coverage and gabro-dioritic rocks. Regarding to the adjacent units, shear zones are marked by trends of potassium or by abrupt fall contents.

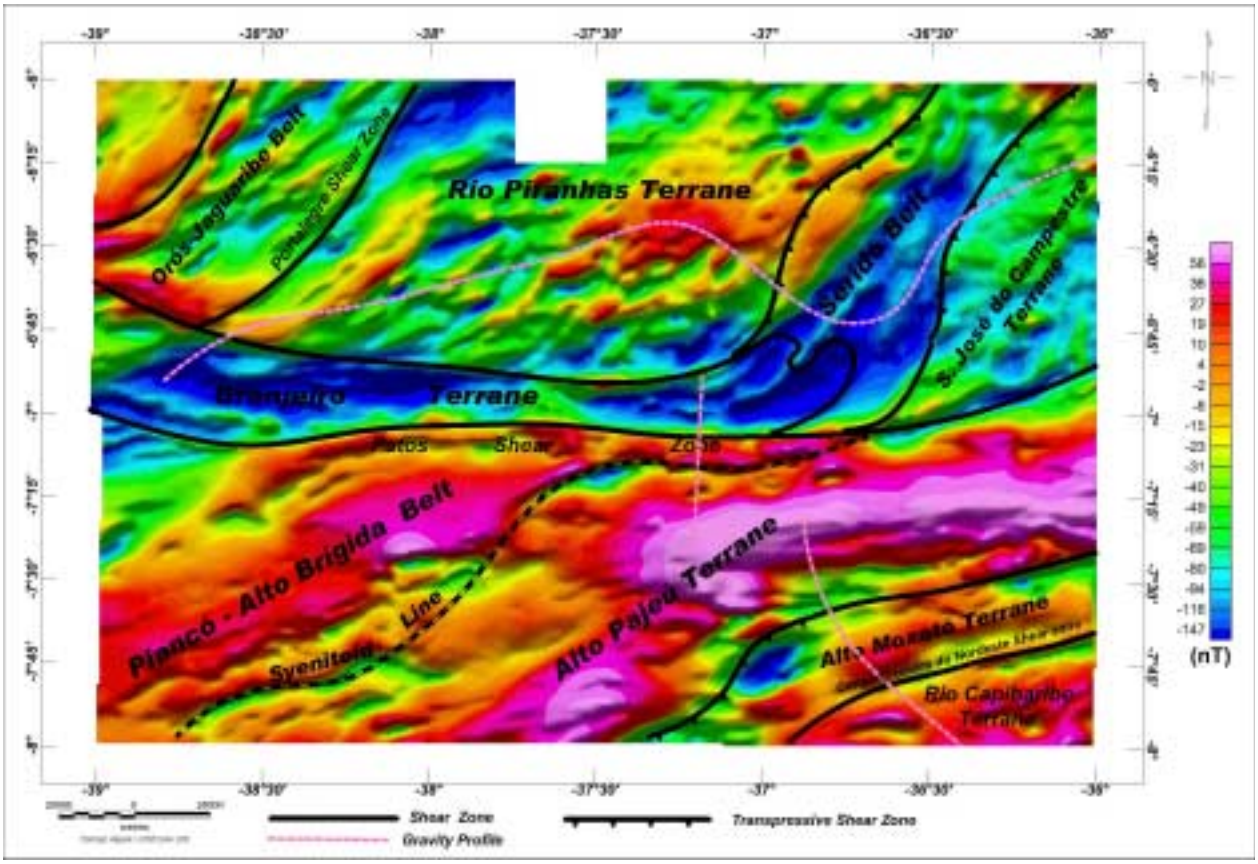

Figure 2 - Colourful shaded total field magnetic anomaly map with shear zones and tectonostratigraphic terranes.

At the south of the Patos shear zone, the potassium distribution is less homogeneous. Apparently that reflects a less intense level of granitization. Elevated contents (>3%) concentrate in trends related with tectonic limits, shear zones or batholiths and isolated syenitic intrusions.

This potassium distribution pattern doesn't repeat in the uranium map. In this case, it's concentrate in

related trends shear zones and in the innermost parts of the batholiths.
The thorium distribution has similar aspects of the uranium, however concentrating inside the bodies and geological structures limits.

c) Gravity Data and Tectonic Limits

The Patos shear zone importance as a deeper crustal limit is confirmed by a bipolar gravity signature (positive-negative) and by geochronologic data.
Two distinct gravity tendencies, separated by a highly horizontal gradient, have been detected in the gravity profile that crosses the Patos shear zone. The positive tendency corresponds to the terranes located at the north of shear zone and negative tendency zone is located at the south. Beyond those main tendencies, have been identified small positive and negative residual amplitudes, related to granitic rocks and metasedimentary units.
In the aeromagnetic data, the Patos shear zone is associated with a negative axis belt. The magnetic regional signal is clearly distinct from north to south of that shear zone. Deeper magnetised bodies (up to 20 km) dominate at the north. Low magnetisation bodies, related with thick bands of supracrustals and intensely granitized rocks, dominate at the south.
A long gravity profile allows the qualitative interpretation of five crustal blocks in the central region of study area. Their limits correspond to positive horizontal gradient stretches. Gravity Bouguer anomalies with maximum amplitudes of 20 mGal are correlated with upper crust structures. Three blocks are constituted for dense upper crust and two for very granitized upper crust. The blocks represented by a dense upper crust are Granjeiro terrane, the east part of Rio Piranhas terrane/Seridó belt (there are no possibility to separate these two terrane by gravity) and internal nucleus of the São José do Campestre terrane. This lasts one with 3.5 Ga archeans rocks. Granitized upper crust occurs in the west part of Rio Piranhas terrane and in the west margin of São José do Campestre terrane.
At the southern of study area, a gravity profile depicted a positive-negative anomalous pair, with amplitude of 40 mGal (peak to peak). The highly horizontal gradient corresponds to the limit between Alto Moxotó and Rio Capibaribe terranes. The profile contains a long wavelength component (about 150 km) that represents the regional gravity field. This signature is related with crustal thickening that increases gradually from north-west to south-east. The apex of this thickening corresponds to central region of the Rio Capibaribe terrane. The residual anomalies (amplitudes between 2 to 15 mGal) overlapped to this regional are related with upper crust heterogeneity. Consequently, has been separated three different crustal compartments. Tow of very granitized upper crust and one of dense upper crust. The compartments that represent very granitized upper crust correspond to the south margins of Alto Pajeú and Rio Capibaribe terranes. The compartment that represents dense upper crust corresponds to the Alto Moxotó terrane.

Conclusions

Correlation of magnetic, gamma-ray spectrometry and gravity data with geological data of Jaguaribe-SE sheet demonstrate to be a useful tool in the study of tectonic compartments and composition of the precambrian crust. The magnetic patterns and alignments present a good correlation with known tectonostratigraphic terranes and faults boundaries. Magnetic, gravity and geochronologic data confirm a deeper crustal limit at the Patos shear zone. Moreover, it's possible to localise unknown terranes and shear zones.

References

Ferreira, C. A. & Santos E. J., 2000. Programa Levantamento Geológico Básicos do Brasil: carta geológica, carta metalogenética previsional (folha Jaguaribe SE, SB.24-Z, escala 1:500.000). CPRM, Recife. (In press).

GETECH & PGW, 1996. South American Magnetic Mapping Project. Technical Report and Survey Atlas. 111 p.

PGW; CPRM; GSC, 1997. Brazil Airborne Radiometric Mapping Project. Technical Report and Survey Atlas. 30 p.

Santos, E.J.; Van Schmus, W. R.; Brito Neves, B. B.; Oliveira, R. G.; Medeiros, V. C., 1999. Terranes and their boundaries in The Proterozoic Borborema Province, Northeast Brazil. VII SNET, Lençóis, Bahia, Brasil, Anais, Sessão 2, p. 121-124.

Acknowledgements

I would like to thank CPRM-Geological Survey of Brazil for permission to publish this work.

Maximization of a Field Characterization Using 3D Seismic: Case Study, C-2 Reservoir, Block VIII, Occidental Basin, Lake Maracaibo, Venezuela.

R. Carrizales, E. Sifonte, T. Aguilar / Petroleo de Venezuela S.A.

Abstract

In this work a methodology is developed in which is applied the advances of applications of seismic 3D (Variance Cube, Seismic Attributes, Three Dimensional Visualization, incorporating Well/Seismic depth cross sections, and others) in the evaluation of the field, integrating it with the disciplines of the geosciences to obtain a static model of the producing reservoir. This study is of great help in the reevaluation and interpretation of areas currently producing and also gives better definition and characterization of remaining prospective reservoir areas.

The study area is from the middle portion of Lake Maracaibo, Western Basin of Venezuela, more specifically in the Seismic 3D cube of Block VIII. The dataset cube embraces an area of 265 Km2; comprised by approximately 700 Inlines and 1400 Crosslines. Later in the project the study was further detailed in a smaller cube of 112 Km2 in order to study the C-2 reservoir of Block VIII. In total there were 152 wells loaded in the database (Fig. 1).

Within the regional stratigraphic column, there were interpreted four (04) seismic reflectors ranges from the Cretaceous period into the Miocene. And these reflectors show strong acoustic impedance and are of great areal extension, which are: Socuy member of the Creatceous Colon Formation, Guasare Formation (Paleocene), Top of Eocene Uncomformity and the Rosa Formation (Miocene). Subsequently the C-2 and C-3 Sands of the Eocene Misoa formation were interpreted in VIII Block.

The objective is to study the C-2 Sand of Block VIII which contains 190.7 MMBLs POES (original oil in place), remaining oil in place of 11.7 MMBLs, and accumulated production of 33.4 MMBLs with an oil retrieval factor of 23.65 % and oil of gravity of 27.5° API. This sand is segregated into six (6) separate reservoirs in this block.

The application of this methodology helped in finding new develoment prospects and increased the net recoverable barrells in the area of

Methodology

· Search, sort and quality control of information.
· Evaluate and load well with Check-Shot.
· Generation of Synthetic Seismograms.
· 3D visualization.
· Interpretation of horizons and faults.
· Generation of maps in time/ attributes
· Evaluation of Slice Time/ Flattening of horizons.
· Maps of thickness in time, isocron
· 3D visualization analysis
· Maps in depth.
· Maps of quality sands.
· Stratigraphic Interpretation.
· Relationship of Seismic Attributes/ Petrophysics
· Reservoir description, pressure units, reserves calculation.

Seismic Analysis

Before beginning the seismic interpretation the well information and markers were analyzed and calibrated to correlate with the seismic reflectors.

Seismic/Well Calibration.

The processes of calibration is accomplished by the creation of synthetic seismograms, consisting of convolution of the sonic and density curves with the appropriate extracted seismic wavelet, and the eventual matching of the geological marker with the correct seismic reflector.

Another processes of calibration are the time-depth curves with which the depths are led to double time of the seismic.|

Velocity Analysis.

The velocity analysis is performed from the conversion of seismic horizons from time to depth, generating a horizon velocity grid for each level integrated from the sonic logs as well as the borehole geophone check-shot data.

Map Generacion.

The maps in time, attributes, depth and sand quality were completed using the applications of Charisma, Indepth and CPS3 belonging to the GEOQUEST software platform.

In the initial part of the study, the seismic volume was generaded with the aplication of variance cube to define the main lineaments in the area, then four (04) regional reflectors were interpreted (La Rosa Fm, Eocene Unconformity, Guasare Fm and Socuy Member) from the Block VIII seismic cube. For each one of the interpreted horizons a map in time

was generated, after which is made an automatic interpolation (ASAP); with which the attribute maps were created: Amplitude, Dip, Azimuth and Correlation Coefficient. These attribute maps serve to define a better pattern of the structural features and main lineaments of the area (fig. 2 and 3).

Local Structural Framework.

The 3D seismic data of Block VIII were interpreted, from which was generated a seismic-structural model represented by two (02) patterns of principal faults, which cross a monoclinal structure type with gentle dips (4-5 degrees) toward the Southeast in the North end. In the Southern part there is major deformation and structural complexity. The creation of the structural model was refined and supported by seismic attributes of Dip, Azimuth and Edge Enhancement, as an addition to the interpretation of seismic Crosslines, Inlines and selected random profiles.

- The first system represents a transcurrent fault trending North Northeast-South Southwest with similar characteristics to the Icotea fault, which also shows additional faulting in the seismic in the perpendicular direction, normal displacement faulting and in some cases inverse displacement. This could be attributed to two factors: orogenic movements of which the basin was subjected or possibly to poor resolution of the seismic. This fault has regional expression and maintains the same lineament across the entire area. Dipping East in Block VIII, with the difference that the fault changes dip at the South end of the area (in Centro Lago Block), and dips toward the West, and there may exist a point of zero displacement between both blocks where it may have a scissor movement (strike-slip).

- The second fault pattern is composed of normal faults generally trending Northwest-Southeast and dipping toward the Northeast, although dip toward the Southwest was determined in some cases. The Southwest dip is evident on some faults on the West Side of the study area where the C-2 sands are productive. Some authors have highlighted both patterns as contributing to the entrapment of hydrocarbons in this field reservoir, as well as also playing a role in sedimentation (fig.4 and 5).

Local Stratigraphy.

The seismic/stratigraphic analysis of the C-2 reservoir of Block VIII started first with the seismic sections (regional and local) in order to identify the sedimentary groups and sequence boundaries, which allows the study to define the direction of sedimentation and measure the geometric relationships; onlap, downlap, toplap, and truncations.

For the next phase, a lithologic analysis from electrical logs was carried out throughout the stratigraphic sections. Five (05) stratigraphic sections were created in the East-West direction and four (04) in the Northeast-Southwest direction covering almost the entirety of the field. They used the tops C2MFS1 and C3MFS1 of the well CLD-04 loaded into the seismic database, and interpreted as maximum flooding surfaces (MFS) for this part of the study. The stratigraphic sections were integrated with the wells: CLD-24, CLD-15, CLD-12, CLD-04, CLD-53 and CLD-08 were used in extrapolating the correlation of these tops, using C2MFS1 as a stratigraphic marker to hang the sections.

Addicionally the lithologic analysis of well logs and sequence stratigraphy allowed the identification of two (02) flooding surfaces in order of deposition (FS2 and FS1) corresponding to shale intervals. The intervals determinated by this method were flooding surfaces and not maximum flooding surfaces because of the scarce core information present in the area, and they represent a maximum flooding from the sea in these intervals, although the readings from gamma rays and conductivity are relativelyhigh values. The total average thickness for the C-2 sand is 450 feet in the wells drilled on Block VIII. We can observe in the annexed sections the correlation of the surfaces as discussed (fig. 6).

After having identified the surfaces FS2 and FS1 in all the wells, the study proceeded to carry out correlations of internal parasequences between these surfaces and the maximum flooding surfaces, C3MFS1 and C2MFS1 respectively. It was posible to differentiate within the C-2 Sand from the base to the top the Highstand System Tract (HST) and Transgressive System Tract (TST) within local internal unconformities. Five (05) genetic sand units were differentiated, of which the UG-2 unit shows the best sand development, which is observed by vertical communication in the wells: CLD-04, CLD-07, and CLD-65.

Sedimentary Environment.

For the determination of the sedimentary environment in which the C-2 sands were deposited in Block VIII. The gamma ray curves were used in order to interpret log facies, as well as the core analysis of CLD-65 and the net sand thickness maps and percentage sand maps, which then identify source areas and direction of sedimentation of sand units. These maps were detailed into the principal production flow units in the

C-2 reservoir (UG-1, UG-2 and UG-3) and they were interpreted for depositional environment for each flow unit.

In general form the sedimentary environment of the C-2 shows preferencial transport of sands in a Northeast-Southeast direction. It has been interpreted as a nearshore environment with a sub-environment of coastal influence caused by tides. Following that is described the sub-environment associated with these sand bodies.

Relation of Seismic Attributes/ Petrophysics.

The seismic attributes generated during the project correspond to the attributes of surface and volume. The cross-plot displayed between these and the petrophysical parameters do not show a direct relationship. This could be due to the poor quality of the petrophysical data. The petrophysical data was done with the values averaged over whole sand intervals, and the seismic data was displayed in 8 bit format, which limited resolution.

The Total Amplitude maps are identified zones of high values, which were related to Sand Unit 2 (UG-2) with the sub-environmant interpreted for the unit. The Total Amplitude map represents a summation of the top of C2 and C3 seismic reflectors. The sand units show a better developed sand quality corresponding high amplitudes on the seismic, and these high amplitudes from the Total Amplitude map correspond to the areas of high oil production. (fig. 16)

Field Analysis And Production Behavior

For this study the information was used of:
Production Histories
Well Histories
Pressure Histories
Objective Depth of Production
Original Oil/Water Contact
Official production and structural map.

In agreement with analysis of actual pressures, the behavior of production and fluid distribution (aquifer intrusion) was found to be compartamentalized by structural framework into four proposed blocks; A, B, C, and D.

Calculation of Net Oil in Place (POES)

With the new structural frame mapped the net oil in place increased by 31MMBls and we were able to increase the recoverable reserves by 17MMBls. This is due to the increase of closure area and change of petrophysical parameters .

Conclusions

1.With the new seismic 3D interpretation and the integration of other geoscience disciplines, the new structural model is consistent with all the geologic and engineering data.

2. As a result of this study the net oil in place of the C-2 field increased from 190.7 MMBls to 221.4 MMBls for a better and more accruate field characterization.

3. The described Sand Unit 2 (UG2) presents the best petroleum sands in the area but locally the Sand Units 1 and 3 show some new prospectivity.

4. The C-2/C-3 Total Amplitude attribute map showed a good relationship between high seismic amplitudes and improved sand quality, which also corresponds to accumulated production in the wells, which allowed the identification of additional prospective zones.

5. 70% of the accumulated production of the field comes from four wells which are associated with the interpreted sub-environment and this map was used to recommend future locations.

6.The reservoirs defined in the area were compartmentalized for the new structural framework, pressures and the fluid distribution.

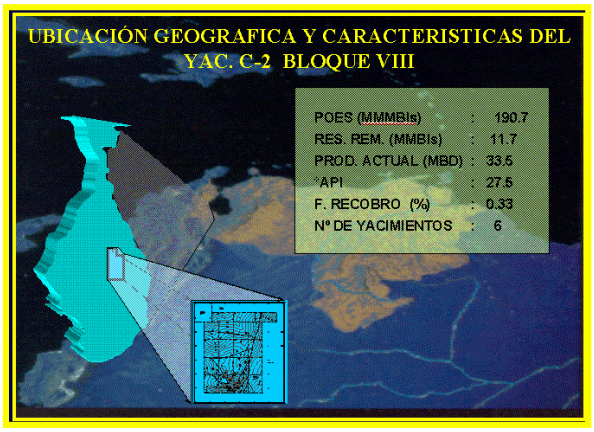

Fig. 1-Location of the area of study, in the central zone of the lake of Maracaibo, Block VIII, and some official characteristics of the location to study.

Maximization of a Field Characterization Using 3D Seismic: Case Study, C-2 Reservoir, Block VIII, Occidental Basin, Lake Maracaibo, Venezuela.

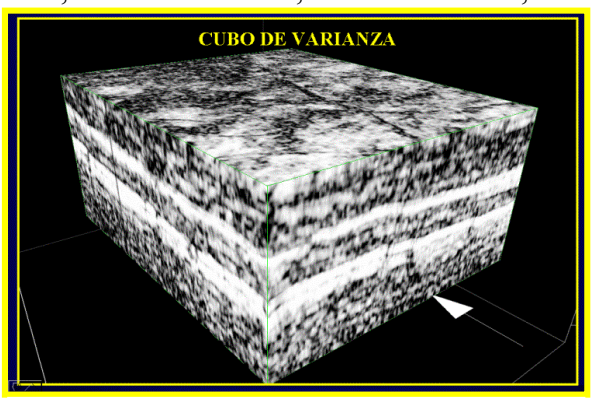

Fig. 2- Variance Cube that facilitates the interpretation of the faults and determine the general structural patterns to study.

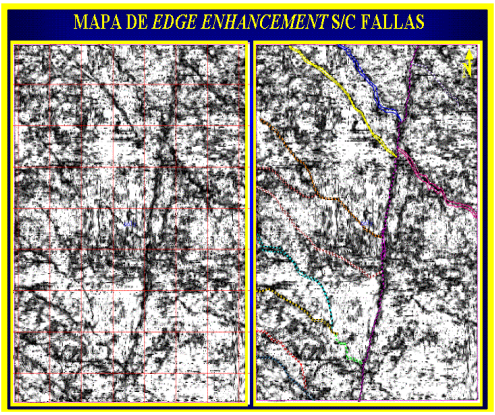

Fig. 3- The maps of structural attributes are another way of visualizing the structural features and main trends.

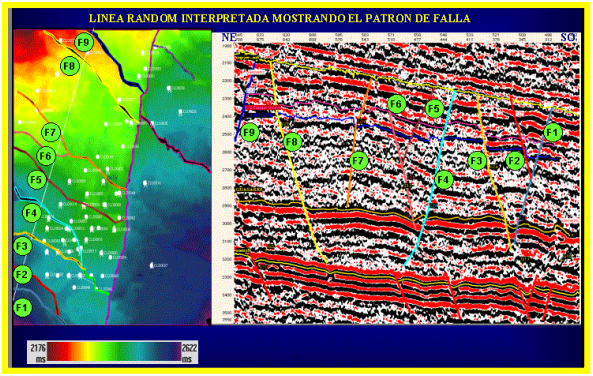

Fig. 4- Structural map in time with the interpreted faults.

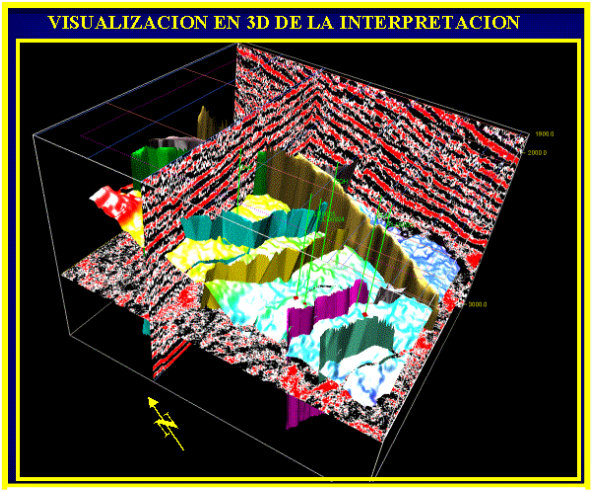

Fig. 5- A three-dimensional visualization which permits to integrate the whole information in order to obtain the better representation of the Structural Model.

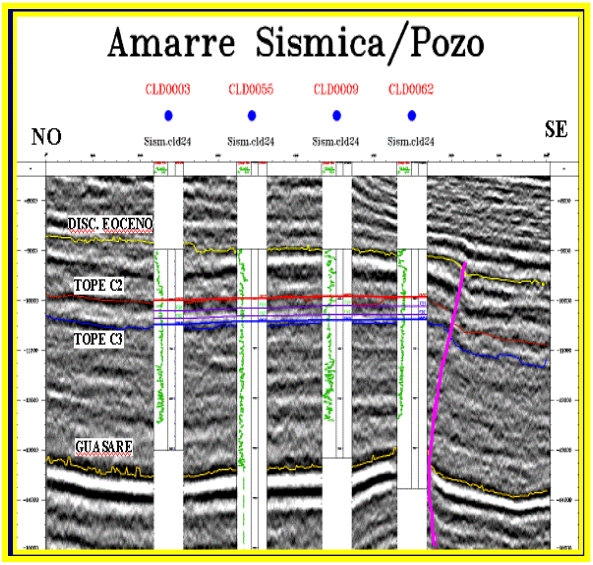

Fig. 6- Picture showing the benefit 3D Seismic for generation of structural sections, allowing to follow the markers of interest across the area.

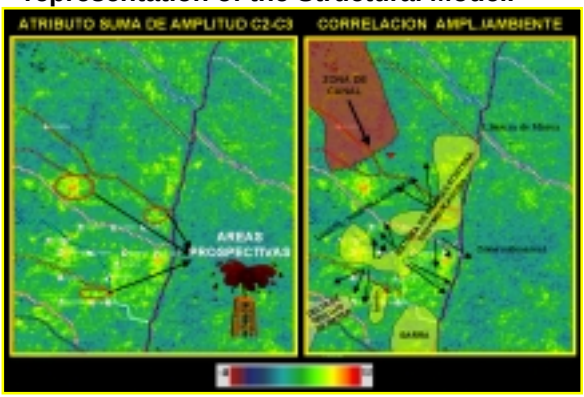

Fig. 7- The Amplitude map shows a relationship between the high amplitudes with the interpreted sub-environments and the best producing areas .

Processamento digital de dados aeromagnéticos, dos Projetos Uraricoera e Rio Branco, Estado de Roraima.

Solange dos S. Costa, UA/IG – UNICAMP, solange@ige.unicamp.br & Elisabete M. Pascholati, IG - UNICAMP, paschol@ige.unicamp.br

Abstract

Some digital processing techniques have been frequently used as a tool in aeromagnetic data to aid geological mapping. In this paper we evaluate images generated from application of filters in the frequency domain. This allowed the determination of six magnetic domain. These domains showed a good correlation with available geological information in the central portion of Estate of Roraima. New magnetic contacts were deduced and additional structures were verified with principal direction NW-SE and secondary NE-SW.

Introdução

Nas últimas décadas, amplos programas de levantamentos geológicos têm sido concentrados no Estado de Roraima. Contudo, devido ao difícil acesso, densa cobertura vegetal, elevado grau de intemperismo e falta de infra-estrutura, o conhecimento geológico atual nessa região ainda é bastante restrito, com grandes áreas mapeadas apenas em pequenas escalas. Devido a tais características, a aplicação das técnicas de processamento digital de imagens em dados aerogeofísicos vem contribuindo significativamente para um melhor entendimento acerca do quadro geológico dessa região.

Na década de 70, foram realizados dois aerolevantamentos no Estado de Roraima, um abrangendo a porção oeste, denominado de Projeto Uraricoera e outro na porção leste, denominado de Projeto Rio Branco (Figura 1). Desses dois projetos, apenas os dados do Uraricoera foram processados digitalmente, segundo Costa & Amaral (1998), Reis (1998) e Costa (1999). Quanto aos dados do Projeto Rio Branco, os mesmos foram utilizados no formato de mapas de contorno e publicados através do Programa de Levantamentos Geológicos Básicos do Brasil nas Folhas Paredão e Ajarani (Brandão *et al*., 1994). Nesta pesquisa serão apresentados os resultados homogeneizados, referentes aos dois projetos supra citados, apresentando a correlação e/ou divergências existentes entre as anomalias magnéticas e as informações geológicas disponíveis da área.

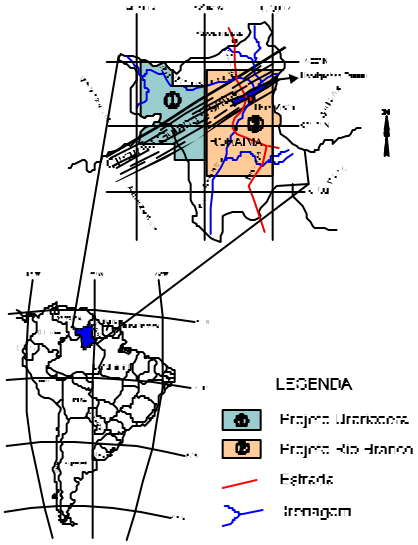

Figura 1 – Mapa de localização da área estudada

Contexto geológico e geotectônico

Geotectonicamnete, o Estado de Roraima está situado no Escudo das Guianas. O arcabouço geológico deste Estado registra núcleos antigos do embasamento, representado por extensos terrenos granito-*greenstone*, cinturões de rochas de alto grau metamórfico e granitóides relacionados ao Paleoproterozóico, além de uma ampla distribuição de granitóides, corpos básicos, ultrabásicos, anortositos e cobertura sedimentar intracratônica ao longo do Mesoproterozóico, culminando no Mesozóico com a reativação do Cinturão Guiana Central, originando o hemigrabem do Tacutu e a distribuição de corpos alcalinos e enxames de diques (Figura 2).

Processamento dos dados

Os procedimentos para o processamento dos dados magnéticos tiveram como suporte teórico, os trabalhos desenvolvidos por Roest *et al*. (1992), Milligan & Gunn (1997), dentre outros. Os dados aeromagnéticos foram interpolados aplicando-se o método de mínima curvatura com espaçamento estabelecido para o tamanho das células de 250 m x 250 m. A partir dessa interpolação, foram evidenciados vários ruídos periódicos, os quais foram

atenuados a partir da aplicação do filtro de coseno direcional. O passo seguinte à interpolação, consistiu na utilização de filtros implementados no domínio da frequência, tais como: redução ao pólo, susceptibilidade magnética aparente, continuação para cima, continuação para baixo, sinal analítico, fase do sinal analítico e derivadas direcionais.

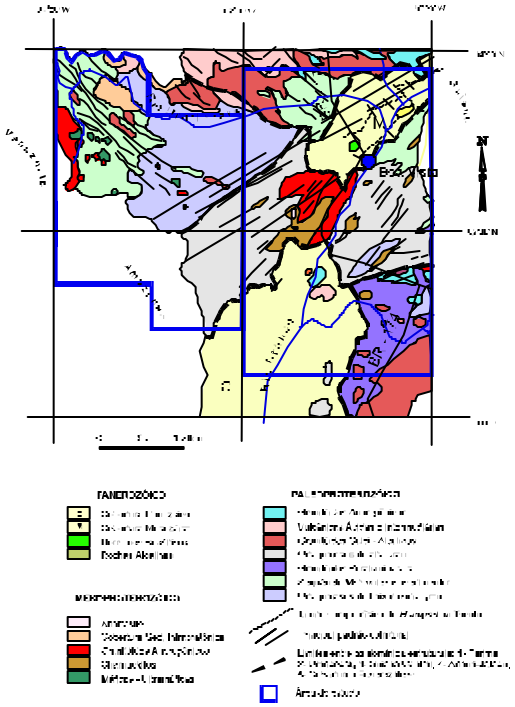

Figura 2 – Mapa geológico simplificado, segundo Reis & Fraga (1998).

Resultados e discussão

A integração entre os dados geológicos e as anomalias magnéticas foi feita a partir da sobreposição desses dados com as imagens geradas a partir da aplicação das técnicas acima mencionadas. Pôde-se observar algumas relações e também divergências entre as respostas magnéticas e as litologias da área(Figura 3).

Na imagem do sinal analítico, pode-se observar a amplitude das anomalias magnéticas variando de 0.000 nT/m a 7.444 nT/m, sendo os valores máximos representados na cor rosa e os mínimos na cor azul. A seguir, serão descritas as correlações entre as unidades geológicas mapeadas por Reis & Fraga (1998) e as fontes causadoras de tais anomalias:

a) Os valores mínimos com intensidade variando entre 0.000 nT/m a 0.039 nT/m, têm correspondência principalmente com os Ortognaisses de baixo a médio grau, localizadas na porção norte, e com as rochas da Sequência Metavulcanossedimentar, na porção oeste da área;

b) Aos valores intermediários (0.040 nT/m a 0.091 nT/m), associam-se na porção sudeste os corpos de Granitóides peraluminosos e os Ortognaisses de alto grau, na porção central os Charnockitos, e aos Granitóides Anorogênicos da porção central e oeste.

c) No intervalo interpretado como de valores máximos (0.092 nT/m a 7.444nT/m), alguns corpos mapeados como Máficas –Ultramáficas, porção oeste, coincidem com esse intervalo, além dos Derrames Basálticos, localizado próximo a cidade de Boa Vista.

Além das correlações existentes entre esses três intervalos de valores mínimos, médios e máximos, foram observadas várias anomalias com propriedades magnéticas semelhantes, dispersas de forma heterogênea por toda a área, como pode ser observado na Figura 4, indicando a existências de seis domínios magnéticos, distintos entre si, denominados de A, B, C, D, E e F, correlacionados a áreas até então, não individualizadas.

Com valores minímos, porém com variações de intensidades, foram delimitados os seguintes domínios: Domínio A - correponde ao Hemigrabem do Tacutu, porção nordeste da área. Domínio B – compreende as mesmas unidades da Figura 3, com evidente mudança no traçado da sua área de influência.

Nos valores considerados como médios, foram definidos os seguintes domínios: Domínio C – abrange os Ortognaisses a oeste da área, Seqüência Metavulcanossedimentar a oeste e norte da área, e os Granitóides Calci-Alcalinos a sudeste da região. Domínio D – está distribuído na porção sudeste, associado aos Granitóides Peraluminosos, na porção central aos Ortognaisses de alto grau e aos Granitóides Anorogênicos. Domínio E – correlacionado aos Charnockitos, na porção central e disperso por todo o restante da área.

Os valores máximos, delimitam o Domínio F – apresentam-se de forma bem distribuida por toda a área, além da delimitação das rochas Máficas-Ultramáficas e dos Derrames Basálticos (Figura 2), diversas contatos poderam ser inferidos

Para uma análise estrutural, foi aplicado sombreamento sintético nas direções de 45^o, 90^o, 135^o e 180^o, nas diversas imagens geradas. A Figura 5 representa o traçado de todos os lineamentos magnéticos obtidos após esse procedimento. A partir de tais feições estruturais foi gerado um diagrama de roseta (Figura 5), onde pode ser melhor visualizada a direção preferencial das estruturas de carater ruptéis traçadas, onde a direção preferencial é para NW-SE,

provavelmente vinculado ao Cinturão Parima e com direção secundária para NE-SW, vinculada ao Cinturão Guiana Central.

Referências bibliográficas

Costa, S. dos S.; Amaral, G., 1998, Processamento digital dos dados aeromagnéticos da Folha Urucuzeiro, Estado de Roraima. In: SBG, Congresso Brasileiro Geologia, 40, Belo Horizonte, Resumos Expandidos, p. 394

Costa, S dos S., 1999, Avaliação do conteúdo geológico em produtos de sensoriamento remoto da porção oeste do Estado de Roraima (Folha NA.20-V-D). Inst. de Geociências, Universidade Estadual de Campinas, Dissertação de Mestrado, 83 p.

Carvalho, A. S., 1997, Integração de Imagens de RADAR/JERS-1, TM/Landsat-5 e geofísicas para o mapeamento geológico da porção nordeste de Roraima, Brasil. Inst. de Geociências, Universidade de Brasília, Brasília, Tese de Doutoramento, 250 p.

Milligan, P.R., Gunn, P.J.,1997, Enhancement and presentation of airborne geophysical data. AGSO Journal of Australian Geology & Geophysics, 17 (2): 63-75

Reis, C. C., 1998, Estudo geofísico do oeste do Estado de Roraima e adjacências com base em dados aéreos de magnetometria e gamaespectrometria e sua aplicação geológica. Observatório Nacional, Rio de Janeiro, Dissertação de mestrado, 73 p.

Reis, N. J.; Fraga, L. M. B., 1998, Geologia do Estado de Roraima. Relatório inédito. Manaus. CPRM. 26 p.

Roest, W.R., Verhoef, J., Pilkington, M., 1992, Magnetic interpretation using the 3-D analytic signal. Geophysics, 57 (1): 116-125.

Agradecimentos

Gostariamos de externar nossos sinceros agradecimentos a Universidade do Amazonas, pela concessão da bolsa CAPES, para a primeira autora desta pesquisa, e a CPRM pela concessão dos dados aeromagnéticos dos projetos Uraricoera e Rio Branco.

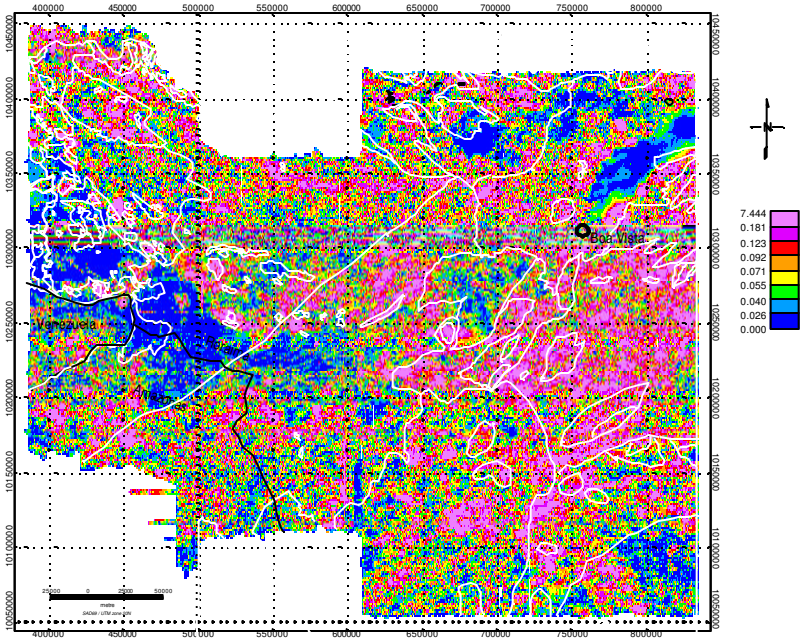

Figura 3 – Integração das informações geológicas com a imagem resultante à partir da aplicação do filtro de sinal analítico.

PDI de dados aeromagnéticos

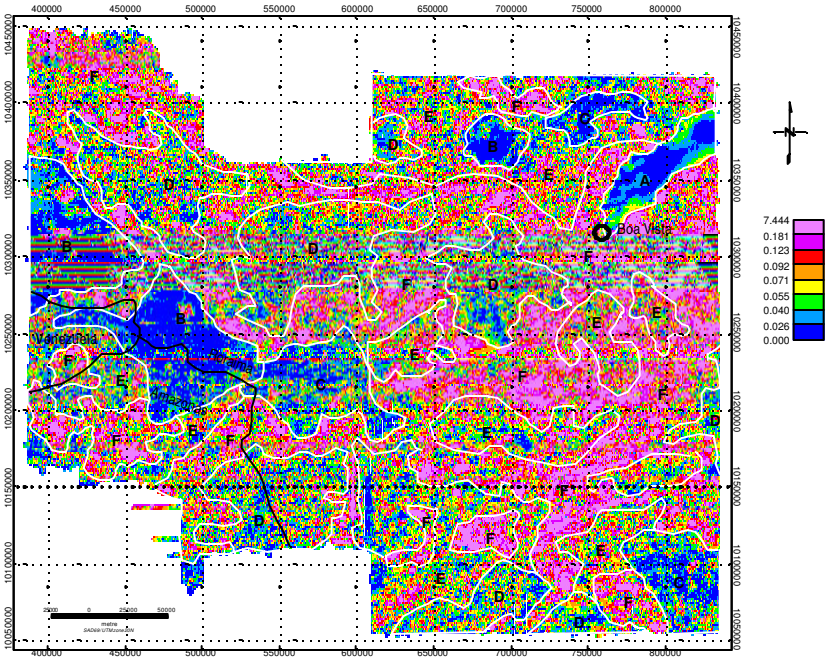

Figura 4 – Domínios magnéticos, traçados à partir da distinção existente entre as propriedades magnéticas da área.

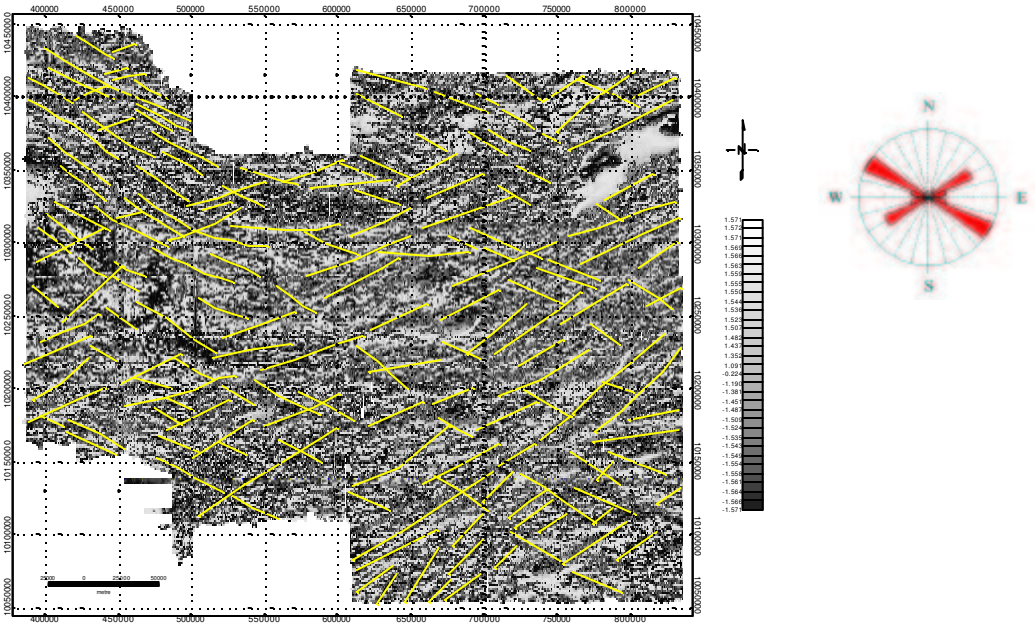

Figura 5 – Imagem da fase do sinal analítico em tons de cinza, com os lineamentos magnéticos evidenciados, em amarelo.

Sonic log prediction using artificial neural networks: Application to Namorado reservoir data, Campos Basin, Brazil

Mércia B. Costa e Silva (mbcs@civ.puc-rio.br), Rafael V. dos Santos (rafael@ele.puc-rio.br), Jorge Leonardo Martins (jlm@civ.puc-rio.br), Sérgio A. B. Fontoura (fontoura@civ.puc-rio.br)*
GTEP/PUC-Rio, Brazil

Abstract
A back-propagation artificial neural network (ANN) is used in order to predict P-wave sonic logs in well locations where such data are unavailable. Further predictions are also intended to be performed where there are no wells. The data set, to which the methodology was applied, covers a mature oil reservoir, the Namorado sandstone, in Campos Basin, Brazil. Basic seismic attributes were used for training the ANN. In this ongoing project, the construction of a 3-D P-wave velocity distribution over the area of the Namorado reservoir is envisaged. Studies of well bore stability are supposed to be a direct application of the results of the project, since improvement in the knowledge of the geologic features of the subsurface is also expected.

Introduction

Optimization of well drilling projects requires an accurate knowledge of rock properties along the trajectory of the wells. During the development stage of an oil field, extensive use of data obtained from offset wells is done. However, such information is inappropriately manipulated since field-drilling experience represents the main source of knowledge. Ideally, both log and drilling data from offset wells should be treated, in a rational manner, in order to generate a model capable of providing better information for drilling purposes.

A project called *Integrated Rock Characterization* is currently under way at the Laboratory of Computational Geosciences of the Pontifícia Universidade Católica do Rio de Janeiro, LGC/PUC-Rio, aiming at establishing a geomechanical model of the crust to be used for drilling purposes. Both geostatistical and artificial intelligence tools are being used for generating such a model. In this paper we present the first set of results generated by using the data set collected over the Namorado oil field, Campos Basin, Brazil. The Namorado data were provided by the Brazilian Agency for Petroleum (ANP).

A back-propagation ANN scheme was used throughout the paper for the generation of P-wave sonic logs. Seismic attributes from a seismic trace in a nearby 2-D seismic line were used in training the ANN. The results seem to indicate that the used ANN represent a feasible methodology to be used with exploratory wells when there are no offset well data for well planning.

Philosophy of ANNs

Neural computing has emerged as an important programming paradigm that attempts to mimic the functionality of the human brain. This area has been developed to solve demanding pattern processing problems, like speech and image processing, which were intractable or extremely cumbersome when implemented using traditional computing (Hecht-Nielsen, 1989).

By analogy with the human brain, ANNs are highly parallel computing systems that rely on relatively simple processors in dense arrangements of interconnections (Treleaven et al, 1989). In their computational implementation ANNs must have an *input vector*, an *output vector* and any array of processors *layers* between each other, connected by *weighted* links (Figure 1). ANNs have demonstrated their ability to deliver simple and powerful solutions in areas that for many years have challenged conventional computing approaches.

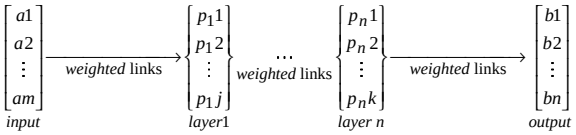

Figure 1: Conceptual network architecture.

Since an ANN is represented by *weighted* interconnections between processing elements, such weights are the parameters that actually define the non-linear function performed by the simulated neural network. The process of determining such parameters is referred to as *training* or *learning*, which relies on training patterns. Thus, ANNs are inherently *adaptive*, conforming to the imprecise, ambiguous and faulty nature of real-world data.

Back-propagation ANNs

The so-called back-propagation ANN algorithm corresponds to the most widely used neural network. This is due to its relatively simplicity and its universal approximation capacity (Hornik et al, 1989). The back-propagation algorithm defines a systematic way to update the synaptic weights of multi-layer networks (multi-layer perceptrons or MLPs). The

supervised learning is based on the gradient descent method, which minimizes the global error on the output layer.

The back-propagation algorithm is performed in two stages (Haykin, 1999): feed-forward and feed-backward. In the first phase, the inputs are propagated through the layers of processing elements, generating an output pattern in response to the input pattern presented. In the second phase, the errors calculated in the output layer are then back propagated to the hidden layers where the synaptic weights are updated in a process of error reduction. This learning process is repeated until some application-dependent user-defined criterion is reached for all patterns in the training set.

The definition of the network size, that is, the number of hidden layers and of neurons in each layer, is a compromise between generalization and convergence. Convergence is the capacity of the ANN to learn the patterns on the training set, while generalization is the capacity to respond correctly to new patterns. The idea is to implement the smallest network possible, so that it is able to learn all patterns and, at the same time, provide good generalization.

Error Measures

Several error measures are used to evaluate the ANN performance in an approximation problem. For this purpose, the *mean absolute percentage error* (MAPE), given by

$$MAPE = \frac{1}{n}\sum_{t=1}^{n} \left| \frac{d_t - e_t}{d_t} \right| \qquad (1)$$

and the *mean absolute deviation* (MAD), expressed as

$$MAD = \frac{1}{n}\sum_{t=1}^{n} | d_t - e_t | \qquad (2)$$

were used for assessing the results presented herein. In both previous equations, n stands for number of tested points; t indexes a particular data being tested; d_t is the desired output (i.e., the data itself) and e_t represents the ANN predicted result. In assessing the results, MAPE was able to give us the error percentage of our predictions, and MAD furnished the level of deviation of our P-wave velocity logs.

Methodology

Some information were missing in the Namorado data set. There were no prestack data available and no processing history of all seismic sections. Moreover, the well logging data contained information only from the reservoir zone. Yet, the absence of some sonic logs suggested the use of ANNs for predicting such information. This was performed in a very similar way as reported in Lira and Pinheiro (1999). Log properties of surrounding wells were then used in ANN training, in order to simulate P-wave sonic logs where their absence was identified. Further to the excellent results (not shown here) obtained with such a procedure, we decided to combine sonic log with seismic attributes to perform estimation of sonic logs via ANN (Russel et al, 1997) where no such data were available.

All ANN prototype implementations were made with MATLAB software. A single hidden layer *back-propagation* ANN was chosen to our application (Figure 2), and at the training phase an "early stopping" method was held, that is, a random validation portion of the training set was kept apart to evaluate the network accuracy after each epoch. The lower error ANN at the validation portion was kept as the result of the training procedure. We ran different network topologies to tune parameters like learning rate, kind of pre-processing data normalization and number of hidden layer neurons. The chosen ones presented both low validation error (< 10%) and smooth training curves. We set 35 processing elements in the hidden layer and used the z-score data normalization.

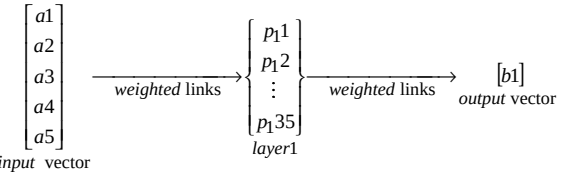

Figure 2: *"5 – 35 – 1"* network architecture.

The training data set used in our ANN experiments were formed by the P-wave velocity log at the chosen well location, and the nearest seismic trace at the same well location with its corresponding basic seismic attributes (Russel et al, 1997). The velocity log was constructed by selecting the main geologic features along the seismic line near the wells (Figure 3). The seismic attributes for such a trace were chosen as follows (Taner, 1992):

- *Trace envelope*: The total instantaneous energy, computed as the modulus of the complex trace;
- *Instantaneous phase*: The argument of the complex trace, is the best indicator of lateral discontinuity;
- *Instantaneous Frequency*: The time rate of change of phase, Corresponds to the average frequency of the power spectrum of the seismic wavelet.

The amplitude of the seismic trace was also used in ANN training, since these events are directly

linked to lithology variations in a true-amplitude seismic section. The last input was the time corresponding to each training point. P-wave sonic log were required to be the output of the ANN. The use of a complete sonic log in the ANN training process was crucial for performing the necessary time-to-depth conversion, which was calculated automatically by the Hampson-Russel software (Geoview).

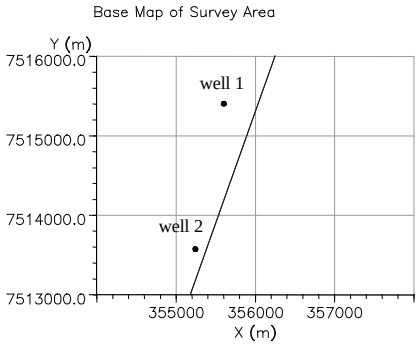

Figure 3: Location of the data, including the seismic line and the corresponding wells used in ANN training and prediction.

Application to Actual Data

The data used in the simulation of P-wave sonic logs through the methodology described previously is from Namorado field (Campos Basin). We made use of a 2-D high-resolution time-migrated seismic line and well log information from two nearby wells (Figure 3).

Only partial information of the sonic log in Well 1 was available, and no information of the same log type in Well 2. Thus, for testing purposes, construction of complete P-wave logs was performed for both wells. To this end, the main geologic features along the seismic line near the boreholes as well as information collected from the literature were interpreted. For the Well 1, the velocity profile is represented in Figure 4, and in Figure 5 for Well 2. Note that only a small part of the sonic data was added to the sonic log of Well 1.

Two strategies, slightly different from those used in Lira and Pinheiro (1999), were chosen for simulation of the corresponding sonic log via ANN at Well 1 and Well 2. The cited authors considered only density and porosity logs as the training set for the ANN. As mentioned previously, basic seismic attributes also took part in the training process of the ANN used in the present experiments.

The description of the first strategy starts as follows. Top and bottom parts of Well 1 were used in training the ANN, while validation was performed with the middle part of the constructed sonic log. The outcomes obtained with this procedure are shown in Figure 4. For this case, the error measures are: MAPE = 9.37 *%*, and MAD = 224.35 *m/s*. The prediction of Well 2, using Well 1 as the training set, represented the other strategy. For this situation, MAPE = 12.30 *%* and MAD = 260.88 *m/s*, and the results are shown in Figure 5. Clearly, high-frequency components of the raw seismic attributes, introduced in the training step, influenced the predictions. Median filters (Bednar, 1984) were then applied to such predictions

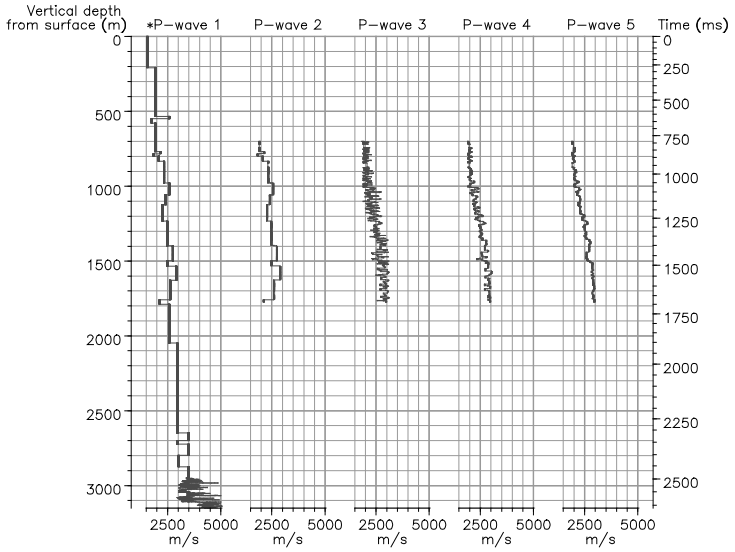

Figure 4 – Results from strategy 1: P-wave 1 is the constructed sonic log at Well 1; P-wave 2 is the part used in ANN validation; P-wave 3 is the simulated sonic log at the well location via ANN; P-wave 4 is the median-filtered version of P-wave 3 (11 points); and P-wave 5 is the median-filtered version of P-wave 3 (21 points).

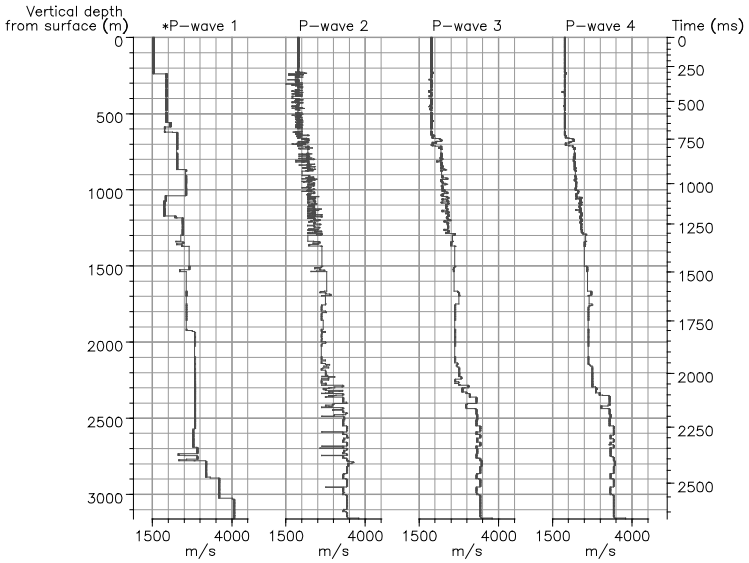

Figure 5: Strategy 2. P-wave 1 is the constructed sonic log at Well 2; P-wave 2 is the simulated sonic log at the well location via ANN; P-wave 3 is the median-filtered (11 points) version of P-wave 2; and P-wave 4 is the median-filtered (21 points) version of P-wave 2.

as an attempt to deal with smoother sonic logs. Improvement of the predictions after filtering application can be seen in Figures 4 and 5.

Final Comments and Conclusions

The joint use of P-wave sonic log information and seismic attributes in the training set of a properly defined back-propagation ANN was crucial in predicting P-wave sonic logs farther away from the data. Results can certainly be improved if a full sonic log is used in the ANN training set. By applying the same methodology, other log properties such as density and porosity can also be predicted. Although a vertical P-wave sonic log is predicted in the experiments shown above, the extension of the methodology to non-vertical sonic log predictions can be performed straightforwardly if a 3-D seismic data set is used. The next step to be pursued within the *Integrated Rock Characterization* project is the joint application of both ANN and geostatistical schemes to generate an improved geomechanical model for drilling purposes.

Acknowledgements

The authors wish to express their gratitude to ANP for releasing the Namorado field data, to CNPq/RHAE and to CAPES for financial support.

References

Bednar, J. B., and Watt, T. L., 1984, Alpha-trimmed means and their relationship to median filters, IEEE Trans. on Acoust., Speech and Signal Process., ASSP-32, pp. 145-153.

Haykin, S., 1999, Neural Networks: A Comprehensive Foundation, Prentice Hall, Upper Saddle River, New Jersey.

Hecht-Nielsen, R., 1989, Neurocomputing, Addison-Wesley, San Diego.

Hornik, K., Stinchcombe, M., and White, H., 1989, Neural Networks, 2, 359.

Lira, J. E. M. and Pinheiro, J. E. F, 1999, Fluid Substitution Using Pseudo-Sonic Logs Generated by Neural Networks: A Modeling Study, 6th International SBGf Congress, SBGf26199.

Russel, B., Hampson, D., Schuelke, J. and Quirein J., 1997, Multiattribute Seismic Analysis, The Leading Edge, vol. 6, pp. 1439-1443.

Taner, M. T., 1992, Attributes Revisited, Rock Solid Images (Revised Sep. 2000, available at http://www.rocksolidimages.com).

Treleaven, P., Pacheco, M., and Vellasco, M., 1989, VLSI Architectures for Neural Networks, IEEE Micro, V. 9, No. 6, pp. 8-27.

Sparseness in inversion and processing

*Tadeusz Ulrych**

Abstract

This presentation deals with the concept of sparseness in inversion and processing with application, in particular, to the problem of signal to noise enhancement. This concept is most easily understood from a Bayesian point of view, where sparseness is introduced by means of a prior probability density function. The minimization of the resulting cost function which is, in general, non linear, results in a model, one of an infinity of possible solutions, that bears the stamp of parsimony.

I will, in the talk, present various examples where the sparseness constraint is used to considerable advantage. Foremost, of course, the famous maximum entropy power spectral method, that has recently been extended to include the computation of high resolution Fourier transform by Sacchi and Ulrych (1998). A parsimonious time series model is the special ARMA representation that leads to a Pisarenko spectral estimate and has been used by Sacchi and Kuehl (2001) in noise suppression. A recent sparse implementation of a hybrid Radon transform by Trad et. al (2001) is a good example of the special role that the choice of basis functions plays in the imposition of sparseness. Finally, I will discuss some results by Zhang (2000) of the application of a two dimensional wavelet to the signal to noise enhancement of seismic sections.

Introduction

In general, the linear or non linear inverse problem that we are faced with in most problems of interest to us, is an underdetermined one. The fact that an infinity of solutions exists should not, and does not, daunt us. Indeed, as is so well known, the problem is always regularized in some manner, the particular regularizer being the architectural signature of the resulting solution. We state the inverse problem as follows,

$$f(\mathbf{m}) = \mathbf{d} = \mathbf{s} + \mathbf{n}$$

where $f(\mathbf{m})$ could represent a linear or non-linear function of the model $\mathbf{m}$, $\mathbf{d}$ are the data and $\mathbf{n}$ represents the noise.

†University of British Columbia, Vancouver, Canada (UBC).

We now call upon Bayes:

$$p(\mathbf{m}|\mathbf{d}) = \frac{p(\mathbf{d}|\mathbf{m})p(\mathbf{m})}{p(\mathbf{d})} \qquad (1)$$

which is written in terms of the appropriate probability density functions or pdf's. Once we have computed $p(\mathbf{m}|\mathbf{d})$, of course, we have all the information that we require about the model $\mathbf{m}$.

Assuming, in standard fashion, the likelihood to be Gaussian and also assuming some knowledge of the data covariance matrix, $\mathbf{C}_d$, in terms of the data variances we obtain $p(\mathbf{d}|\mathbf{m})$ in a straight forward manner.

Now comes the question of assigning the prior probability of our model (Ulrych et al., 2001). This is where so much argument and confusion has arisen, needlessly in my humble opinion. Prior knowledge in the form of $p(\mathbf{m})$ is only used to suggest a particular population model to fit to the data. This choice is not cast in stone. If, after checking against the data, the prior appears unreasonable, it is discarded. For example, if the problem is to find a source wavelet, we may suppose that we know a priori that the model is smooth in a first derivative sense. Clearly, this would not be an appropriate supposition for a problem concerning the earth's reflectivity where an appropriate pdf might be heavy tailed.

The point is that $p\mathbf{m}$ is an expression of *information*, information which most of us use in everyday personal decisions that govern our lives. Bayes allows us to incorporate such information into our quest and we would indeed be remiss not to. Often, parsimony or sparseness, is a particularly useful prior concept that has very strong physical roots. Models that explain our data can be very complex but we should, perhaps, begin with the hypothesis that the fewest parameters that accomplish the task lead to most plausible initial results.

In this abstract, I will deal very briefly with two examples where sparseness is, in some manner, an issue of central importance. The first is the hybrid Radon transform (Trad et al., 2001) that attempts to separate signal in the form of hyperbolic events form coherent "linear noise". The second example has a purpose similar to the first, but the implementation is by means of a two dimensional wavelet where the concept of sparseness, I will argue, is implemented by the tailoring of the basis functions to the problem at hand.

A hybrid linear-hyperbolic RT

One application of the Radon transform (RT) is to map events with different curvature in the data space to different areas of model space, such that these events can be separated or filtered before returning to the data space. This ability of the RT is in practice diminished by the fact that data contain events with different shapes. Linear events due to ground roll (GR), for example, are superimposed on hyperbolic events from reflections. Both events cannot be simultaneously focused with the standard RT. Recently, Trad et al. (2001) have presented a hybrid Radon transform to perform a sparse representation in the model space of data containing events with different shape. The RT is performed by two operators, each one with a different set of basis functions, which we call a hybrid operator.

In both the linear RT (LRT) and the parabolic and hyperbolic RT (PRT and HRT) there is an operator that maps the model space to the data space, and its adjoint (or conjugate transpose) that performs the reverse mapping, from data to model. Whatever the shape of the basis functions, the RT can be defined in terms of summation along paths as

$$\mathbf{d} = \mathbf{L}\,\mathbf{m}\,, \tag{2}$$

where $\mathbf{d}$ and $\mathbf{m}$ represent the data gather and the Radon transform (model), respectively. The operator $\mathbf{L}$ can be applied frequency by frequency when the curve is time invariant (linear, parabolic, and pseudo- hyperbolic RT). Conversely, the time variant HRT operator has to be applied in the time domain, usually using sparse matrix techniques.

Strong linear events are often present in the data superimposed on the hyperbolic reflections. An appropriate forward modeling of these data is given by

$$\mathbf{d} = \mathbf{L}_1\mathbf{m}_1 + \mathbf{L}_2\mathbf{m}_2, \tag{3}$$

or equivalently

$$\mathbf{d} = [\mathbf{L}_1\ \mathbf{L}_2] \begin{bmatrix} \mathbf{m}_1 \\ \mathbf{m}_2 \end{bmatrix}, \tag{4}$$

where the forward operator is $[\mathbf{L}_1\ \mathbf{L}_2]$, and the adjoint operator is $\begin{bmatrix} \mathbf{L}_1^T \\ \mathbf{L}_2^T \end{bmatrix}$. These two operators, forward and adjoint, are all we need to solve for the model $\begin{bmatrix} \mathbf{m}_1 \\ \mathbf{m}_2 \end{bmatrix}$ using, for example, a least square conjugate gradient algorithm. The two components of the model, $\mathbf{m1}$ and $\mathbf{m}_2$, are the linear and pseudohyperbolic Radon transform spaces. In the examples shown here, $\mathbf{L}_1$ is the Linear RT operator that maps lines to points, and $\mathbf{L}_2$ is the pseudo hyperbolic Radon transform (PHRT) operator of Foster and Mosher (1992). This second operator has basis functions following the equation $t = \tau + pg(h)$, where $g(h)$ is a function of offset and depth. Once a particular depth is chosen, the PHRT maps hyperbolas with apex at this particular depth to points. Looking at the general system in equation (3) we could think of any combination of Radon operators. This kind of hybrid RT could be applied whenever the data have events with different shapes.

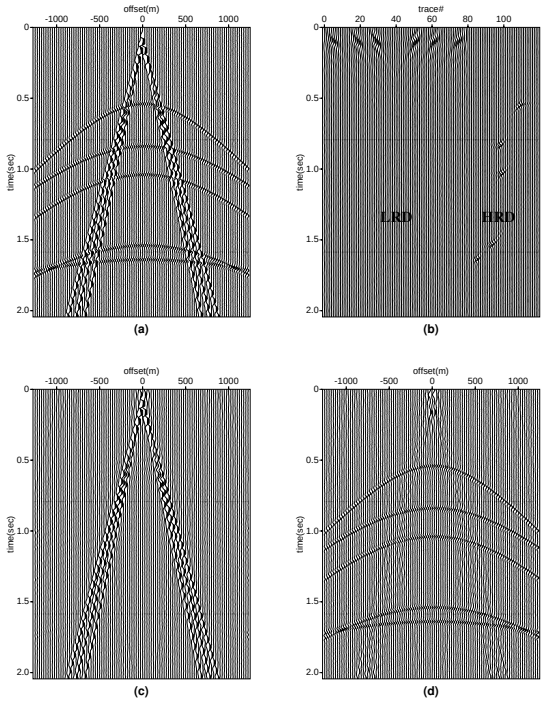

Figure 1: Hybrid inversion with sparseness constraints

The mapping of different events to different spaces where they can be separated is possible as long as the two spaces do not overlap, in other words, the basis functions are quite different. The separability is directly related to the sampling and aperture of the data, because imperfect information results in a lack of resolution, a lack that can often be diminished by appropriate constraints on the model space, or regularization.

The path to follow, then, is to design a transform, with a wide availability of basis functions suitable for a sparse representation of different events, and apply some sparseness constraint to overcome the lack of information in the model

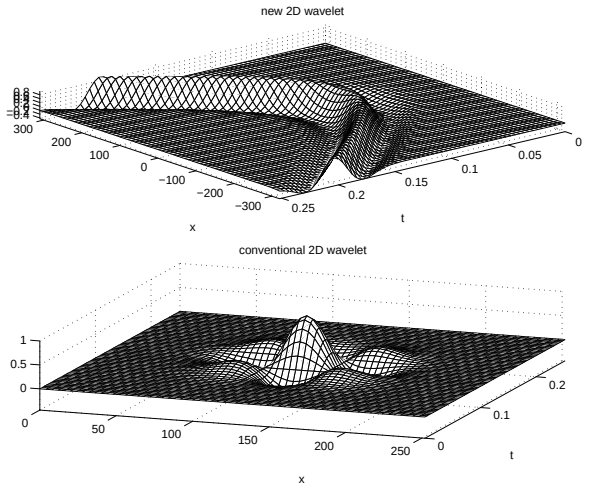

Figure 2: Images of the two kinds of wavelet

space. The approach of Trad et al. (2001) to this problem consists of the implementation of a hybrid Radon transform to map with maximum sparseness two different kinds of events: linear and hyperbolic.

The constrained inversion is solved by first defining a cost or objective function. The inverse Radon operator is found by minimizing the cost function

$$J = \|\mathbf{W}_d(\mathbf{L_1 m_1} + \mathbf{L_2 m_2} - \mathbf{d})\|_2^2 \quad (5)$$
$$+\|\mathbf{W}_{m1}\,\mathbf{m}_1\|_2^2 + \|\mathbf{W}_{m2}\,\mathbf{m}_2\|_2^2, \quad (6)$$

where $\mathbf{W}_d$ is a matrix of diagonal weights containing the inverse of the standard deviation of the data and $\mathbf{W}_{m1}, \mathbf{W}_{m2}$ are matrices of model space weights that we can set to enhance the resolution of the RT.

In applying the hybrid RT (Figure 1), the first operator maps the linear events to the first area of the model, the linear Radon domain (LRD), while the second operator maps the hyperbolic events to the pseudo hyperbolic space, the hyperbolic Radon domain (HRD) (Figure 1b). To avoid distortion of the linear events, NMO correction is not applied, therefore a PHRT approximates better the reflections than a parabolic RT. A mute applied in the hyperbolic space removes the signal, and after an inverse RT is applied, only the linear events are predicted (Figure 1c). The subtraction of the linear events from the data leaves the hyperbolic events intact. Only a small amount of noise remains, in particular at the top of the linear events (Figure 1d), probably because of non perfect destructive interference of the noise.

Physical wavelet frame denoising

In as much as the previous example is one where sparsness enters by virtue of the topography of the model, so, in this example, sparsness will be imposed by means of the design of a new wavelet frame. In fact, this approach represents the construction of a basis that most parsimoniously captures the essence of the signal.

Based on the nature of seismic data, Zhang (2000) has constructed a new wavelet frame for noise suppression. Since conventional wavelet denoising methods use a standard wavelet, they may be versatile, but certainly not optimal for seismic data. A frame is composed of atoms or wavelets, and the observed data can also be regarded as being composed of atoms. The more similar that the two kinds of atoms are, the more efficient is the signal extraction that can be achieved. Because of the trace to trace correlation that is exhibited by seismic data, denoising methods require a 2D geometry.

Conventional 2D wavelet denoising methods use a 2D wavelet that is created via a tensor multiplication of 1D wavelets and, consequently, only emphasis the vertical and horizontal connection between data. If the angle parameter is used, other directions corresponding to this angle can be taken into account.

The signal in seismic sections is, in general, located along a curve. For instance, in prestack data, signals may be assumed hyperbolic. It appears natural therefore to construct a 2D wavelet that is based on these specific curves. Since, for a hyperbolic function the independent variables are not separable and the orthogonal wavelet property no longer exists, frame theory is required in the design, a theory basic to the analysis and reconstruction of functions.

For a frame, the form of its atom ψ_k can be arbitrary provided that it satisfies the frame condition. For the wavelet frame, the atom ψ_k has the form

$$\psi_{s,b}(t) = |s|^{-\frac{1}{2}}\psi(\frac{t-b}{s}), \quad (7)$$

where s and b are the scale parameter and the translation parameter respectively. This atom also satisfies the admissable condition for a wavelet. The reconstruction formula becomes

$$f = \sum_s \sum_b < f, \psi_{s,b} > \widetilde{\psi_{s,b}}. \quad (8)$$

where $\widetilde{\psi_k}$ is the re-constructional frame. The 2D

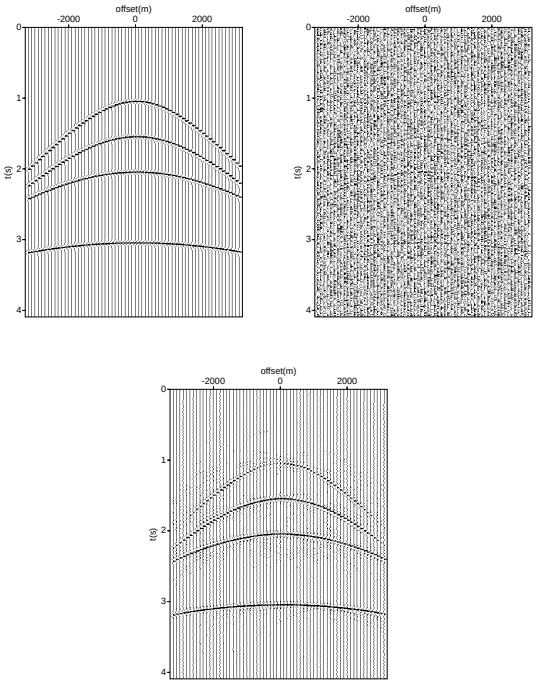

Figure 3: Denoising by PWFD

wavelet is

$$\psi_{s_x b_x, s_t b_t}(x,t) = |s_x s_t|^{-\frac{1}{2}} \psi(\frac{x-b_x}{s_x}, \frac{t-b_t}{s_t}). \quad (9)$$

For prestack seismic data, in time, the atom is a seismic wavelet, in space it is a hyperbola. The form of the real seismic wavelet can be highly variable, but a useful approximation is Mexican Hat wavelet. A conventional 2D wavelet is compared with the new wavelet in Figure 2. These two wavelets exhibit very different behavior with change of scale parameters. Specifically, both the shape and curvature of the new wavelet will change.

Denoting the data as

$$f = S + N \quad (10)$$

where S represents the signal, N the noise, we project f onto another space spanned by the basis ψ_{sb} and hope that S and N will be separable.

$$< f, \psi_{sb} >=< S, \psi_{sb} > + < N, \psi_{sb} > \quad (11)$$

Denoising is simple and effective. First, the data containing noise are projected onto the new seismic wavelet frame. Simple thresholding is performed and, finally, the data are reconstructed.

Figure 3 illustrates some results with synthetic data. The first panel shows the hyperbolic reflections, and the second panel illustrates this signal contaminated with random noise with SNR=1. The third panel shows the result of the new denoising techniqu present more detailed results, in particular for real data.

Conclusions

Regularization of inverse problems is well understood in a Bayesian context. the regularization is imposed by means of prior information, the form of which, shapes the solution. In this paper, we have emphasized and illustrated the role that sparseness plays in various scenarios, when imposed as a prior constraint. I would like to reiterate that sparseness can take many guises. Thus, model weights which enter into an objective function when chosen in accord with a Cauchy pdf, will lead to a sparse result. However, sparseness is also implicit in an image explained by a few principle components, or by a wavelet decomposition where only a few coefficients are of importance. Sparseness, to my mind, is intimately related to such concepts as parsimony and simplicity, concepts often related to science and beauty.

References

Foster, D.J., and Mosher, C.C., 1992, Suppression of multiple reflections using the Radon transform, Geophysics, 57, 386-395.

Sacchi, M., and Ulrych, T., 1995, High-resolution velocity gathers and offset space reconstruction: Geophysics, **60**, 4, 1169–1177.

Sacchi,M,D., Ulrych,T.J., and Walker, C., 1998, Interpolation and extrapolation using a high resolution discrete Fourier transform, IEEE Trans. on Siganl Processing, 46, No 1, 31-38.

Sacchi,M.D., and Kuehl,H., 2001, ARMA formulation for f-x prediction error filters and projection filter, Journal of Seismic Exploration, 9, 185-197.

Trad D., Sacchi M., and Ulrych M (paper in preprint). Journal of Seismic Exploration, A hybrid linear-hyperbolic Radon transform.

Ulrych,T.J., Sacchi,M.D., and Woodbury, A., 2001, A Bayes tour of inversion: A tutorial, Geophysics, 66, No.1, 55-69.

Zhang, R., 2000, Physical wavelet frame denoising, CDSST Annual Report, U. of British Columbia, 171-181, (submitted to Geophysics).

Using Geostatistical Techniques For Mapping A Reservoir In Eastern Venezuela

Carlos Selva,[1] Fred Aminzadeh,[2] Miguel Diaz B.,[1] Jesús Porras M.[1].
[1] Perez Companc S.A , [2] FACT/ dGB-USA

Abstract

A horizon-based statistical analysis method was used to map a reservoir unit in Eastern Venezuela. This resulted in about three-fold increase in the original volumetric oil reserve estimates. Communication between four previously identified individual units became apparent leading to a single reservoir unit interpretation. The study involved a data set comprised of 23 wells and a 3-D stacked migrated seismic data set covering approximately 80 Sq Km. The sedimentary column studied, consists of fluvial to shallow marine deposits interpreted as part of the Miocene Foredeep Sequence, going from 3rd to 5th Order Sequences. The R4U reservoir is interpreted as a 5th Order Low Stand System Tract (LST). Many statistically likely net-sand maps were generated by co-kriging the RMS amplitude from seismic with net sand values from well data. An average sand distribution map was generated from one hundred simulations with equal statistical weights. The net sand map showed a clear E-W channel shaped sand body that could not be identified previously using well data or seismic data alone. These results were used as an input to a proposal to drill two new horizontal wells in order to drain the upgraded recoverable reserves of 4.8 MMbbls.

Introduction

Lobo Field was discovered in 1,952. Since then, 23 vertical and 5 horizontal wells were drilled. A total of 25 hydrocarbon bearing reservoirs are present, with 7 of them contributing to 90% of the OOIP of 150 MMBbl. Reservoir units are between 5,500´and 6,400´ in depth with the oil gravity ranging from 10° to 16° API. The consensus was that by drilling horizontal wells parallel to structure would allow production under very limited draw-down. This in turn will lead to a limited deformation of the OWC, reducing water coning and sand production, thus increasing the life of the well. Also, because of the reservoir exposure with 1,000 feet of horizontal sections, it was expected to increase the productivity index by a factor of five with respect a vertical well, this being the main justification for drilling horizontal wells. Decision to further develop the field with horizontal wells has led to major improvements in the performance. Consequently, mapping techniques presented here, are of paramount importance to select future well locations.

Geological Setting

The Lobo field is located in the southern margin of the Eastern Venezuela Basin, in the Greater Oficina Area. The location map is shown in Figure 1. Is an extensional province with associated normal faulting trending N60°E.

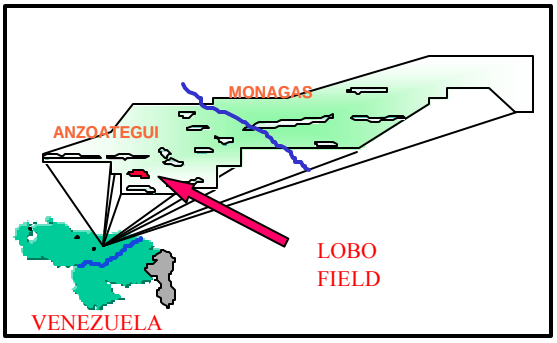

Figure 1. Location map of Lobo field

Locally, the trap is a homoclinal truncated by a normal fault, which provides the structural closure. Lateral closure is estimated as stratigraphic. Main reservoirs are located in the foot-wall block of the fault, showing a preferential NW-SE trend. Production becomes from Oficina and Merecure formations, developed in a complex fluvial-deltaic system. The units, from medium Miocene to Oligocene, interpreted as foredeep deposits, overly passive margin (Cretaceous) sedimentary rocks. Most reservoirs consist of interbedded sandstones and shales. Coal layers are common in the column.

The stratigraphic column of Lobo Field encompasses sediments of the first order passive margin and foredeep sequences. The passive margin sequence consists of interbedded cretaceous sands and shales that overly metamorphic and igneous rocks of the Guayana Shield. On top there is a major regional unconformity. The foredeep sequence, comprise siliciclastic sediments ranging from Late Oligocene-Early Miocene to Recent. Two second-order cycles were identified in this sequence: a transgressive cycle that contains the Merecure,

Oficina and Freites formations, and a regressive cycle that include Las Piedras and Mesa formations. The Late Oligocene-Early Miocene to Medium Miocene, is represented by the Merecure and Oficina formations, last conformed by interbedded deltaic to shallow marine sands and shales. The Merecure Formation showing a fluvial characteristic is interpreted as the lowstand phase of the foredeep sequence. Medium to Late Miocene is represented by the Freites Formation, with shaly sediments deposited in an outer shelf marine environment. For more details on the geologic setting and stratigraphy in this area see Parnaud et al (1995).

Detailed stratigraphy distinguished ten third-order sequences within the foredeep cycle. Reservoir units represent fourth to fifth order sequences. Each sequence can be separated into stratigraphic system tracts. These high order sequences are from local tectonic pulses and sea-level oscillations that affected the foreland basin. The R4U reservoir consists of fluvial-meandering channel deposits that include a sandy bed-load channel facies and an overbank. The channel shows a SW-NE trend.

The reservoir is composed of medium-grained, medium-sorted and unconsolidated sandstones with porosities in the range of 21% to 27% and permeabilities from 300 to 2,000 md. Average net pay thickness is 15 feet. Initial pressure of the reservoir is 2,550 psi, with a permanent datum of 6,070 feet. Water drive is the main production mechanism. Previous interpretations assumed four individual reservoirs and placed four different oil-water contacts in them. On the basis of this new reservoir characterization study it was determined that we have a single reservoir with a common oil-water contact estimated at 6,200 ft.

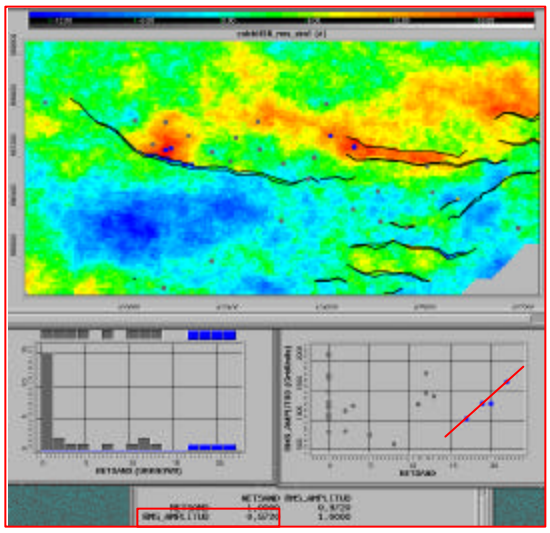

Figure 3. Histogram of the net sand and its correlation with RMS used to generate kriged net sand distribution.

Methodology

To accomplish the task of reservoir characterization (generating the porosity and thickness maps), we followed a conventional geostatistical method. Figure 2 shows the flow diagram of the process that was used to generate final results. Data preparation and examination is very important to do quality control and to get a general feel for the available data and to understand the ranges of different parameters. Examination of data is facilitated by use of different statistical tools such as histograms, cross plots, matrix plots and cross correlation as shown at the bottom of Figure 3. At the top section of

Figure 2. Flow diagram

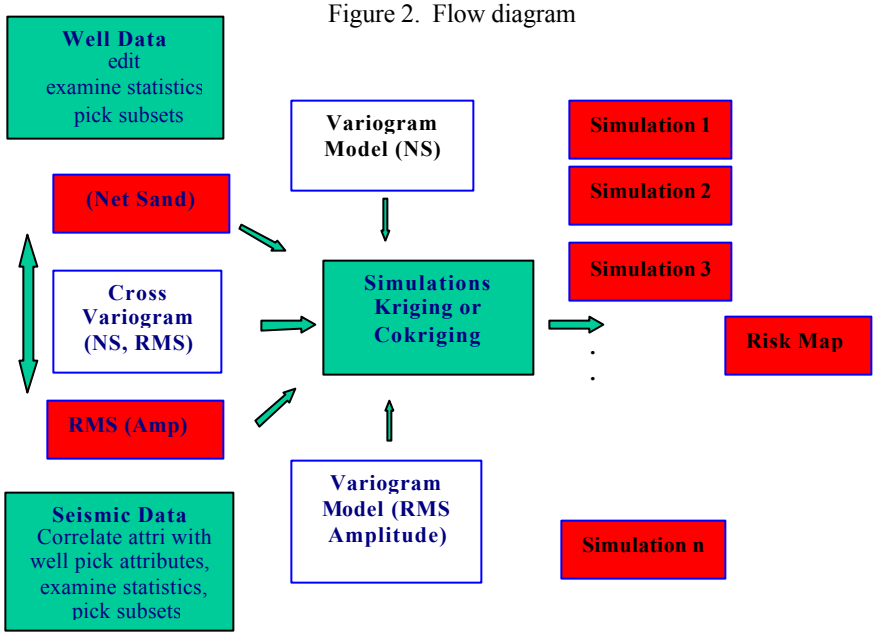

Table 1- Step by step description of the methodology

Step	Details and Comments
Data Preparation	Data editing, Choice of boundaries for mapping and grid size
Data examination	Creation of histograms and matrix plots
Attribute choice	Compare seismic attributes and well properties correlations
Spatial statistics	Calculate variograms and correlograms
Kriging	Extrapolate well properties away from the well using well property variogram models
Kriging with external drift	Extrapolate well properties away from the well using variogram models and seismic at grid points as a guide
Colocated Kriging or Cokriging	The same as kriging except the seismic information usage is not limited to grid points only
Cokriging	Extrapolate well properties away from the well using variogram and cross-variogram models and seismic data
Simulation	Create multiple 100) realizations of co-kriged results
Risk analysis and interpretation	Based on the simulation results, create the predicted value and associate uncertainty at the proposed well location
Ground Truth Test	Test the prediction results against new wells and examine to ranges of predicted values and true drilling results

Figure 3 we show the intermediate kriging result of net sand using well data alone. We examined different seismic attributes to constrain extrapolation of well data for kriging with external drift or for co-kriging. This was accomplished by comparing the correlation coefficients of different seismic attributes (at well locations). RMS amplitude was selected as the most reliable attribute in establishing reasonable relationship with net sand and to a lesser extent with porosity. Table 1 shows the major steps for our geostatistical study. For technical details and other methods see Deutsch and Journel (1998). It should be noted that to make full use of all seismic attributes combination (clustering) of different attributes, should be considered. This can be best accomplished by factor analysis of the original attributes and establishing optimum correlations with well properties. For an example of such analysis see Aminzadeh and Chatterjee (1984).

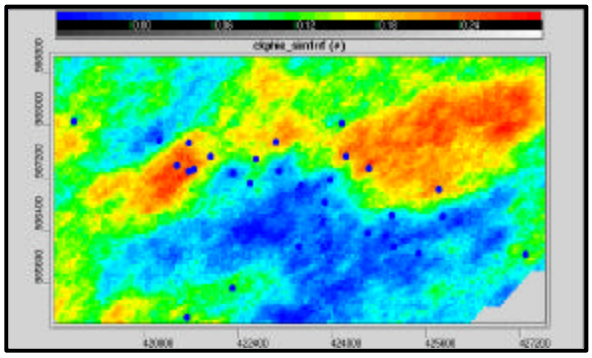

Figure 4. Cokriging of porosity using seismic and well data.

Alternatively, as shown in Aminzadeh et al (2000) and Aminzadeh and de Groot (2001) neural networks could be utilized.

Results and Conclusions

In this section we provide several examples of the analysis results and main conclusions of the study. As we note from Figure 3 extrapolating only well data by kriging provides a map which shows general trends which lacks the details that seismic data contain. As we outlined in Table 1 different kriging and cokriging methods can be used to include seismic information in extrapolating well information away from those locations. Among these method are: kriging with external drift, colocated cokriging and cokriging. The latter methods use well data, seismic, cross-variogram of the RMS amplitude and net sand, as well as variograms of each data component.

All these methods can be applied to create any reservoir property. The confidence level on mapping results however is dependent on the well coverage and the extent of correlation between the well properties and seismic attributes. Figure 4 shows an example of porosity map generated from cokriging of porosity against RMS amplitude.

Given the fact that many other realizations of the net sand map can be derived from the same data set, we generated a large number of simulations. A number of those simulation results are shown in Figure 5. The net sand map showed a clear SW-NE channel shaped sand body that could not be identified previously using well data or seismic data alone. An average

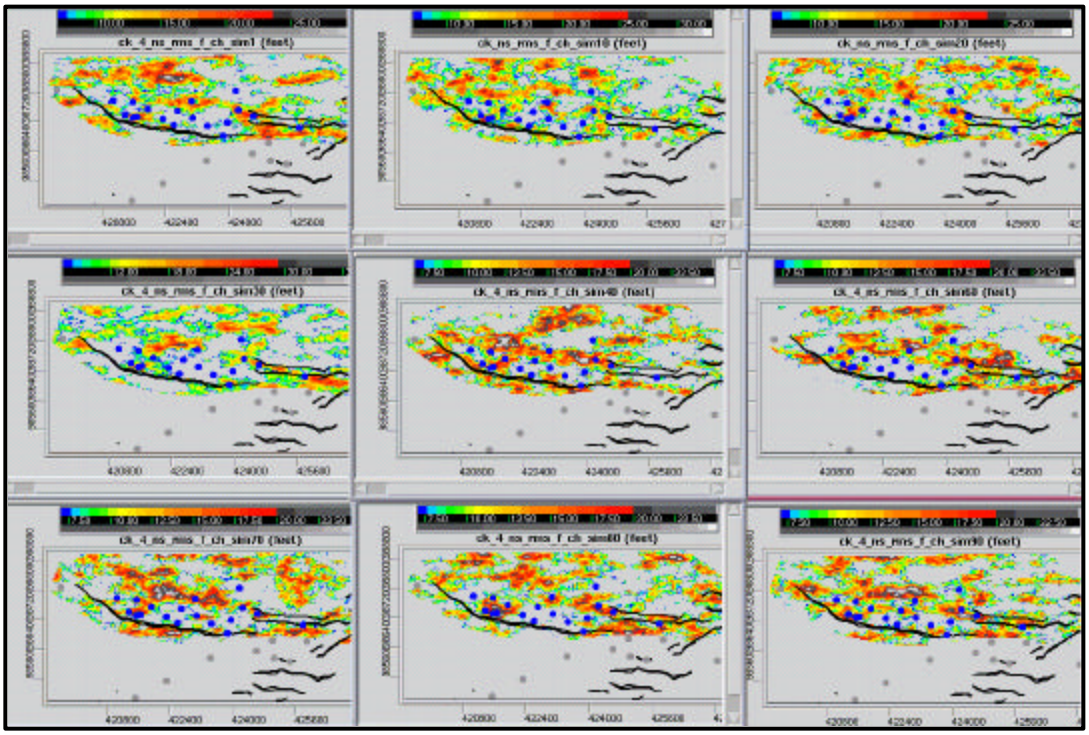

Figure 5. Selected number of simulation cokriging results of net sand.

sand distribution map was generated from those simulations as shown in Figure 6.

To evaluate results and their level of uncertainties, we calculated the mean and standard deviations of net-sand distribution at a location where a new well was drilled, not used in the original data set for extrapolation. At that location we calculated a mean and variance values of 21 and 4.4 feet. The actual well showed a net sand value of 25 feet. Predictions for several new well locations were made with the associated uncertainties. These estimates were used as an input to a proposal to drill two horizontal wells in order to drain the newly upgraded recoverable reserves of 4.8 MMbbls.

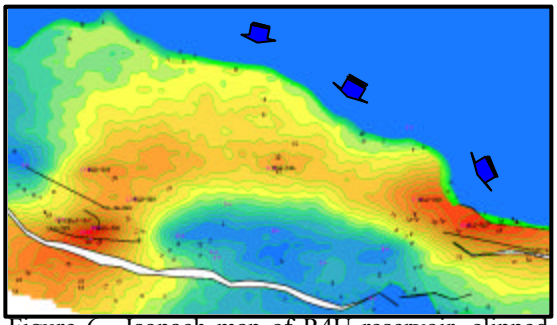

Figure 6. Isopach map of R4U reservoir, clipped at the original water-oil contact.

References

Aminzadeh, F. & Chatterjee, S. 1984, Application of clustering in exploration seismology, Geoexploration, Vol. 23, pp. 147-159.

Aminzadeh, F. Barhen, J. Glover, C. W. and Toomanian, N. B., 2000, Reservoir parameter estimation using hybrid neural network, Computers & Geoscience, Vol. 26 pp 869-875.

Aminzadeh, F., and de Groot, P., Seismic characters and seismic attributes to predict reservoir properties, 2001, Proceedings of SEG-GSH Spring Symposium.

Deutsch, C. W. and Journel, A. G., 1998, GSLIB Geostatistical software library and user´s guide, Oxford University Press.

Parnaud F., Pascual J. C., Truskowsky I., Gallango O., Pasalacqua H. and Roure F., 1995, Petroleum geology of the central part of the Eastern Venezuelan Basin, in Petroleum Basins of South América, AAPG Memoir 62.

Acknowledgments

The authors gratefully thank Perez Companc management for permission to present this paper.

USING OLD GEOPHYSICAL DATA AS A TOOL FOR MODERN GEOLOGICAL MAPPING IN SEMI-ARID TERRANES: AN EXAMPLE FROM THE SERIDÓ BELT, NORTHEASTERN BRAZIL.

Elton Luiz Dantas[1], Adalene Moreira Silva[1], Tati Almeida[2]

[1]University of Brasília, Brazil; [2]Brasilian Army, COTER, Remote Sensing Center.

Abstract

The Seridó belt, of northeastern from Brazil, is an excellent example that illustrates the usefulness of radiometric data in the support understanding of modern geological mapping in semi-arid terranes. We propose a strong relationship among geochemical, isotopic and geophysical signatures of each different crustal block recognized in this region. This kind of approach is fundamental for investigating the regional structural framework and helps to better define the boundaries of the different lithostratigraphic units present in all of the complexly deformed Precambrian belts in Brazil.

Introduction

Airborne gamma-ray data are often used as an aid to both mineral exploration and lithological mapping. Many times, there is a good correlation between patterns in the radiometric data and unweathered rocks (Gunn *et al.,* 1997). The Seridó region is characterized by an abundance of fresh to moderately weathered bedrock; owing to the semi-arid climate of NE Brazil.

The aim of this paper is to present the results of the processing, enhancements and interpretation of the radiometric data previously collected in the Seridó region. The principal goal is to integrate these data with field mapped geological units (which have also been dated by modern geochronological methods). Examining the geophysical data along with the field and laboratory data may prove useful for future extrapolations of analogous, but less well-studied areas.

The data

The Seridó geophysical data was obtained in 08/1973 to 03/1974 by CPRM (Brazilian Geological Survey) and DNPM (National Department of Mineral Production). The radiometric data was acquired with an EXPLORANIUM spectrometer, model DGRS-2000 with 1.012,5 cubic inches of NaI (Tl) (Sodium iodide crystals treated with thallium). The instrument recorded four windows that corresponding to total count, potassium, uranium and thorium. The CPRM could not rescue the digital data. Because of that, the original stacked profiles (38 sheets in 1:50.000 scale) were digitalized by Paterson, Grant & Watson Limited (PGW, Canada) using the back-calibration technique, as a part of the Brazil Airborne Radiometric Mapping Project (BARMP). One of the uranium sheets (SB.24-Z-B-III-1) was not found and is missing in the XYZ dataset (Mourão, written communication). The EW flight lines were flown 1,000 meters with orthogonal tie lines flown every 20,000 meters at 135 meters above the ground surface.

The Regional Geologic Setting

The geological framework of the central part of Borborema Province (BP), in NE Brazil, includes several Neoproterozoic supracrustal sequences overlying an Archean to Paleoproterozoic basement complexes, which are intruded by voluminous granitic plutons at 600 Ma ago (Figure 01).

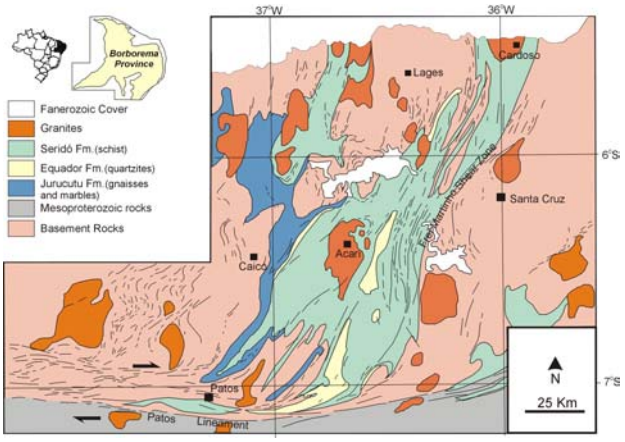

Figure 01 – The geological sketch of the Borborema Province (BP).

Geodynamical evolution models from that region suggest a complex evolutionary history that include the amalgamation of different tectonostratigraphic terranes during the Neoproterozoic orogenic collage (Van Schmus *et al*., 1995; Jardim de Sá, 1994 and Castro *et al*., 1998).

The basement in the BP is characterized by orthogneisses and granitoids intruded and metamorphosed during the Transamazonian cycle (2.2 to 1.9 Ga). These granitoids represent 30 % of BP exposed

lithologies and show a common geological evolution that defines a single Paleoproterozoic crustal block.

In the interpretation of the BP Gravity survey (Castro *et al*., 1998) identified a complex pattern of anomalies that suggested different lithospheric crustal blocks delimited by large-scale shear zones. The structures reflect the boundaries of these terranes or collisional sutures such as the lithospheric discontinuity represented by the Patos Lineament.

Data Processing

Flight line data were converted into grids that allowed for immediate application of enhancement techniques. Initial processing involved flight line editing, the application of a gridding algorithm, and the leveling of all data to a common base. The irregularly spaced data were gridded to a 500-meter interval using a Geosoft-Montaj software v.5.06 based on a minimum curvature technique (Briggs, 1974).

Data interpretation and integration for modern geological mapping

The three radiometric maps (potassium, thorium and uranium) were individually enhanced by their histograms and then displayed in pseudocolor. The aim was to use these data by determining if a spatial correlation exists between the radiometric data and lithological units.

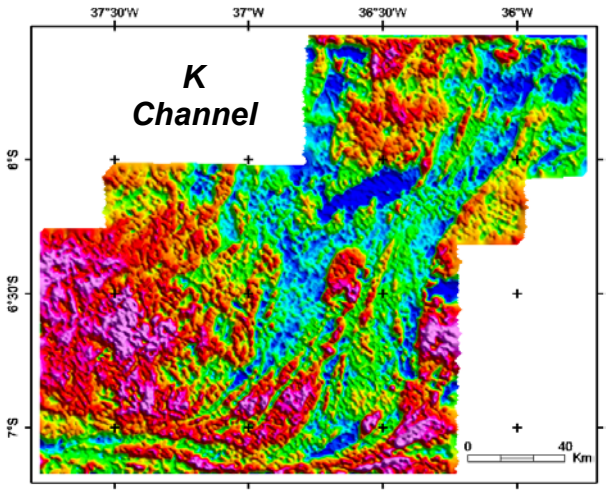

Figure 02 – Potassium image for the Seridó Belt after microlevelling.

Figures 2, 3 and 4 show the potassium, thorium and uranium maps of the Seridó Belt after microleveling. There are good correlations with the known geological maps, mainly with the Phanerozoic

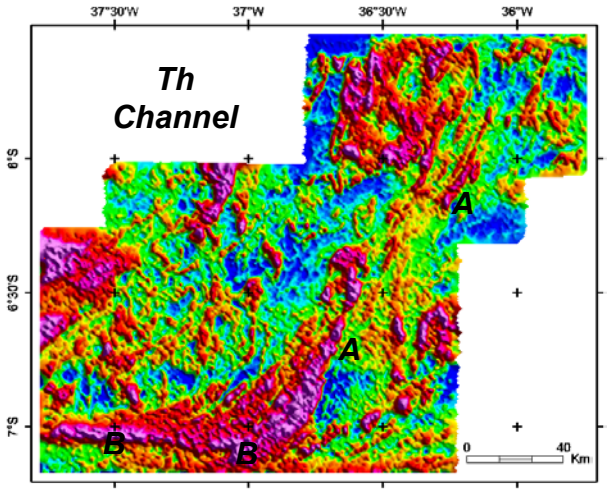

Figure 03 – Thorium image for the Seridó Belt after microlevelling. A – Frei Martinho Shear Zone, B – Patos Lineament.

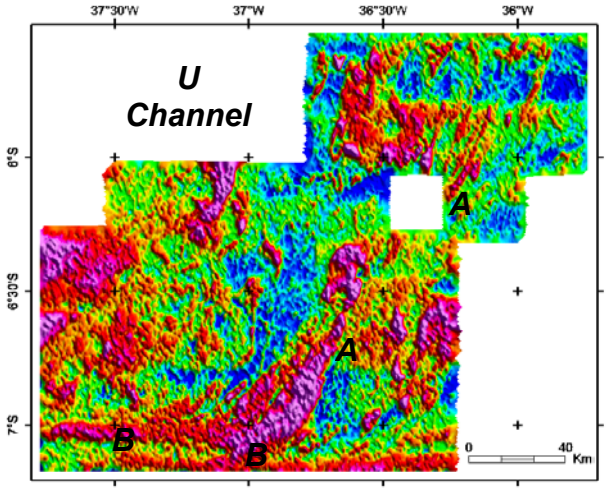

Figure 04 – Uranium image for the Seridó Belt after microlevelling. A – Frei Martinho Shear Zone, B – Patos Lineament.

units (A), Neoproterozoic schists (B), Paleoproterozoic basement (C) and granitoid rocks (D). Anomalies in the thorium and uranium data (Figures 3 and 4) define the structural boundaries in the region.

Potassium, thorium and uranium were assigned to the red, green and blue to create a composite RGB color model. The resulting image (Figure 5) comprises colors generated from the relative intensities of the three components and represents subtle variations in the ratios of the three bands. Potassium was assigned to red, thorium to green and uranium to blue. Two granitoid bodies (the Acari and Cardozo

plutons) are well defined due to high K, U and Th anomalies, as well as their different petrographic facies rich in potassium. An occurrence of marbles, quartzites and amphibolites from Jucurutu Formation intercalated with schists could be distinguished by their high potassium contends. The Tertiary Covers in the Serra de Santana display low K, Th and U signatures.

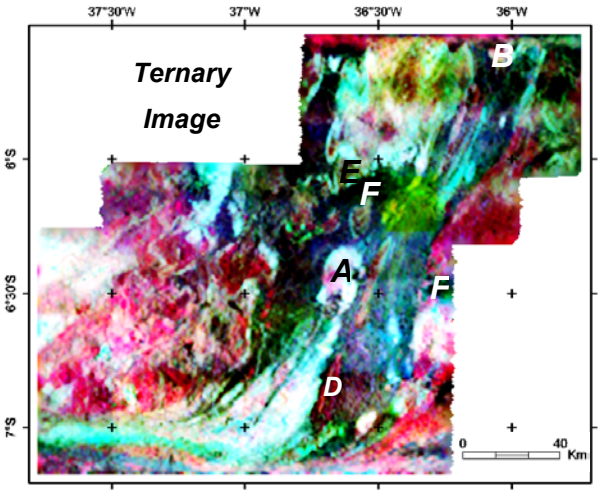

Figure 05 – Gamma-ray spectrometric image (RGB= KThU) for the Seridó Belt. A – Acari Pluton, B – Cardoso Pluton, C – Marbles (Jucurutu Fm.), D – Quartzites (Equador Fm.), E – Amphibolites (Basement Rocks), F – Fanerozoic Cover.

The ratio image tends to remove lithological differences and effects in the data caused by variations in the soil moisture, non-planar source geometry, and errors associated with altitude correction. According to Darnley (1972), lithological differences tend to be removed because radioelement concentrations frequently vary with lithologic changes. The eU/eTh, eU/K (Figures 6 and 7) were useful for determining important lithological changes and contacts.

The radiometric data was also a powerful tool to identify regional and local structures. The displacement of the structures caused by the widespread branching system shear zones is evident in south part of the area (Patos lineament) and the precise definition of the boundaries between the Seridó schist and the basement rocks (Frei Martinho-João Camara Shear zone). Large-scale folding and ductile shear zones are well defined in the Th channel (feature D in Figure 2) in the Lages and Caicó region.

We can separate the basement rocks of the area into three major crustal blocks, possessing different isotopic Nd signatures (Caicó, Lages and Santa Cruz blocks in Figure 2) Dantas (1998). The same differences are observed using the aerogeophysical

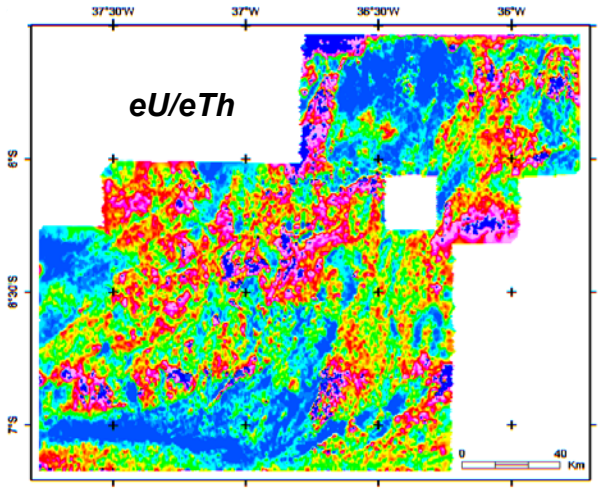

Figure 07 – U/Th ratio of Seridó Belt.

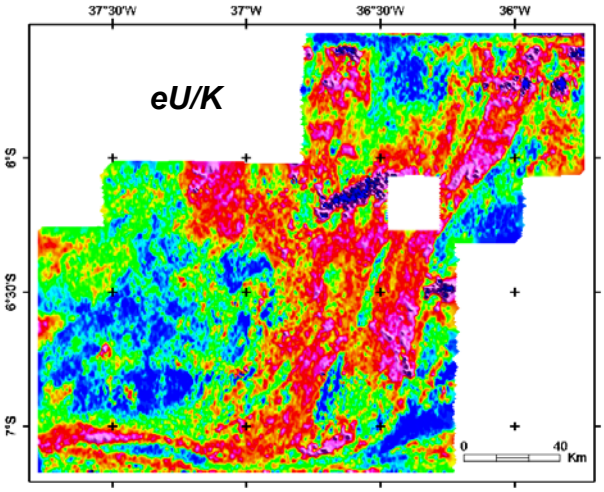

Figure 08 – U/K ratio of Seridó Belt.

data. These data reflect distinctive geochemical and petrogenetic variations (medium to high-K) in the calc-alkaline rocks that occupy this region.

The second order magnitude anomalies, however, are the most important aspects of this study, as they show contrasting features in the inner basement rocks of the Caicó block. One important point is that the Seridó region is well studied and mapped at 1:50000 detail scale. These maps shows that the basement is constituted by differentiated plutonic rocks yielding U/Pb zircon crystallization ages of 2.15 Ga (Hackspacher *et al*., 1990). The composition of these orthogneisses range from gabbroic to

granitic, with tonalitic to granodioritic rocks predominating. The geophysical data suggest a geological architecture consistent with that of a zoned batholith complex. This compositional heterogeneity is also observed in the magnetic data.

A predominant NW trend in these structures is evident, mainly in the Th and ternary image data. Another important enhanced feature is the bending of the NW to NE trending structures caused by the large ductile trascurrent shear zones present in this area. Its possible to discern the dextral sense movement of the shear zone and several complex fold interference patterns in the image (E).

Discussions and Conclusions

The three radiometric maps (potassium, uranium and thorium) were individually enhanced by manipulation of their histograms and then displayed in pseudo-color. There is an obvious relationship between the some mapped geologic units and the radiometric data. These data were imaged as ternary displays (R: B: G = K: U: Th). Individual lithological units can be traced due to their distinctive radiometric response. The difference observed in the basement rocks show that reprocessing available data of this kind can provide a cost-effective definition of structures and lithologies in a diverse geological terrane. Because a large geophysical (radiometric) database already exists for all of Brazil, it may be possible to employ these data in reprocessed form in order to gain a better understanding of the geology of poorly studied or inaccessible regions of the country.

References

Briggs, I. C. 1974. Machine Coutouring Using Minimum Curvature. *Geophysics*, **39** (1): 39-48.

Castro, D.L., Medeiros, W.E., Jardim de Sá, E.F., Moreira, J.A.M., 1998. Gravity map of part of northeast Brazil and adjacent continental margin and its interpretation based on hypothesis of isostasy. *In*: Revista Brasileira de Geofísica, **16**, 2-3: 115-132.

Dantas, E.L. 1998. Geocronologia U_Pb e Sm_Nd de terrenos arqueanos e paleoproterozóicos do Maciço Caldas Brandão, NE do Brasil: *Tese de doutorado*, UNESP, Rio Claro – SP.

Darnley, A.G. 1972. Airborne Gamma-Ray Survey Techniques. In: Uranium Prospecting Handbook. S.H. Bowie, M. Davis, And D. Ostle, Eds., London, The Institute Of Mining And Metallurgy: 174-211.

Gunn, P.J.; Minty, B.R.S.; Milligan, P.R. 1997. The Airborne Gamma-Ray Spectrometric Response Over Arid Australian Terranes. *In*: Exploration 97: Fourth Decennial International Conference On Mineral Exploration, *Proceedings*..., Edited By A.G. Gubins, 1997: 733-740.

Hackspacher, P.C., Van Schmus, W.R., Dantas, E.L., 1990. Um embasamento tranzamazônico na Província Borborema, *Anais* XXXVI Cong. Bras. Geol.: 1683-2696.

Jardim de Sá, E.F., 1994, A Faixa Seridó (Província Borborema, NE do Brasil) e o seu significado geodinâmico na cadeia Brasiliana/Pan-Africana: *Tese de Doutorado*, UNB, Brasília - DF.

Van Schmus, W. R., Brito Neves, B.B., Hackspacher, P.C. & Babinski, M., 1995, U/Pb and Sm/Nd geocronological studies of the eastern Borborema Province, northeastern Brazil: initial conclusions. *J. South America Earth Sciences*, **8**: 267-288.

Acknowledgments

We would like to thank CPRM (Brazilian Geological Survey) for permission to use the radiometric data for this research. We are also grateful to the colleagues Roberto Alexandre Vitória de Moraes and Marcelo Lawrence de Bassay Blum for the enormous help in data processing. Finally, thanks to Dr. Allen Fetter for the reviews and comments on this paper.